Nuclear Fusion Project
Semi-annual Report of the
Association KfK/EURATOM

April 1986 — September 1986

Projekt Kernfusion

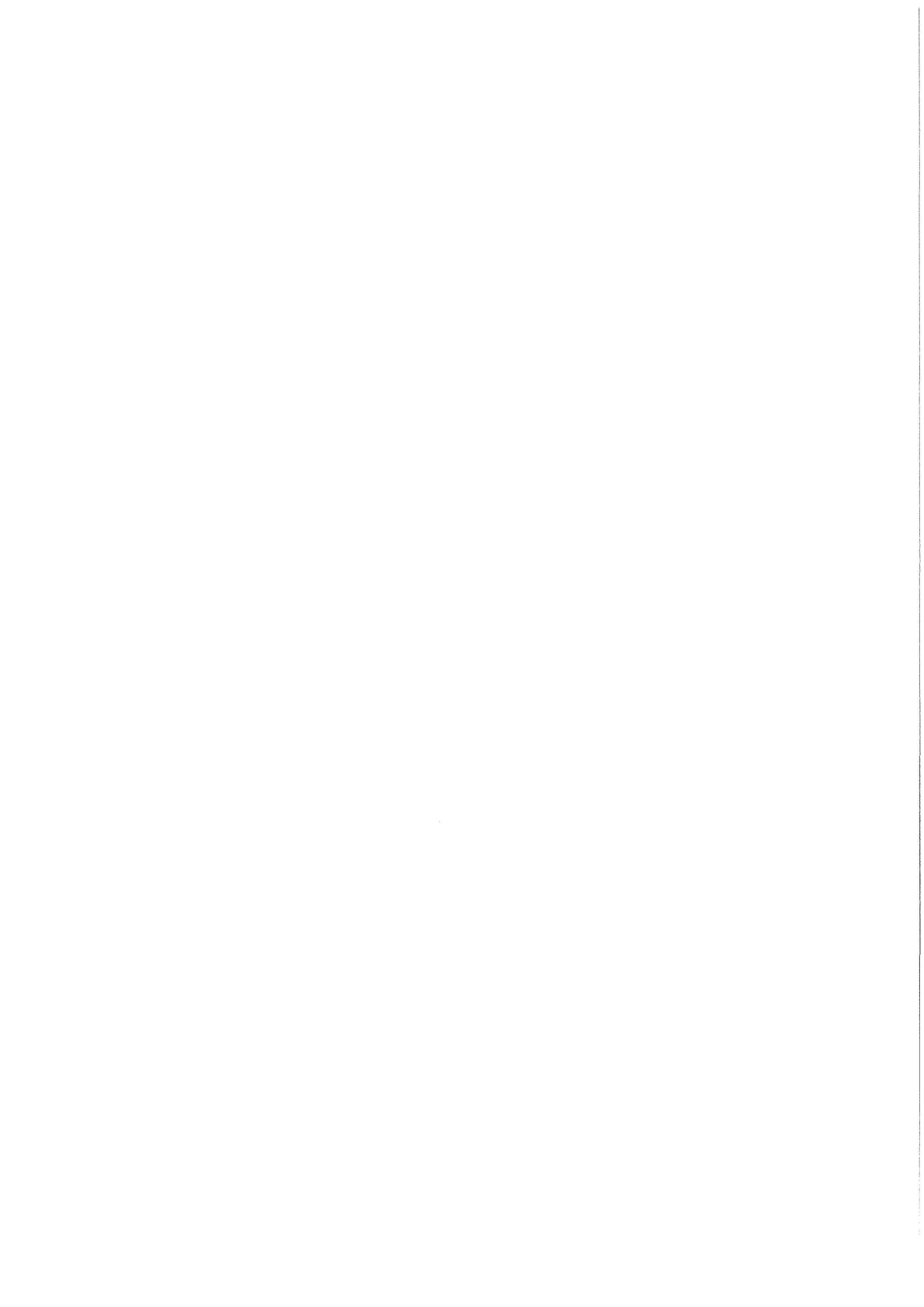# Kernforschungszentrum Karlsruhe

KERNFORSCHUNGSZENTRUM KARLSRUHE

Projekt Kernfusion

KfK 4165
EUR 10534 e

Nuclear Fusion Project

Semi-annual Report
of the Association KfK/EURATOM

April 1986 - September 1986

CONTENTS

Preface

The Karlsruhe Nuclear Research Center (KfK) is engaged in research and development predominantly in the field of nuclear technology, safety, and protection of the environment.

Nuclear fusion is one of the main activities of KfK. It is organized as a project under the Directorate of Reactor Development and Safety. The work of KfK concentrates on technology aspects of nuclear fusion with magnetic confinement. It is part of the European Fusion Programme where KfK participates as an association to EURATOM. Close links have been established to the Max Planck Institute for Plasma Physics (IPP). In the Entwicklungsgemeinschaft Kernfusion KfK and IPP cooperate for the development of future fusion experiments joining the experience gained in plasma physics (IPP) and materials, safety, and nuclear technology (KfK), respectively.

As in the present strategy of the European Fusion Programme the Next European Tokamak (NET) is foreseen as the major next step, most of the activities of KfK address this subject. In addition to the contributions to NET, studies are carried out to innovate INTOR, the worldwide cooperation for an experimental reactor under the auspices of IAEA. Furthermore, the Entwicklungsgemeinschaft Kernfusion has evaluated the feasibility of a fusion reactor with a stellarator confinement.

In the preliminary design phase of NET the technology programme aims at establishing the necessary data base and at selecting appropriate technical solutions to be incorporated into the NET design. Consequently, the tasks performed at KfK cover a wide range of still very fundamental studies.

However, based on the established KfK knowhow on one side, and following the needs of NET and a balance of contributions among the different contributors on the other side, major activities have crystallized out within the KfK fusion programme.

Recent tests of the superconducting coil sent to the Large Coil Test Facility at Oak Ridge have confirmed the data obtained in pretests and are a basis for the NET related activities. Conductor development, coil design and preparation of prototype testing of toroidal and poloidal field coils for NET are one of the focus points of KfK's programme. About one third of the laboratory's fusion effort is devoted to this activity.

In view of the still limited know-how on tritium handling in civilian applications KfK has decided to contribute to the important area of fusion fuel production and recycling by building and operating a tritium processing laboratory. Under preparation, in some cases already in operation, are different experiments on fuel extraction and reprocessing which are described in this report partly as blanket and partly as tritium tasks.

NET is planned to be an experimental machine with high flexibility to accomodate different technological developments and to demonstrate their usefulness for reactor applications. KfK has undertaken to analyze the feasibility and the trade-offs of this flexibility with respect to an insertion of different breeding blanket modules and the associated remote maintenance problems.

Among the candidates of breeding blankets for NET KfK has chosen two design options, which are described in this report (B 1 task). Furthermore, engineering of first wall, shield, and divertor modules is in progress.

It is expected that from the evaluation of the engineering studies and the accompanying experiments at least one of the concepts can be further developed to a full blanket insert for NET.

Remote handling is a working area which recognizes growing importance within the KfK laboratory, as the development is driven by different applications in the nuclear and non nuclear fields. To prepare for the challenging needs of NET, remote maintenance systems are developed for the TFTR fusion experiment at Princeton, USA, and for JET. The progress made for the European Fusion Programme is described as RM tasks.

In the materials qualification and development programme KfK has concentrated on ferritic steel and its modification to obtain low levels of long term activation. The dual beam irradiation facility is the most advanced tool for evaluating irradiation phenomena of these materials. Further work relates to materials for the protection of the first wall and to rf insulators for very high frequencies.

Safety studies address questions of component availability, safety, accident sequences, accidental release and impact of these releases on the environment. These studies are conducted in particular close interrelation with partner laboratories and with the NET team.

In the Plasma Physics Programme KfK sets the basis for a later industrial development of powerful gyrotrons for mm wave lengths. Effects limiting the output power and mode stability of these sources of electron cyclotron heating power are being studied.

About two hundred scientists, engineers and technicians contribute to KfK's fusion programme. The work is contracted to and supported by the Commission of the European Community. A list of the tasks and NET study contracts is given in the appendix.

I hope that this report conveys some information on the KfK fusion project to the supervisory bodies, to our collegues, to visitors, and to all those who are interested in the progress of fusion technology.

J.E. Vetter

B 1   Blanket Design Studies

Two design concepts are studied by KfK: a helium cooled ceramic blanket and a blanket with LiPb eutectic as breeder material and coolant. The study includes small scale experiments and collaboration with industry for special feasibility problems. The studies are coordinated with efforts of CEA and UKAEA in a common working group.

In both of the designs blanket and first wall (F.W.) form a unit with a common coolant flow. Thus, the first wall studies are included here and described in more detail under Task N 1, Plasma Facing Components.

Helium Cooled Ceramic Breeder Blanket

The helium cooled ceramic breeder blanket concept previously described was modified to cope with the recent NET design requirements:

- double null (DN) divertor configuration with 48 segments,
- high surface heat load (20-100 W/cm^2),
- graphite tiles on the whole surface,
- copper saddle loops for passive plasma stabilization.

STAINLESS STEEL
FIRST WALL

STAINLESS STEEL
COOLING TUBE
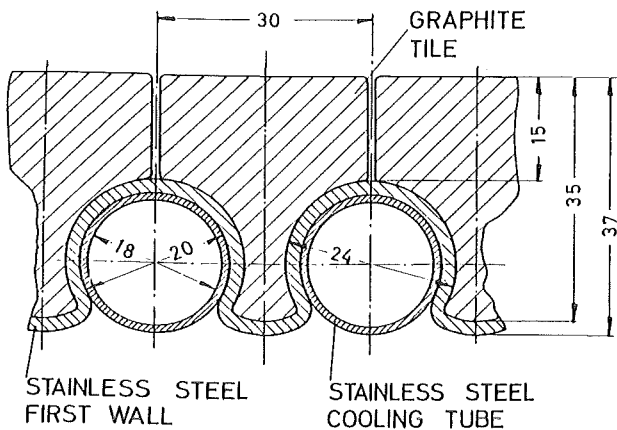
Fig. 1: Helium cooled first wall with graphite protection tiles

Fig. 1 shows the supporting arrangement for the graphite protection tiles on the outboard first wall. This is based on a suggestion of Malang (semiannual report KfK 3979) which is modified to maintain the double containment principle. Graphite temperature and

thermal stresses in the first wall limit the design to a maximum heat flux of 20 W/cm^2 outboard and 10 W/cm^2 inboard.

The saddle loops are realized by 2.2 mm thick and 500 mm wide copper plates brazed on the back of the first wall in the upper and lower F.W. region, and by 13 mm thick copper plates attached to the side walls of the outboard blanket vessel.

The graphite tiles, the more limited space on the inboard side due to the divertor supply tubes, and the copper plates reduce the tritium breeding ratio to TBR = 1.12 for 100% coverage. Without inboard breeding the decreases to a value of 0.97.

Feasibility of piping and closed box were investigated by INTERATOM. With a very tight arrangement of pipes for coolant and purge gas supply a design with a closed blanket segment box seems feasible. Fig. 2 indicates the arrangement principle.
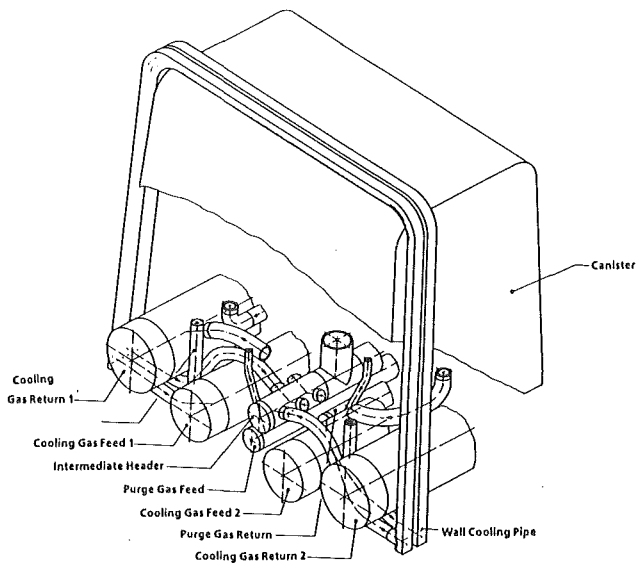
Fig. 2: NET-DN outer blanket segment - isometrical view of piping arrangement

On the basis of recent pebble bed heat conductivity measurements two-dimensional temperature distribution calculations for the canister with the highest heat load 20 W/cm^3 ceramic, 14 W/cm^3 canister wall) were done. Fig. 3 shows the results in a radial cut through the canister. The maximum temperatures are 700°C and 442°C in pebble bed and canister wall, respectively.

An important feasibility issue of the solid breeder canister blanket concept investigated at KfK is the
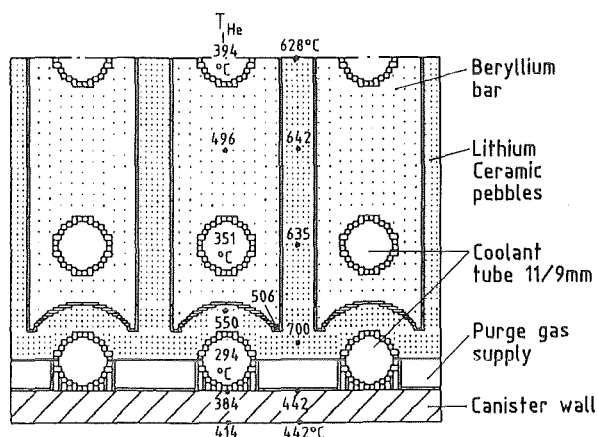
Fig. 3: Temperature distribution in a pebble bed canister

behaviour of the pebble bed under thermal cycling conditions. It is estimated that the difference in volume expansion between the pebble bed and the canister is $\Delta V/V 2.0\%$ when going from room temperature to operating temperature. This change of volume should not generate excessive loads on the walls or destroy pebbles. To study this load a 16 mm inner diameter, 20 mm high steel cylinder, inductively heated to 600°C, is filled with Li_4SiO_4 pebbles. After the pebbles are filled in and are vibration compacted the cyclinder is sealed so that no empty room is left. Then the cylinder is suddenly dipped into cold water to shrink the steel capsules on the pebbles. This corresponds to $\Delta V/V=2\%$. Heating and cooling is repeated 300 times.

The device has been installed and tested. Results will be reported in the next period.

Liquid Metal Cooled Blanket

The development of a blanket concept where the eutectic lithium-lead alloy $Li_{17}Pb_{83}$ serves both as breeder material and as coolant has been continued. The present design is based on the NET double null divertor configuration. Breeding blankets are arranged at the outboard side only. The lower breeding rate was compensated by introducing beryllium as a multiplier in the front part of the outboard blanket. There are gas-cooled steel reflectors arranged at the inboard side, leading to a tritium breeding ratio > 1.1. Graphite tiles as first wall protection at the inboard

as well as at the outboard side were included in the neutronics calculation.

Blanket design work has been concentrated on three subjects:
- First wall and multiplier cooling.
- Double containment of the liquid metal by a composite wall.
- Layout of modular interface units between liquid metal cooled blankets and the plant water-cooled system.

The first wall of the blanket is cooled by liquid metal flowing in toroidal direction. Fig. 4 shows a
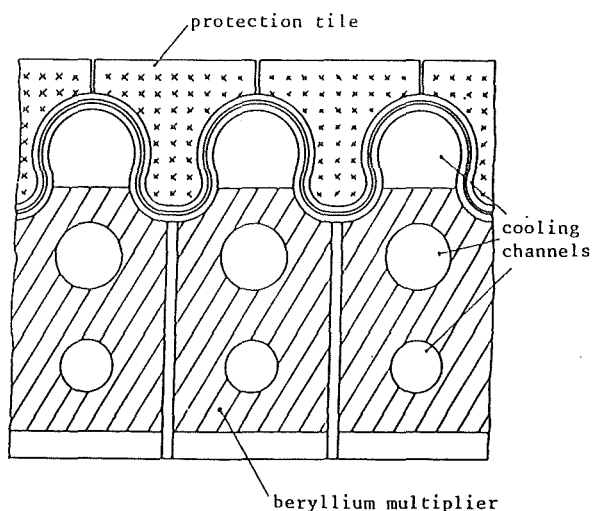

Fig. 4: Cross section of the toroidal front channels

cross-section of the toroidal front channels containing beryllium blocks serving as neutron multiplier. Liquid metal flows parallel to the magnetic field through holes in the beryllium blocks. The flow velocity in these channels can be adjusted to the local heat generation to achieve an identical exit temperature for the three channels. Protection tiles are fitted loosely between the cooling channels and have a heat-radiating surface opposite to the cooling channels twice as large as the plasma facing surface. This results in lower temperatues and thermal stresses compared to other concepts.

A composite structure as shown in Fig. 5 is used for the outer wall of the blanket segment. An intermediate layer of pure iron is used to stop or at least slow down the growth rates of cracks caused by the cyclic operation of the machine. Integrated in the composite wall is a network of grooves which can be pressurized
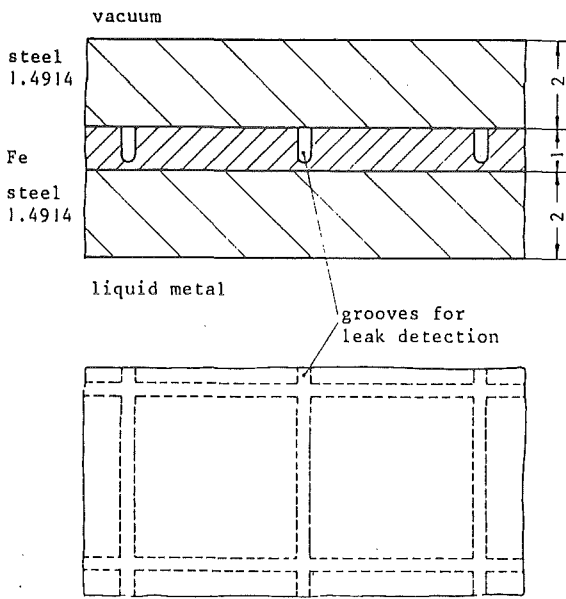
Fig. 5: Composite wall with grooves for leak detection

to an intermediate pressure. Monitoring this pressure enables the detection of cracks prior to leakages of liquid metal into the plasma chamber. Therefore, this design provides a real double containment of the liquid metal without the complexity of a separate coolant.

The conceptual design of a modular unit has been started, serving as interface between the liquid metal cooled blankets and the plant water-cooling system. This unit contains an intermediate heat exchanger (liquid metal/water), a primary circulation pump and a tritium extraction system. Double walled tubes are used in the heat exchanger and a secondary liquid metal (Na or NaK) is flowing through the gaps between the concentric tubes. Tritium permeates into the secondary liquid metal and is extracted by cold-trapping.

The use of such interface units results in three major advantages:

1. Large flexibility of blanket insertion. It offers the possibility to replace water - or gas-cooled blankets by liquid metal-cooled ones and to add additional blanket segments.

2. High availability of the machine. The interface units are exchangeable, avoiding time-consuming in situ repair work.

3. Electrical insulation between neighboring segments. Plasma control requires segmentation of the torus and electrical insulation between the segments including the cooling loops. The use of interface units allows the insulation of each blanket segment (if necessary). Fig. 6 shows this case where each of the 48 blanket segments is connected to a separate interface unit. The height of the unit will remain constant and the outer diameter will be increased from 2 m to 3.5 m if 3 segments (one sector) are connected to a common unit.
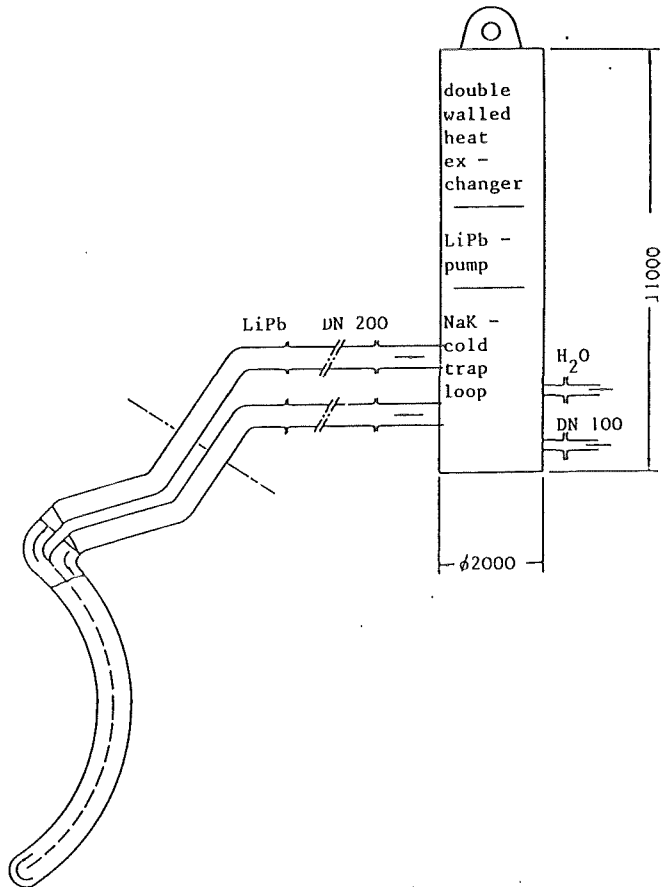
Fig. 6: Interface unit between liquid metal cooled blanket segments and plant cooling water system

Tritium Recovery System for the Self-cooled Blanket

For a self-cooled blanket with an intermediate loop or a double walled heat exchanger the most promising method for tritium separation is to permeate the tritium into the fluid of the intermediate loop (Na or NaK) and to separate it by cold trapping. To recover the tritum, the cold trap is decoupled from the flow, the fluid is drained and the cold trap is heated up.

The elemental tritium which results from thermal decomposition at about 400°C is pumped off and stored with a getter bed. Fig. 7 shows a flow sheet proposed
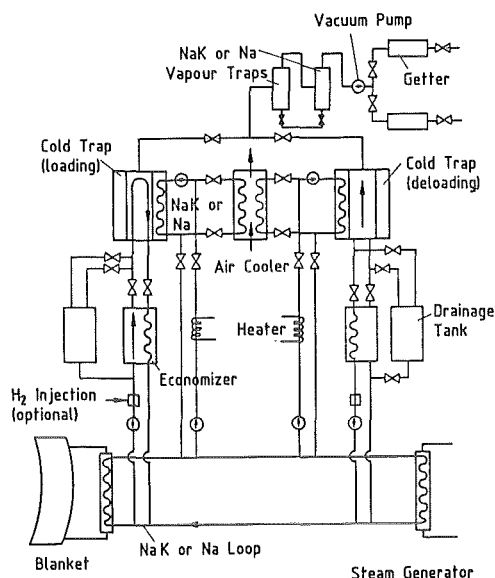
Fig. 7: Tritium separation and recovery in an intermediate loop

for NET: Na was chosen as fluid, a tritium partial pressure of 0.01 Pa is achieved by using 4 cold traps (diameter 0.8 m, height 1.3 m), a mass flow rate of 10 kg/s, a cold trap temperature of 130°C and an addition of protium of three times the tritium mass flow rate (isotope swamping). For NaK and a lower cold trap temperature, the addition of protium would not be necessary.

Another method, studied in the frame of NET contract 223/86-2/FUD NET, is the tritium permeation through a highly permeable wall and the subsequent catalytic oxidation in a gas stream. Critical issues are the development of permeation barriers at the Li-Pb-wall interface and the mechanical behaviour of the metallic bond.

Publications:
M. Dalle Donne, U. Fischer, G. Sordon, E. Bojarsky, H. Reiser, P. Norajitra, E. Bogusch: "Pebble Bed Canister: A Ceramic Breeder Blanket with Helium Cooling for NET". 14th Symp. on Fusion Technology, Avignon, 7.9. - 12.9.1986

M. Dalle Donne, S. Dorner: "Tritium Control in a Helium Cooled Ceramioc Blanket for a Fusion Reactor", Fus. Techn. 9 484 (1986)

S. Malang, V. Casal, K. Arheidt, U. Fischer, W. Link, K. Rust: "Liquid Metal Cooled Blanket for NET". 14th Symp. on Fusion Technology, Avignon, 7.9. - 12.9.1986

J. Reimann, S. Malang: "A Study on Tritium Separation from LiPb by Permeation into Na or NaK and Cold Trapping". KfK 4105, 1986.

J. Reimann, P. Dinner, S. Malang, C. Wu: "Tritium Separation from LiPb Blankets by Permeation into a Gas Stream or into NaK". 14th Symp. on Fusion Technology, Avignon, 7.9. - 12.9.1986

Staff:
K. Arheidt
E. Bojarsky
V. Casal
M. Dalle Donne
U. Fischer
C. Günther
B. Haferkamp
M. Küchle
W. Link
S. Malang
P. Norajitra
J. Reimann
H. Reiser
K. Rust
G. Schumacher
G. Sordon

B 2   Development of Computational Tools for
       Neutronics

The KfK-activities within the B 2-frame comprise the evaluation and processing of nuclear data for fusion applications and the development of adequate computational tools for use in fusion neutronics. For this purpose a general multi-dimensional anisotropic transport code system making full use of double-differential cross-sections (DDX) is under development.

The one-dimensional anisotropic transport module ANTRA1, treating the anisotropic neutron scattering in a rigorous way, had already been set up. For the provision of the 3-d transfer matrices (dependent on the incoming and outgoing energy group and on the segment of the scattering angle) needed in this procedure, a corresponding processing code system has been established. The 3-d transfer matrices are generated from basic DDX-data and/or are reconstructed from conventional single-differential data (SDX).

Comparative neutronic calculations have been performed for a lead spherical assembly around a 14 MeV neutron volume source. The basic nuclear data are taken from the European Fusion File EFF-1. The comparison of first results (Table 1) suggests that for lead the

experiments for both lead and beryllium will be performed.

Monte Carlo methods are adopted for treating complex geometrical arrangements in fusion reactor blankets in two and three dimensions. The Los Alamos code MCNP is in routine use at KfK for such applications. Fig. 8 shows a typical example of a heterogeneous arrangement of beryllium, breeding ceramics and helium cooling pipes in a solid breeder blanket requiring a two dimensional neutronic analysis.
Efforts continue to improve the MCNP data base. For this purpose the corresponding data-preparation code ACER had been adapted. At present the cross-sections of Fe-56 and Cu-63, needed in the analysis of the forthcoming neutronic experiments, are treated.

The group constant generation code NJOY is in routine use at KfK for the calculation of group constants from ENDF/B-formated nuclear data files (EFF, JEF, ENDF/B). In the past half year several errors have been detected and removed from the NJOY code and the linked modules JOYFOR and MITRA. These latter programmes perform the formating and testing of the group constants, calculated by NJOY, for further use within the KfK programme system.

Pre-equilibrium effects are often neglected in the

programme	ANTRA 1	ANTRA 1	ONETRAN	MCNP
data base	EFF-1	EFF-1	ENDF/B-IV	ENDF/B-IV
group structure	30LANL[a)]	30LANL	25 UW[b)]	continuous
method	rigorous (DDX)	P_4	P_3	equally probable scattering intervals (SDX)
neutron multi-plication	1.338	1.338	1.342	1.342 ± 0.003

a) Los Alamos group structure
b) University of Wisconsin group structure

Table 1: Comparison of the neutron multiplication for a spherical lead
         assembly (14 MeV neutron volume source with a radius of 5 cm
         surrounded by a spherical lead shell of 5 cm thickness) as
         calculated by different procedures and data

usual Legendre expansion method is sufficient and, moreover, that there are no significant differences in the nuclear data between ENDF/B-IV and EFF-1 for natural lead. It is expected, however, that the situation is completely different when going to light nuclei, especially for beryllium. At KfK neutronic

evaluation of the neutron emission spectra resulting in an underestimation of the emission probabilities at high energies; this even holds for EFF-1 data, especially if materials from the ENDF/B-IV file had been taken over. Of special interest in the forthcoming neutronic experiments at KfK is the
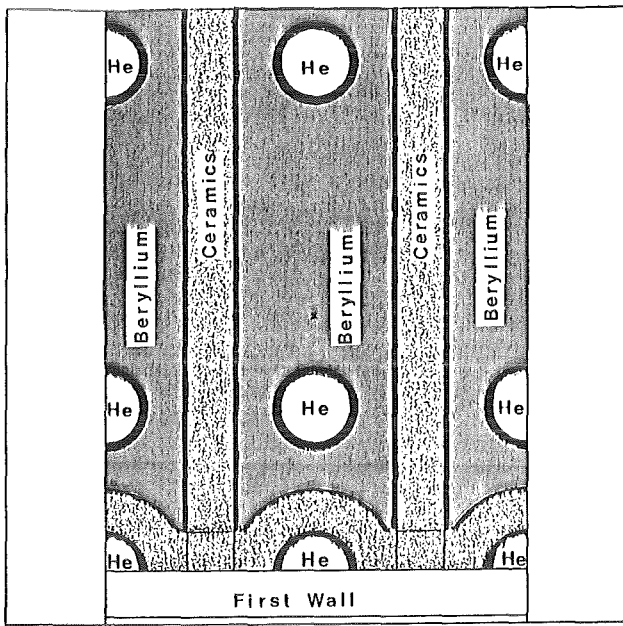
Fig. 8: Heteorogeneous beryllium/breeding ceramics arrangement analysed with MCNP

spectrum of Cu-63 (at an incident neutron energy of 10 MeV) compared to the distribution contained on EFF-1. After completion and testing of the evaluation these data will be made available for EFF.

Publication:

U. Fischer: Optimal Use of Beryllium for Fusion Reactor Blankets, 14th Symp. Fusion Technology, 8.-2.Sept. 1986, Avignon

Staff:
I. Broeders
U. Fischer
B. Goel
B. Krieg
H. Küsters
A. Schwenk
E. Stein
E. Wiegner

neutron emission spectrum of natural copper. Therefore the secondary energy distribution of the neutron inelastic continuum scattering is being calculated for copper, taking into account the pre-equilibrium emission of neutrons.

Fig. 9 shows the newly calculated neutron emission
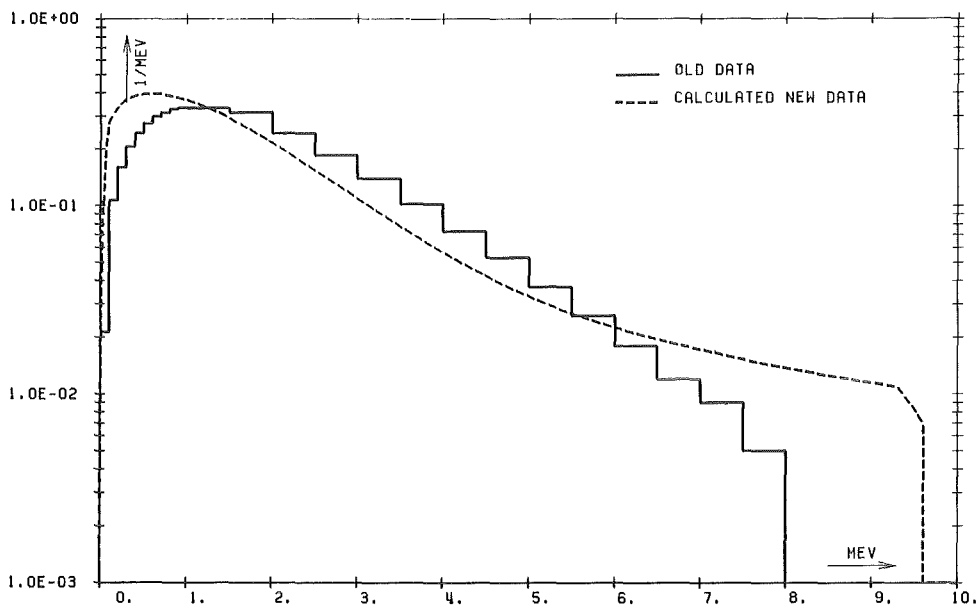
Fig 9: Neutron emission probabilities of Cu-63 at 10 MeV incident neutron energy

B 6   Corrosion of Structural Materials in Flowing Pb-17Li

Corrosion of structural materials by flowing liquid Pb-17Li alloy can be the temperature limiting process for a fusion reactor blanket using liquid metal as blanket fluid. Therefore, we intend to study the corrosion behaviour of the martensitic steel 1.4914 (X18CrMoVNb 12 1) in a loop in which the eutectic alloy Pb-17Li is circulated by means of an electro-magnetic pump. We have made a new construction of the hot leg of the Pb-Li loop. The main changes refer to the material of the hot leg piping. We have chosen a ferritic steel no. 1.4713 (X10CrAl 7), which is available in tubes of the necessary dimensions. We have introduced a new heater with energy input from outside and a heat exchanger. The hot and cold legs are connected by means of flanges in order to avoid welding of the ferritic tubes to the austenitic tubes of the cold leg. Fig. 10 shows the new design of the

detection limit of iron, chromium and nickel could be lowered below the μg/g range using atomic absorption spectroscopy in a graphite furnace. Preliminary results show that the uptake of iron and chromium even after 9000 h at 420°C does not exceed 5 μg/g, but nickel has been leached and the concentration raised to 100 μg/g. The determination of oxygen in Pb-17Li has been improved by vacuum hot extraction. The detection limit is 1-2 μg/g.

Staff:
Ch. Adelhelm
H.U. Borgstedt
G. Drechsler
G. Frees
M. Grundmann
Z. Peric
G. Streib
S. Winkler
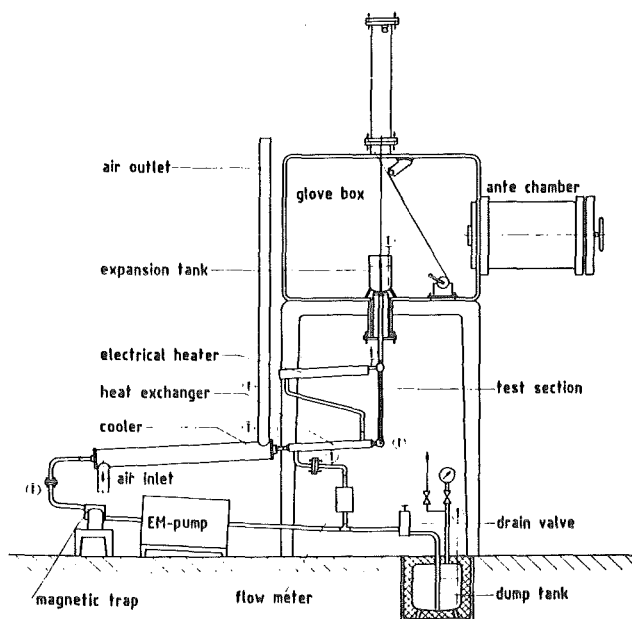
Fig. 10: Flow scheme of the Pb-Li Loop II integrated in an inert gas glove blox

loop. The enlarged volume of the loop has made necessary the replacement of the drain tank by a larger one (20 l). The loop is nearly completed and will be commissioned before the end of the year.

Analytical studies of Pb-17Li have been continued. To determine the amount of corrosion products in Pb-Li, sensitive analytical methods have been proved. The

B 6.3   Fatigue of Structural Steel under Liquid
        Eutectic Environment

The low cycle fatigue behaviour of the martensitic
steel X18CrMoVNb 12 1 (1.4914) will be tested at 550°C
in the liquid alloy Pb-17Li. The electromechanical
testing machine (INSTRON 8062, 125 kN) was put into
operation and some room-temperature tests with
austenitic steels have been performed to check the
testing machine. Capsules for the in liquid metal
tests are already prepared. Hour glass shaped speci-
mens for LCF tests are under preparation. The tests
with and without hold time at the strain maximum will
be started in October 1986.

Staff:
H.U. Borgstedt
M. Grundmann
Z. Peric

B 9 Tritium Extraction based on the Use of Solid Getters

Several methods were proposed to extract tritium from the liquid Pb-17Li blanket material. Task B 9 will study the use of solid getters. The advantage of this method will be its simplicity and a low tritium inventory in the blanket.

Compatibility tests in static Pb-17Li were performed in batch type experiments. The material first selected was zirconium.

The preparation of all samples was done in an argon atmosphere with less than 1 ppm oxygen. A superficial layer on the Pb-17Li was removed and the eutectic was remolten twice. 50 to 60 grams were used in the experiments. The samples were cast into crucibles of molybdenum, which were preheated to 1000°C under a pressure of less than 10^{-5} mbar for 2 hours.

The zirconium was used in the form of foils (12 x 50 x 0.1 mm), obtained from GOODFELLOW (99,8 %). It was preheated to 1000°C under vacuum similar to the crucibles to remove any surface layers and to release dissolved gases. The foil was fixed in the crucible to avoid floating.

Compatibility experiments were performed at temperatures from 300 to 600°C and up to 1000 hours. Experiments under vacuum could only be performed up to 400°C because at higher temperatures evaporation of the liquid metal reduced the lithium-concentration. Most of the tests were therefore performed in an argon atmosphere of 6.0 purity.

After the test the samples were brought into the glove box, and the Pb-17Li was molten and cast into pieces. All the metal, as well as metal remaining on the crucible surface, was dissolved in nitric acid. The solutions were analyzed by ICP - AES - analysis. Some Pb-17Li still remained on the surface of the zirconium sample; this was not yet analyzed. The zirconium samples will be used for metallographic investigations.

Assuming that only a minor amount of dissolved zirconium remained on the samples, the zirconium found in the Pb-17Li corresponds to the corrosion rates. Fig. 11 shows the results.
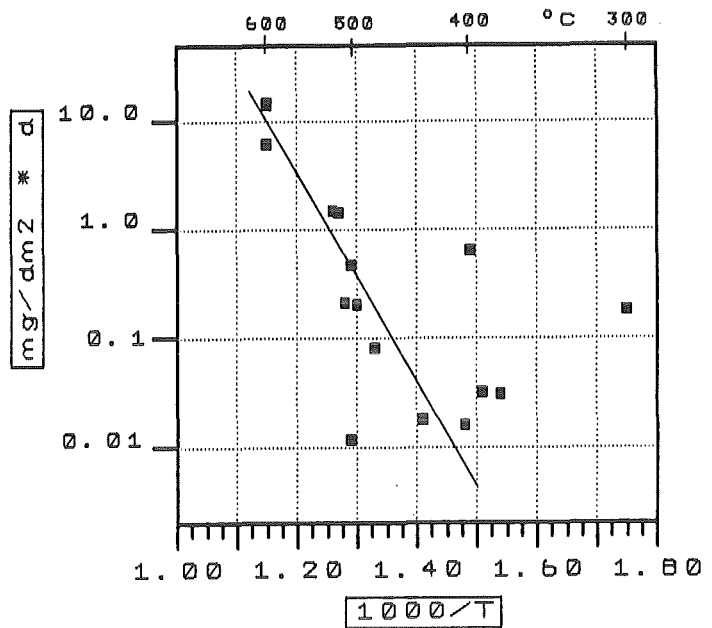
Fig. 11: Corrosion rate of zirconium in liquid Pb-17Li

From the Arrhenius plot one obtains the corrosion rate as a function of the temperature

$$\ln K_{Zr} \; [mg \cdot dm^{-2} \cdot d^{-1}] \; = 28 - 22700°K/T$$

The activation energy for the process was found to be

$$H_a = - 188 \; kJ/mol$$

The experimental technique has been improved from experiment to experiment. At the beginning the Pb-17Li samples showed a strong oxidation effect. Later, no crusts were formed anymore. Though one might suspect a disturbance of the Li-content due to its preferential oxidation the Li-concentration in the eutectic after all tests was still higher. Nevertheless in all experiments the Li-concentration after the test was still higher than 0.6 % by weight. (All data are included in the figure).

From the corrosion rates found one can expect, that zirconium is sufficiently stable in liquid Pb-17Li to be used as a possible getter. However the influence of oxygen has to be investigated, because a real reactor system certainly will not be oxygen-free. Furthermore there may be some enhancing influence of flowing liquid metal on the corrosion, even if the flow rate through a getter will be low. Another problem will be

the poor wetting behaviour below 400°C. In such cases samples will have to be pre wetted at a higher temperature.

The experimental program will continue with zirconium, studying the influence of stirred Pb-17Li, wetting and different surface treatments of the zirconium. Other getter materials will be studied in the near future.

Staff:
H. Feuerstein
H. Gräbner

B 11-16 Development of Ceramic Breeder Materials

1. Fabrication and Characterization of Ceramic Breeder
   Materials (B 11, B 12)

Preparation and fabrication of lithium containing monosilicates, especially Li_2SiO_3 and Li_4SiO_4, are under development to be used as breeder materials. Monosilicate powders, normally sintered to pellets with cylindrical shape, were prepared for irradiation tests and basic material studies. Concerning the KfK pebble-bed canister design for a fusion blanket the preparation of nearly spherical particles with dia- meters in the range of 0.5 to 1 mm could be prepared in a small range for irradiation experiments.

Preparation of Li_2SiO_3 aud Li_4SiO_4 Pellets

A number of Li_2SiO_3 and Li_4SiO_4 pellets were prepared to obtain information on the physico-chemical properties as well as on the irradiation behavior, based on the preparation method already described in detail. The different samples were prepared and characterized according to the specifications given in Table 2.

Preparation of Spherical Granulates

It has been shown that nearly spherical particles can be prepared from the spray-dried powders by extruding the wetted monosilicate powders with subsequently rounding on a special rotating disk using microcrystalline cellulose (Avicel) as a binding agend. The prepared particles were dried by fluidizing bed methods and sintered in a rotating kiln at temperatures up to 1100°C for some hours. 80% of all particles per batch are in the size of 0.5 to 1 mm. Batches in the range of some hundred grams can be prepared by this method with our equipment. Using larger rotating disks the batch size can be scaled up to some kilograms per batch. Continuously working machines are under development in industry.

Characterization of Ceramic Breeder Materials

The characterization of the ceramic breeder materials prepared for irradiation experiments and the measurements of physico-chemical properties covers besides chemical analysis, ceramography, scanning electron microscopy, X-ray diffractometry, image analysis, mercury intrusion porosimetry and the measurement of the permeability coefficient. Up to now

analyses have been carried out of Li_2SiO_3 and Li_4SiO_4 specimens of the irradiation experiments DELICE 01 and 02 (OSIRIS reactor at Saclay), LISA 1 (SILOE reactor at Grenoble) and, recently, of the VOM-23H experiment of the Japan Atomic Energy Research Institute. The latter experiment is performed within the IEA framework, known as BEATRIX-irradiation program. The shape of the specimens of the first three experiments was cylindrical (diameter 5 and 8 mm, respectively), whereas it was spherical in the VOM-23H experiment. The diameter of the spheres was 4 mm. They had a density of 2.11 g/cm^3. The fraction of open porosity was about 48%. The effective channel diameters (assuming cylindrical shape of the channels) ranged from 0.05 to 1.0 µm (Fig. 12). The analysis of the
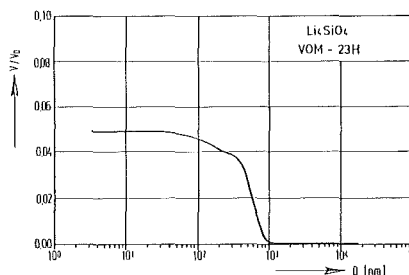
Fig. 12: Relative amount of open porosity versus mean effective channel diameter in the Li_4SiO_4 spheres of the VOM-23H experiment

crystalline phase composition of the spheres made out of Li_4SiO_4 showed that a very small amount of Li_2SiO_3 existed in the specimens. The lithium density was 0.47 g/cm^3. The mean value of the effective diameters of cross sections through the grain of the specimens was about 14 µm. This value was about half of that one observed in the Li_4SiO_4 pellets of the LISA 1 experiment.

Publications:

A. Skokan, H. Wedemeyer, D. Vollath, E. Günther, "Thermal Properties and Application of Potential Lithium Silicate Breeder Material", 14th Symp. on Fusion Technology (SOFT), Avignon, 8-12.9.1986

D. Vollath, H. Wedemeyer, "On the Preparation of the Lithium-Silicates from Li_2SiO_3 to Li_8SiO_6 in alcoholic media", International Conf. on Fusion Materials (ICFRM-2), 13.-17.4.86, Chicago

experiment	material	density (% th.d.)	shape	diameter (mm)	number of specimens	remarks
ELIMA-o2	Li_2SiO_3	9o	pellets	5	16	
	Li_4SiO_4	65	pellets	5	16	irradiation test, KNK II
		9o	pellets	5	16	
		9o	particles	o.5-1	2o g	
DELICE-o3	Li_2SiO_3	9o	pellets	5	16	
	Li_4SiO_4	65	pellets	5	16	irradiation test, OSIRIS
		9o	pellets	5	16	
		9o	particles	o.5-1	2o g	
BEATRIX	Li_2SiO_3	8o	pellets	9.5	8	
	Li_4SiO_4	9o	pellets	9.5	8	irradiation test, EBR II
		9o	pellets	16.5	1o	
		9o	particles	o.5-1	2ö g	
TRIDEX-o1	Li_4SiO_4	9o	pellets	8	65	irradiation test, DIDO
LISA-o2	Li_4SiO_4	9o	pellets	8	2o	irradiation test, SILOE
		9o	particles	o.5-1	2o g	
IMF I	Li_4SiO_4	8o	pellets	9	35	thermal shock
		9o	pellets	9	35	resistance test
			powder		2oo g	compatibility tests
			powder		1oo g	effect of water
IMF III	Li_4SiO_4	9o	pellets	7.5	37	HIP-experiments
IRCH	Li_2SiO_3	8o	pellets	5	25o	solubility
		8o	particles	2	1oo g	of hydrogen
INR	Li_2SiO_3	8o	pellets	5	2o	
		8o	pellets	1o	3	
		8o	disks	1o	3	
			granules	o.o25	5 g	
			granules	o.o5-o.1	5 g	
			granules	o.2 -o.25	5 g	effect of geometry on tritium release
	Li_4SiO_4	65	pellets	5	2o	
		9o	pellets	5	2o	
		8o	pellets	1o	3	
		8o	disks	1o	3	
			granules	o.o25	5 g	
			granules	o.o5-o.1	5 g	
			granules	o.2 -o.25	5 g	

Table 2: Prepared Samples of Li_2SiO_3 and Li_4SiO_4

Staff:
B. Dörzapf
H. Elbel
E. Günther
R. Hanselmann
J. Heger
W. Jahraus
E. Kaiser
W. Laub
H. Nagel   D. Vollath
R. Scherwinsky   M. Wittmann

2. Measurement of Physical, Mechanical and Chemical Properties (B 13)

Constitution and Thermodynamics

The investigation of the phase relations in the Li_2O-rich part of the Li_2O-SiO_2 system was continued in order to establish the phase diagram in this region. Differential thermal analyses were performed with encapsulated samples that yielded the liquidus line between Li_2O and Li_4SiO_4. The revised Li_2O-SiO_2 phase diagram where all new results are summarized is shown in Fig. 13. Contrary to the assumed regular liquidus

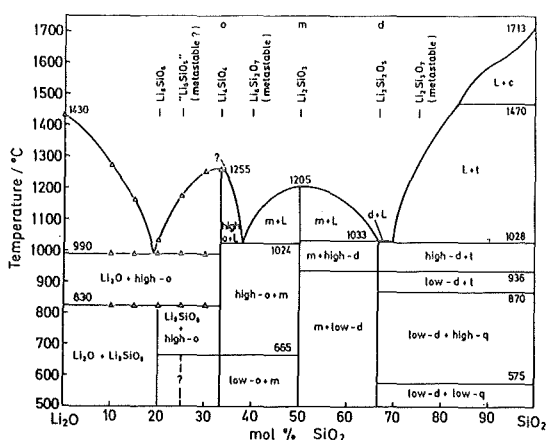
Fig. 13: Revised Li_2O-SiO_2 phase diagram

line between Li_2O and Li_4SiO_4, a eutectic exists at 990°C close to the composition Li_8SiO_6. This new finding implies, that the incongruent melting of Li_4SiO_4 has to be called in question because it would only be consistent with a small two phase field of liquid-liquid separation that seems rather unlikely for the chemical composition of Li_4SiO_4. Li_8SiO_6 is the only phase between Li_2O and Li_4SiO_4, that was found to be thermodynamically stable. The compound Li_6SiO_5 is probably metastable, for it could not be synthesized in the dry system. Li_8SiO_6 is unstable at open air conditions. It reacts with H_2O vapour and CO_2, forming $LiOH$, Li_2CO_3 and Li_4SiO_4. Its linear thermal expansion coefficient, determined by high-temperature X-ray diffraction in helum, is

$$\alpha = (10.46 + 1.73 \cdot 10^{-2} \, T) \cdot 10^{-6} \, K^{-1} \quad (300 \, K \leq T \leq 1075 \, K)$$

The investigation of the interaction with water vapour was continued and extended for the compounds Li_4SiO_4, Li_2SiO_3 and $LiAlO_2$. In addition to the

thermoanalytical methods, continuous isothermal experiments were conducted. Preliminary tests on the reliability of different moisture measuring instruments were necessary; compromises concerning sluggish response, bad resolution or insufficient stability of the zero line had to be found. The experiments were performed during a period of 10 days at 773 ± 1 K in inert gas containing 100 ± 5 vpm H_2O with a flow rate of 25 l/h. Pellets (Li_4SiO_4) as well as powder samples (Li_2SiO_3 and $LiAlO_2$) were used. Insignificant losses of weight (0.025-0.05%) were observed for all samples likewise after this treatment. X-ray diffraction examination yielded no indications for the formation of other crystalline phases.

Publication:

D. Vollath, H. Wedemeyer, in: EUR 9611e (1985) p.9

Physical and Mechanical Properties

Samples of γ-$LiAlO_2$ produced by a sol-gel process (C. Alvani, University of Rome), which is now the third process applied for the preparation of γ-$LiAlO_2$-powder, were received. Fig. 14 shows the
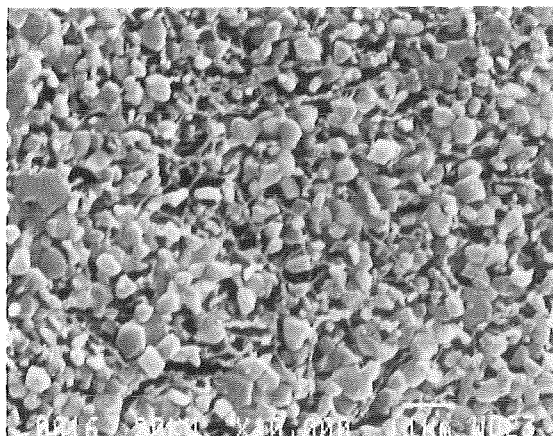

Fig. 14: Scanning electron micrograph of γ-$LiAl_2$ (Italian production), 10 000x

microstructure in a SEM picture. The samples had a density of 78% of theoretical. All porosity is in the submicron range. The thermal diffusivity data measured up to now were corrected for the pellet porosity. One gets the following equations for the temperature range $300 < T < 900$ K:

γ - $LiAlO_2$ (of KfK powder) $\alpha = \dfrac{1}{-6.17+0.109\,T}$ cm^2/s

γ - $LiAlO_2$ (of French powder)$\alpha = \dfrac{1}{-12.4+0.129\,T}$ cm^2/s

γ - $LiAlO_2$ (of Italian powder,$\alpha = \dfrac{1}{-7.42+0.120\,T}$ cm^2/s
see above)

In cooperation with the Unsiversity of Stuttgart, the specific heat of Li_2SiO_3 (Fig. 15) and Li_4SiO_4 (Fig. 16) were measured. The maximum of c_p for Li_4SiO_4 corresponds to the phase transition in that temperature region.
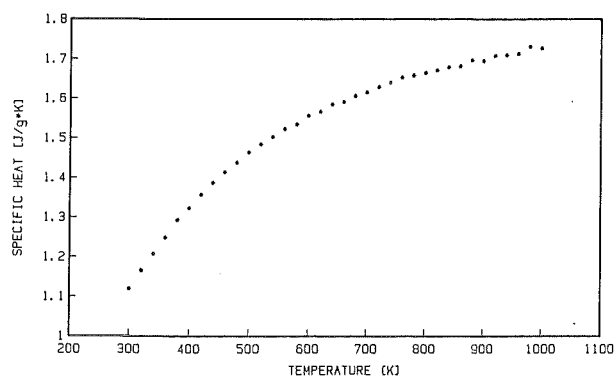
Fig. 15: Specific heat of Li_2SiO_3
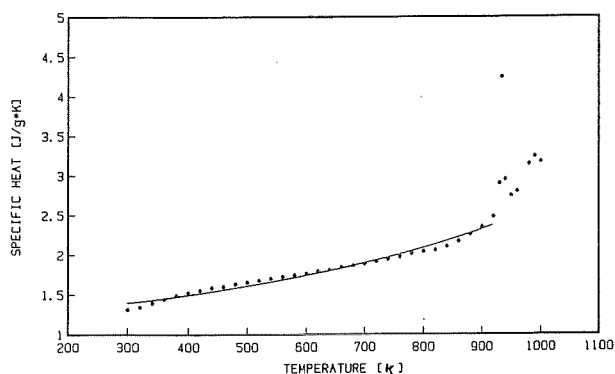
Fig. 16: Specific heat of Li_4SiO_4

The compressive creep rate of Li_2SiO_3 pellets of KfK production was measured in the temperature range between 750 - 1000°C. The pellets with densities between 94 and 78% TD were tested under stresses from 5 to 40 MPa. The measuring period of each data point was $\leq$ 200 h. Tests with changes of temperature and load revealed an activation energy of about 470 kJ/mol

and a stress exponent between 1 and 2. Fig. 17 shows the mean creep rate in the first 100 hrs of the tests at 900°C and under the stress of 10 MPa as a function of porosity. The creep rate seems to be nearly independent of other structural parameters than density.
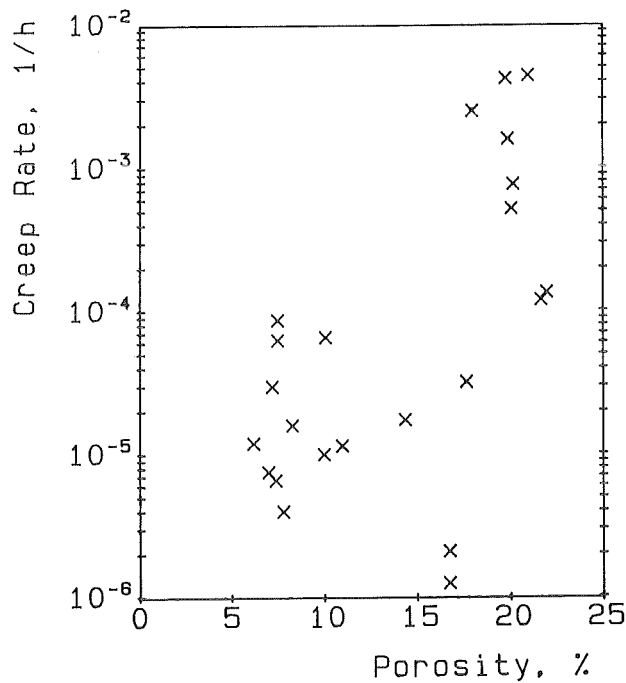
Fig. 17: Compressive creep rates of Li_2SiO_3 pellets from various production charges, at 10 MPa and 900°C, versus porosity

The creep rate level and the activation energy determined suggest that Li_2SiO_3 can be considered rigid at temperatures up to 800°C even at porosities of about 20%.

High Temperature Mass Spectrometry

For the design of the blanket of a fusion reactor detailed information on the thermochemical behaviour of the employed breeding ceramic is needed. From a knowledge of the high temperature equilibria of the blanket material its rate of vaporization can be obtained and an upper limit to the range of operational temperature of the reactor blanket can be estimated.

Among the methods employed in the past for the high temperature characterization of solids, mass spectrometry by means of a Knudsen cell has proven to be particularly useful, on one hand because the samples can be examined over a very wide range of temperatures

and on the other hand because the volatilized species can be identified unambiguously. For investigations of this nature a new MAT 271 mass spectrometer from Finnigan is now in operation at the Institute of Radiochemistry. In first experiments the temperature at the Knudson cell, which is measured with a Keller type PB 60 AF 38 pyrometer and a Pt/PtRh thermocouple, is being carefully calibrated with a Mo Knudsen cell containing Ag. For this purpose the melting point as well as the well known vapour pressures of the metal are useful (see Fig. 18).

Ion	I_i^+ (mV)	collector	E_e- (eV)	T (°C)
Li^+	350,00	Faraday	8,4	1545
LiO^+	1.27	Faraday	12,0	1508
Li_2O^+	< 0,50	Faraday	9,4	1508
SiO^+	0,58	Faraday	14,0	1508
$Li_2SiO_3^+$	1,40	Faraday	11,3	1490
$Li_2SiO_3^+$	2,58	S.E.V.	11,3	1490

Table 3: Ions detected during the vaporization of Li_2SiO_3 employing a Pt Knudson cell (due to the incongruent vaporization of Li_2SiO_3 the ion intensities were found to be time dependent)
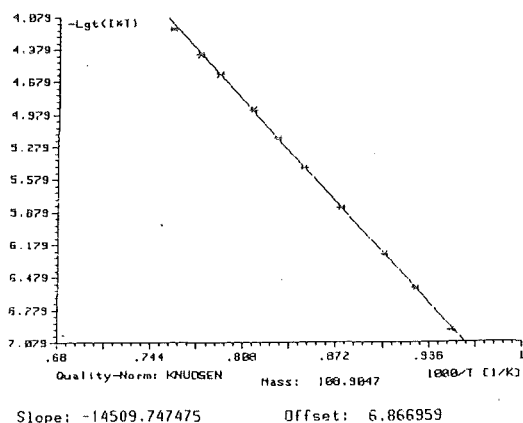
Fig. 18: Calibration with ^{109}Ag in a molybdenum Knudsen cell

Additional calibrations are now in progress with Au in a graphite Knudsen cell. To improve the ion intensity measurements of Au a resolution of the electron multiplier system lower than that employed for Ag was used (the vapour pressure at the melting point is about 25 times lower for Au than for Ag). The above described calibrations also allowed ionization effiaciency measurements (e⁻ voltage).

To test the suitability of the mass spectrometer for the investigation of the high temperature chemistry of lithium metasilicate has been performed. The following specimens were detected in the saturated vapour over Li_2SiO_2: Li (g), LiO (g), SiO (g) and Li_2SiO_3 (g) (see Table 3 and Fig. 19).

These still preliminary results are in good qualitative agreement with the only other high temperature study of Li_2SiO_3 found in the literature (J. Nucl. Materials 102, 292 (1981)).

Fig. 19: Parent peak of Li_2SiO_3 detected at 1490°C with a resolution of 260

Staff:
H. Ihle
R.-D. Penzhorn
P. Schuster

3. Compatibility with Stainless Steels (B 14)

The 600, 700 and 800°C annealing tests with oxide breeder materials pressed into capsules of ss 316 and 1.4914 (11% Cr, martensitic-ferritic) showed, that up to 700°C the attack on 1.4914 is not stronger than on 316. Only at 800°C the situation became much worse for Li_2O and 1.4914 (Fig. 20). On the other hand, Li_4SiO_4 and Li_2SiO_3 did not produce more cladding attack on 1.4914 than on 316 in 500 h at 800°C, probably because of their slower reaction rate. It should be possible to use these breeder materials in contact with 1.4914 at higher temperatures than tolerable for Li_2O.
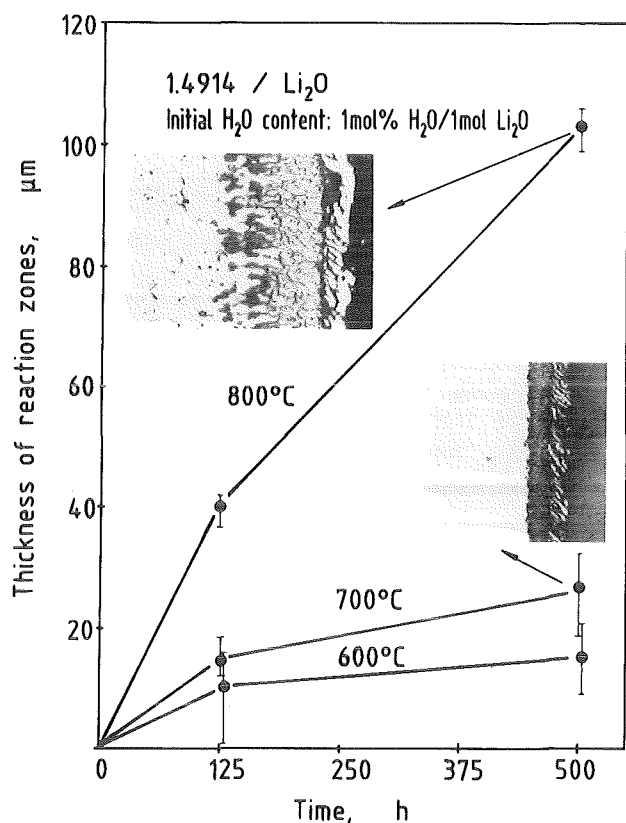
Fig. 20: Reaction zone in ss 1.4914 (11% Cr, martensitic-ferritic) at the interface with Li_2O

The annealing tests have been continued at 800, 900 and 1000°C. For Li_2O and Li_2SiO_3 the results seem to fit the extrapolation of scattering bands from lower test temperatures and also some literature data (on Li_2O). At 1000°C Li_2O in contact with 316 made a reaction depth of about 150 μm after 100 h, while Li_2SiO_3 stayed at 25 μm only. The attack by Li_4SiO_4 was somewhat faster than by Li_2SiO_3, but the difference was considerably smaller than in preceding tests at lower temperatures. Thus it must not be excluded that, under the aspect of cladding compatibility, Li_4SiO_4 could be applicable to similarly high operating temperatures as suggested for Li_2SiO_3 (maximum cladding temperature about 900°C).

To determine the composition of the reaction zones of oxide breeder material with ss 316 and 1.4914, cross sections of the samples are analyzed microanalytically by High Resolution Auger Electron Spectrometry and Scanning Secondary Ion Mass Spectrometry (SIMS). Preliminary results show, that the reaction of Li_2O with steel in presence of 1 mol % H_2O ast 800°C after 500 h (see Fig. 20) led to a ceramic phase consisting mainly of Li, Cr and O. Lithium has been definitely identified by SIMS.

Staff:
Ch. Adelhelm
M. Blumhofer
J. Burbach
W. Dienst
G. Haase
P. Hofmann
K.-H. Kurz
H. Metzger
E. Nold
V. Schauer
G. Schlickeiser
B. Schulz
A. Skokan
H. Strömann
H. Zimmermann

4. Irradiation Testing of Ceramic Breeder Materials (B 15)

The post irradiation examinations of the 45 lithium metasilicate samples columns from the first KfK irradiation DELICE 01 in the OSIRIS reactor have just begun in the hot cells. Start-up difficulties in authorization of sample transport and in the procurement of auxiliary equipment have caused some delay. The irradiation DELICE 02 of 20 sample columns of Li_2SiO_3 and Li_4SiO_4 in the OSIRIS reactor was finished in May, the transport of the samples to KfK is foreseen for autumn 1986.

The two carriers with twelve sample columns each for temperature ranges of 400-450°C and 650-700°C for irradiation in the fast reactor KNK II (B 15.3) are already mounted (For more details see last semi-annual report). For requirements imposed by the operation of the reactor the begin of this irradiation ELIMA 1 will be delayed until early 1987, the irradiation will last about 100 full power days. After this irradiation the experiment ELIMA 2 should immediately follow.

It is intended to perform the two experiments ELIMA 2 in the fast reactor KNK II and DELICE 03 in the thermal reactor OSIRIS, respectively, with identical specimen matrices in order to get a comparison of the influence of different neutron spectra. Both irradiations should lead to a comparable material damage of about 5 dpa caused by fast neutrons and by

	ELIMA 1		DELICE 03		
	Matrix I KNK II 400-450 °C	Matrix II KNK II 650-700 °C	Matrix III OSIRIS 400-450 °C	Matrix IV OSIRIS 650-700 °C	Sum
KfK Karlsruhe	1 Li_2SiO_3 3 Li_4SiO_4 *)	1 Li_2SiO_3 3 Li_4SiO_4	1 Li_2SiO_3 3 Li_4SiO_4	1 Li_2SiO_3 3 Li_4SiO_4	4 12
CEA Saclay	4 $LiAlO_2$ *)	4 $LiAlO_2$	4 $LiAlO_2$	4 $LiAlO_2$	16
UKAEA Springfield	2 Li_2O *) 2 Li_2ZrO_3 *)	2 Li_2O 2 Li_2ZrO_3	2 Li_2O 2 Li_2ZrO_3	2 Li_2O 2 Li_2ZrO_3	8 8
CEN Mol	3 Li_2SiO_3 *)	3 Li_2SiO_3	3 Li_2SiO_3	3 Li_2SiO_3	12
ENEA Casaccia	3 $LiAlO_2$ *)	3 $LiAlO_2$	3 $LiAlO_2$	3 $LiAlO_2$	12
Sum	18 samples *)	18 samples	18 samples	18 samples	72 samples

*) different characterization (density, grain size)

Table 4: Composition of the sample columns for the ELIMA 2/DELICE 02 comparative irradiation

α +t recoil particles and therefore last about 150 FPD. It is foreseen to encapsulate the different ceramic materials fabricated by the involved EC partners according to their individual specifications under the same conditions in the KfK laboratories in stainless steel claddings, thus forming the samples for irradiation. The foreseen loading matrix of the different sample columns in this comparative irradiation is shown in table 4.

Staff:
E. Bojarsky
E. Elbel
H.E. Häfner
H. Werle

5. Tritium Recovery from Ceramic Breeder Materials (B 16)

Some results of the first inpile test LISA 1 /1/ have been discussed in the last report. The main conclusions concerning the lithium silicate samples were:

- Metasilicate, release inconsistent with diffusion for both types of purge gas (He or He + 0.1% H_2)
- Orthosilicate, release very fast and for He + 0.1% H_2 purge gas consistent with diffusion.

In the mean time transient release data of LISA 1 have been evaluated /2/. The results confirm that for He + 0.1% H_2 the release from the orthosilicate sample is consistent with diffusion. On the other hand, out-of-pile annealing of irradiated samples confirm that the release from metasilicate, for both types of purge gases (Ar and Ar + 0.1% H_2), is inconsistent with diffusion.

The next inpile test, LISA 2, will be performed by end of this year. Because of the good results for ortho-silicate in LISA 1, LISA 2 will concentrate on this material (Table 5). Other parameters are chosen to match the requirements of the present KfK blanket design: samples in the form of pellets, lower temperatures down to 350°C. In addition, the effect of adding a small amount (10 ppm) O_2 to the purge gas, will be studied. It is expected that the tritium will be oxidized and therefore tritium permeation will be small.

Specification for LISA 2

Irradiation	Start November 86 Duration 1 or 2 cycles à 20 d)
Purge gas	He + 0.1% H_2, He + 10 ppm O_2
Temperature	350 - 600°C

Publications:

/1/ H. Werle et al., "The LISA 1 Experiment: In-Situ Tritium Release Investigations, Second Int.Conf. Fusion Reactor Materials (ICFRM-2), April 13-17, 1986, Chicago

/2/ R.G. Clemmer, H. Werle, M. Briec, "Evaluation of
     In-Situ Tritium Release Results from the LISA 1
     and TRIO In-Pile Tests", Int. Symp. Fusion Reactor
     Blanket and Fuel Cycle Technology, October 27-29,
     1986, Tokai-mura, Japan

Sample	Material		Sample		TD	
Nr.	Type	Manuf.	Type	Manuf.	(%)	
1	Alu	CEA	Pellets	CEA	78	Ref.
2	Ortho	KfK	Pebbles .5 mm	Schott	98	
3	Ortho	KfK	Pebbles 1.5 mm	Schott	98	
4	Ortho	Ventron	Pebbles .5 mm	Schott	98	
5	Ortho	KfK	Pebbles .5 mm	KfK	?	
6	Ortho	KfK	Pellets	KfK	90	

Table 5: LISA 2 loading scheme

Staff:
R.G. Clemmer
H. Elbel
H.E. Häfner
H. Wedemeyer
H. Werle

M 1   The Large Coil Task (LCT)

The LCT proceeded successfully with the single coil tests, in which the individual coils and its facility related components have demonstrated the readiness for the six coil test. The prehistory of testing is presented in Table 6.

Coil	Single Coil test performed before the test in the six coil array
JAERI (JA)	Domestic, partial array test in the IFSMTF*)
SWISS (CH)	Partial array test IFSMTF, only cryogenic behaviour
GENERAL DYNAMICS (GD)	Partial array test in the IFSMTF*)
GENERAL ELECTRICS (GE)	none
EURATOM (EU)	Domestic test in TOSKA up to 10 kA current
WESTINGHOUSE (WH)	none

*) International Fusion Superconducting
   Magnet Test Facility, ORNL, USA.

Table 6: Testing history of the LCT coils

The test sequence (following the order of Table 6) was started at the end of the last reporting period with the JAERI coil and could finally be successfully finished at the beginning of June with the Westinghouse coil. The results look encouraging. All coils are suitable to be operated in the torus as background or test coil.

Each test run was performed in the following steps
   - Low current checkouts
   - Design current test
   - Dump tests
   - Determination of the operation limits

The two coils cooled by pool boiling (JA, GD) could mainly reproduce their properties measured in tests before. The test of the GE coil demonstrated that all problems with winding shorts by instrumentation leads could successfully be overcome by a burnout technique. A dump from 80% of the rated current confirmed no detectable shorts in the winding.

A main interest of the single coil tests was concentrated on the three forced flow cooled coils

with their advanced technologies. Two coils (CH, EU) could demonstrate due to their rigid conductor and winding design safe operation far beyond the regime of cryogenic stability.

The applicability of Nb_3Sn material in a forced flow cooled conductor for large coils was demonstrated by the Westinghouse single coil test.
The test run of the Euratom LCT coil was performed in only four days. It was the shortest test time needed to run the whole test programme of a coil. This demonstrated excellent handling properties of the Euratom LCT coil.

The Euratom coil could be ramped up to its design current (Table 7) without any sign of instabilities and detectable losses with the fastest ramp rate allowed by the power supply.
The mechanical stresses were lower than in the TOSKA test (Fig. 21). This was expected, because the clamping against the central bucking post avoided the coil to be deformed into a circular shape.

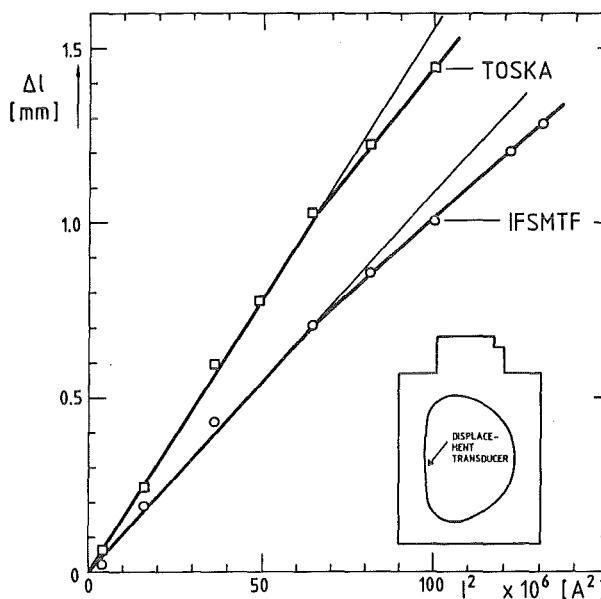Fig. 21: The gap between winding and coil case in TOSKA and IFSMTF-single coil test. The stiffening effect of the central bucking post led to a reduction of the gap

The coil was dumped seven times from currents above 4000 A. This was the highest number of dumps performed with a coil in the single coil test series. The Euratom LCT coil had the lowest losses during dumping and therefore a short recovery time (Table 8).

Cryogenic values		
mass flow, winding	150 g/s	
" ", coil case	50 g/s	
inlet temperature	3.9 K	
inlet pressure	1.24 MPa	
Electrical values	**Design**	**Measured**
rated current	11.4 kA	11.4 kA
fastest ramp rate up to the rated current	3 A/s	4 A/s
no. of ramping-ups to rated current during testing		3
Magnetic field at 11.4 kA		
reference point mid plane	5.55 T	5.56 T
max. field point	6.45 T	6.63 T

Table 7: Operation parameters and key values measured in the design current test

voltage	2.52	kV
time constant	6.79	s
stored energy	103	MJ
total losses	2	MJ
winding	∿ 0.4	MJ
case	∿ 1.6	MJ
recovery time	80	minutes
case temperature	17.5	K
winding temperature	6.4	K
state of the winding during dumping	superconducting	

Table 8: Some values characterizing the dump properties at rated current

The pressure rise and the absolute pressure level was moderate. Investigation of them under boundary conditions given by the IFSMTF, are shown in Fig. 22. It could be confirmed as already demonstrated in TOSKA that the coil could be dumped from rated current without losses of Helium gas, if a cold buffer volume is available.

Two dumps were triggered by a normal zone initiated by current sharing measurements described later. After the normal zone grew up to the length of about a half

turn the resistive voltage reached the 50 mV setting level of quench detector which then dumped the coil automatically. These tests were also a confirmation of the faultless operation of the quench detection system which was specially designed for the coil.

CURRENT [A]	dp/dt [kPa/s]	PROTECTION VALVE POSITION	QUENCH
● 8030	87	INLET a. OUTLET CLOSED	YES
▲ 6300	56	INLET a. OUTLET CLOSED	YES
□ 11400	132	INLET a. OUTLET CLOSED	NO
○ 8474	104	INLET OP., OUTLET CLOSED	NO
△ 5600	42	INLET OP., OUTLET CLOSED	NO
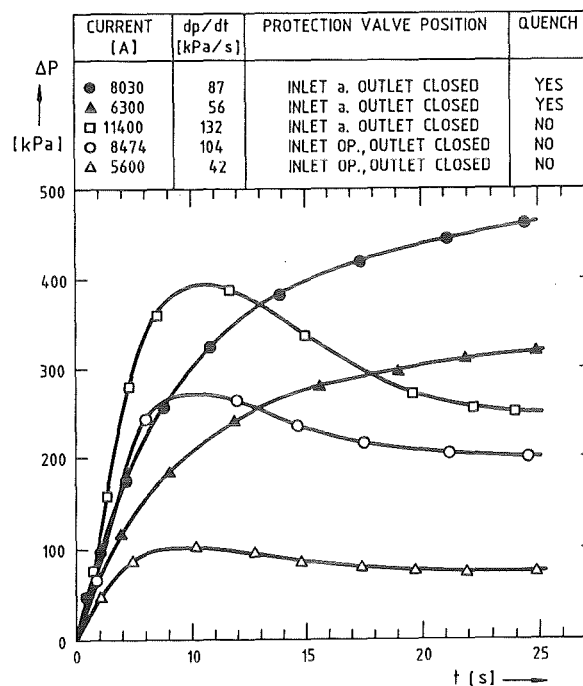
Fig. 22: Pressure increase for the Euratom LCT-coil during dumping under different conditions (position of the protection valves, quench)

In the TOSKA test it was shown that the coil had a low disturbance energy level and can work near its current sharing temperature. In order to determine the operation limits more accurate a gaseous helium slug was heated at the exspected current sharing temperature and injected in the cooling path over some seconds. This was performed in quarters of the current square of the rated current. A current sharing voltage of several hundred μV was observed (Fig. 23). Some verification tests indicated that an increase in current at constant heater pulse temperature and an increase in temperature at constant current lead to a quench. From short sample measurements of the single strands and upscaling to the cable an I_c/T_c-diagram was derived in which the local lines of max. and min. field of the heated pancake determined the current sharing temperature. The measured values are in fair agreement with the expected values (Fig. 24). It was demonstrated that with this method the operation limits of the coil could be predicted.
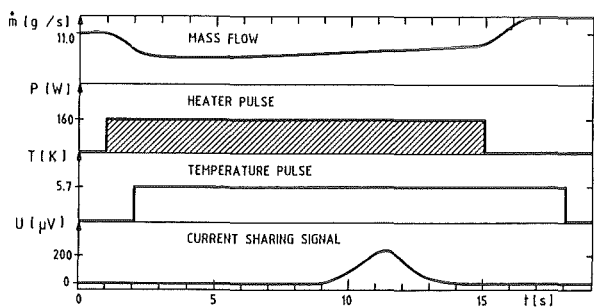
Fig. 23: Time relation between heater pulse, massflow,
temperature and current sharing signal
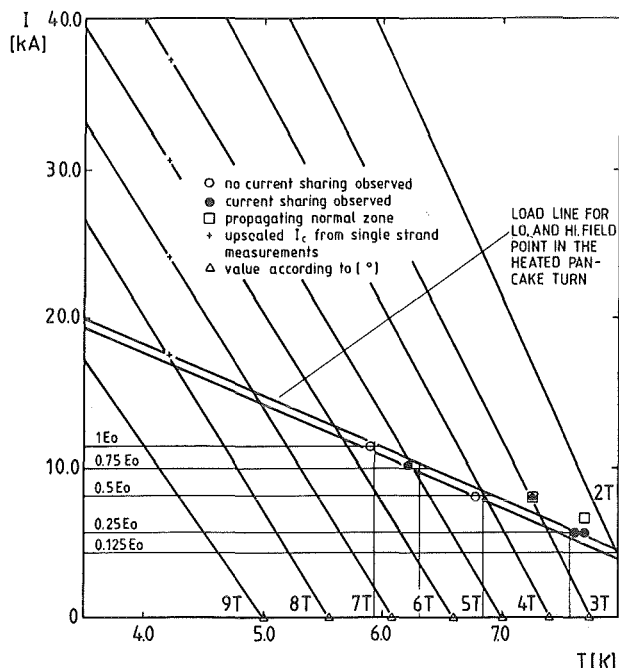
Fig. 24: Load line of the heated pancake in the I_c-T_c
diagramm derived from single strang
measurements up-scaled to the cable.
(see H. Brechna, Supercond. Magnet Systems
Springer Verlag, Berlin, 1973)

The same testing method was also successfully applied
to the Westinghouse coil with good results.

Immediately after the single coil test programme
multicoil tests were started. The main purpose of
these tests was the balancing of the quench detection
system and adjustment of the power supplies for the
six coil operation. Balancing of the quench detectors
in a way that a quench in a single coil did not affect
the neighbouring coils, failed. As a consequence, for
future tests, in case of a quench in a single coil,
the energy of the whole torus has to be dumped. Helium

losses, heavy charging of the cryogenic equipment and
long recovery times of the system are potential
consequences of such an event which is assumed to be
of low probability.

In August, the first run of standard I tests was
successfully performed. In this kind of tests, 5 coils
are operated at 80% of nominal current to form the
background field for the sixth coil, which is run up
to nominal current and submitted to extensive
measurements. Each coil will successively be put into
the full current position. In a later series of tests,
called "Standard II", a pulsed field component will be
added to the coil of the respective test coil.

Staff:
G. Friesinger
G. Nöther
L. Siewerdt
A. Ulbricht
F. Wüchner
G. Zahn

M 3 Development of Composite High Field Super-conductors

Neutron Irradiation of Nb₃Sn Wires

In the last years, the optimization of Nb_3Sn wires has led to the alloying of elements like Ti and Ta, which are substituted in the A15 phase and cause an enhancement of the critical current at magnetic fields above 11 T. In order to decide whether alloyed Nb_3Sn wires would also be useful for fusion applications, different binary and alloyed Nb_3Sn wires were exposed to neutron irradiation. The available condition at the Lawrence Livermore Laboratory did not precisely correspond to the real conditions in a fusion environment, but allow nevertheless to draw some important conclusions.

The irradiation were carried out at the RTNL neutron source, with neutrons of 14.8 MeV, the irradiation temperature being 25°C. Five wires were analyzed, 2 binary ones with 19 cores and 10.000 cores and 3 alloyed ones with 1.6 % Ti, 7.5 Ta and 0.6 % Ni / 3 % Zn, respectively. The decrease of T_c with fluence, shown in Fig. 25, shows that alloyed wires exhibit a larger decrease of T_c with dosis. At a dose of 3 x 10^{18} n/cm², the highest dose attained in the present experiments, the change of critical temperature ΔT_c was 2.5 K for binary and 3.2 K for alloyed wires. This surprising effect, which was detected for the first time, shows that radiation induced disordering on the A15 lattice sites occurs in a different way when a small quantity of alloying elements, $\lesssim$ 3 at%, are added to Nb_3Sn. It is at present not sure whether the disordering mechanism by focusing replacement collision sequences is really affected by the additions or if the latter have a particular influence on the electronic density of the states of the super-conductor.

The behavior of the critical current density I_c in binary and alloyed wires is very different, as shown in Fig. 26 and 27, where I_c/I_{co} and B_{c2}^* are plotted vs. fluence for binary and alloyed Nb_3Sn wires, respectively.
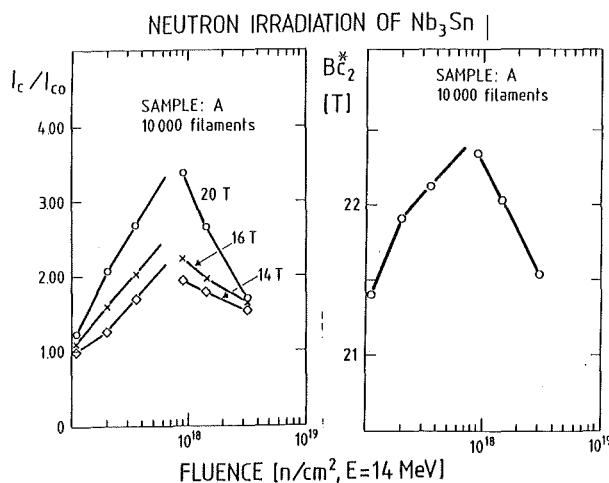
Fig. 26: I_c/I_{co} and B_{c2}^* for a binary Nb_3Sn wire after neutron irradiation at 25°C

Fig. 25: T_c, vs. φ_t for several binary and alloyed Nb_2Sn wires after 14.8 MeV neutron irradiation at 25°C.
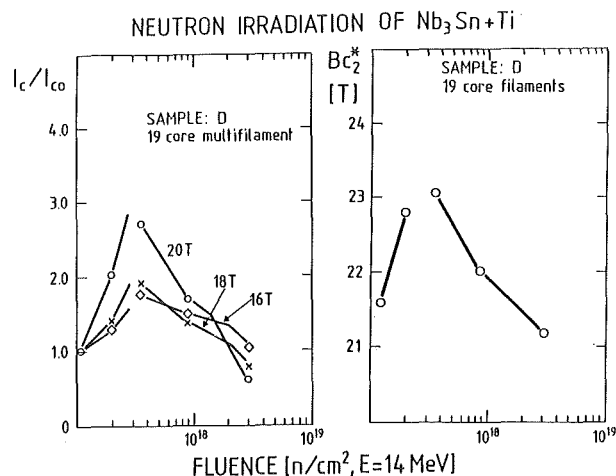
Fig. 27 : I_c/I_{co} and B_{c2}^* of a Ti alloyed Nb_3Sn wire after neutron irradiation at 25°C

The most evident differences between neutron irradiated binary and alloyed Nb_3Sn wires are:

a) The dose rate where I_c/I_{co} peaks is four times higher for the binary Nb_3Sn wires compared to the ternary alloyed $Nb_3Sn + Ti$. The same effect is observed for Ta and Ni+Zn additives and seems thus to be a general property of alloyed Nb_3Sn wires.

b) The enhancement of I_c/I_{co} at comparable b* values is smaller than for the binary wire (b*=B/B$_{c2}^*$). At b* $\simeq$ 0.7, I_c/I_{co} for the Ti and Ta alloyed wires is $\sim$ 3 and 1.2, respectively, compared with $\sim$ 2.2 for the binary 1000 core wire.

c) At a fluence of $\varphi_t = 3 \times 10^{18}$ n/cm^2, I_c/I_{co} for the binary wire at all magnetic fields is higher than before the irradiation, in contrast to the alloyed wires where at this dosis level the ratio I_c/I_{co} is always smaller.

The above findings have a common origin:
the enhancement of ρ_0 after irradiation is <u>smaller for the alloyed wire</u> than for the binary one, due to the higher initial value of the latter.

The presently discussed ordering effect is without any doubt of most importance for applications: <u>NET fusion magnets producing fields of $\sim$12 T will be wound with binary Nb_3Sn multifilamentary wires</u>, even if alloyed Nb_3Sn wires exhibit higher critical current densities.

<u>Staff:</u>
W. Barth
M. Beckenbach
M. Brünner
P. Duelli
U. Fath
<u>R. Flükiger</u>
S. Förster
F. Gauland
S. Gauss
W. Goldacker
A. Kling
B. Lott
G. Nöther
A. Nyilas
H. Orschulko
H. Raber
T. Schneider
W. Specking
S. Stumpf
<u>P. Turowski</u>

M 4   Superconducting Poloidal Field Coil Development

Introduction

The task aims at the development and test of all necessary components to build and operate a superconducting poloidal field coil in the real tokamak environment of TORE SUPRA in 1990. The development shall be relevant for NET.

In order to test the components under TORE SUPRA load conditions, a model coil of 3 m diameter is under design to be operated in the KfK-TOSKA test facility 1987/88.

Model Coil Design

It has been decided to use two different types of cable in the model coil. Two double pancakes will be made with an insulated subcable and two more with a CuNi strip wrapped around the subcables.

The insulated subcable does not allow the internal current transfer from subcable to subcable. If one subcable goes normal, the whole cable is expected to quench. Equal current sharing among subcables is therefore essential during operation.

The CuNi wrapped subcable allows for internal current transfer but has higher losses in a.c.-fields. The cable might go normal in a rapid discharge of the coil.

All other design features are the same for the two types of cable.

A call for tender for the model coil has been placed to European industry followed by detailed discussions with four interested firms. The final order is under preparation.

Conductor Development

First industry made cable samples were produced by two industrial companies. The cabling procedure is now established. The laser welding of the outer section has been performed with a lot of detailed metallurgical inspection of the weld. The welding temperature on the protection tube does not exceed 400°C.

Beam sharing technology is under development for the simultaneous weld of two seams.

The outer steel casing will now be fabricated from 4 sections (see. Fig. 28). Shear strength measurements
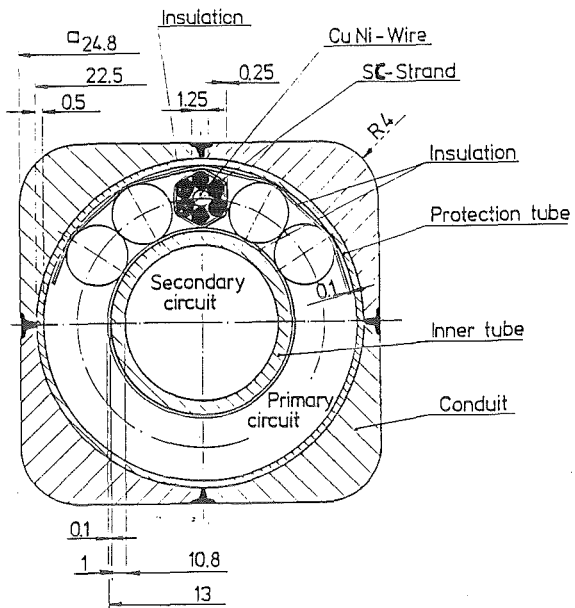
Fig. 28: Superconducting cable for the poloidal field coil

at 77 K of the insulation system gave values as high as reached by soldering ($\sim$ 27 MPa with lap joint samples).

A.C.-Loss Measurements

On laboratory made cable samples with CuNi tape the contact resistance between subcables was measured as function of the degree of cable compression by the outer protection tube. From this contact resistance the losses of the cable in magnetic field pulses are estimated.

Stability of Single Wires

The stability of different wires from VAC, Hanau, Alstom, Belfort and, Autokumpu, Pori has been measured. The wire diameters were 1 mm and 1.25 mm, respectively, with filament diameters between 6 and 12 µm.

The measurements were done in bath conditions, in supercritical He and in liquid He under closed volume conditions. The aim was to evaluate the influence of the different cooling conditions on stability. The results have still to be analyzed. In general all wires were stable against pulse rates up to several hundred T/s.

Reception Tests of Wires

Tests have been performed on the cable samples fabricated by industry to measure the coupling loss time constant τ, the rest resistivity ratio (RRR), and the critical current I_c. For the wire chosen and ordered for the model coil, $\tau = 0.2$ ms; RRR = 170 and $I_c = 310$ A (5 T, 4.2 K) were obtained with a wire diameter of 125 mm and 1632 filaments of 10 µm diameter.

The results show fairly high resistances so that this cable has its potential not only for NET but even for the higher requirements of TORE SUPRA. Test results in the model coil test and cost comparison will give the means to decide which cable should be used in future applications.

Stability of subcable connections against field pulses current up to 2400A could be induced in one subcable loop using the transformer principle. The loop was closed by soldering the subcable ends. The stability of the soldered connection was then measured in a pulsed dipole field which was originated by a capacitor discharge.

A field amplitude of 0.34 T and a pulse length of T/2 = 10 ms (half cycle of a sinosoidal pulse) did not quench the subcable.

An additional shielding copper cylinder surrounding the subcable connection reduced the pulsed field component inside by a factor 50 - 100. With this shielding cylinder added, the subcable connection therefore will not give rise to problems in the model coil operation from the pulsed field point of view.

The resistance of the soldered connection was measured to be about 30 nΩ. The cable connection thus has losses below 1.5 W at 24 kA conductor current. The measurements will be continued comparing different connecting techniques.

2-Phase Flow Experiment in the TOSKA Facility

After the first experiments mainly with stationary adiabatic and nonadiabatic two-phase flow for investigation of pressure drop a second test run with additional instrumentation was made.

A specially developed measuring cell for measuring the vapor content was installed. This cell was developed together with the University of Bochum.

Furthermore, a tubular heating section equipped with 4 thermometers at the circumference was installed. The purpose of this section is to measure temperature differences around the circumference to check the wetting of the wall or the flow pattern, respectively. This test section was made by CEA, France.

The object of the experiments is to find out at what minimum mass flow a safe operation with a pulsed heat load is possible. The pulsed heat load simulates the AC-losses in the conductor. A typical picture of the pulsed operation and the subsequent temperature and mass flow changes shown in Fig. 29.
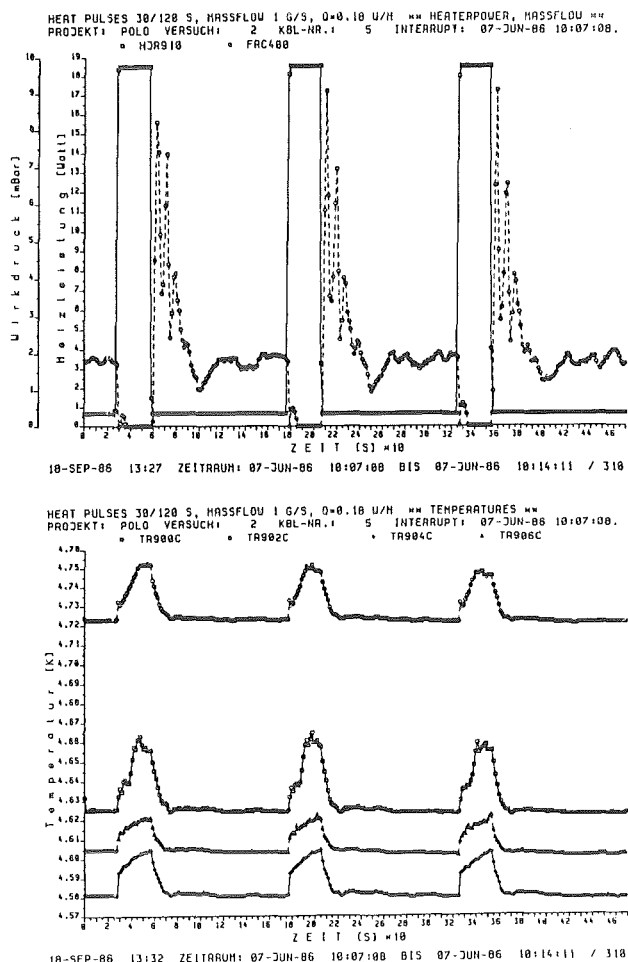
Fig. 29: Temperature and pressure drop after heat pulses in the two phase cooling pipe

Due to the small overall pressure drop there is a considerable change in mass flow during a heat pulse. Therefore it seems necessary to use a pump in order to provide a stable mass flow.

The experiments will be continued with the installation of two glass viewing sections in order to gain optical insight into the flow pattern, heat transfer and mass flow during pulsed operation using video recording equipments.

Diagnostics

The electrical signals of the temperature and quench diagnostics have to be separated from the high voltage potential before being transferred to the data acquisition system.

Special insulated amplifiers are under development using fibre optics to transfer the measuring signals from high voltage potential to earth potential. Several components have already been tested in the high voltage laboratory.

Modifications and extensions of the data acquisition system of the TOSKA facility to handle the large number of transient data during the model coil test have started.

Staff:

H. Bayer
F. Beckenbach
F. Becker
I. Donner
P. Duelli
S. Förster
G. Friesinger
P. Gruber
J. Harneit
W. Heep
U. Jeske
H. Katheder
P. Komarek
W. Lehmann
J. Lühning
G. Nöther
A. Nyilas
U. Padligur
H. Raber
K. Rietzschel
L. Schappals
G. Schenk
C. Schmidt
K. Schweickert
E. Specht
H.-J. Spiegel
F. Süß
M. Süßer
A. Ulbricht
R. Wagner
D. Weigert
F. Wüchner
G. Würz

M 8   Design and Construction of a Poloidal Field
Coil for TORE SUPRA as NET-Prototype Coil

1. Requirements

The objective of the task is the development and test
of an External Field Coil (EF Coil) with parameters
relevant for NET. The reliable operation of a super-
conducting PF-coil shall be demonstrated in a real
tokamak environment with the rapid field variations
due to start up, plasma position control and
disruptions. The development has to confirm the coil
construction process proposed for NET on a fairly
large scale.

For this purpose, the upper ring coil "E_h" of TORE
SUPRA will be replaced by a superconducting coil "ES".
Design and construction will be based on the results
of the already running task M 4.

In Table 9, a comparison of some important parameters
is given for TORE SUPRA, the model coil (task M 4),
NET and for Asdex-Upgrade as alternative device.

NET requires a high induction at the PF conductors of
5 - 6 T compared with the 1.75 T of Tore Supra.
The cable used for the "ES" coil to be inserted in
TORE SUPRA will therefore have the full NET induction

	Tore Supra Coil "E" (copper)	Coil "ES" (sup.cond)	Model Coil	NET (all coils)	Asdex-Upgrade Coil V1 (copper)
Geometry					
mean Radius R_m [m]	3.77	3.91	1.5	4.2-11.2	1.62
cross section of the winding [m²]	0.38 x 0.27	0.33 x 0.22	0.22 x 0.19	0.5x0.5- 1.x0.6	0.36x0.79
electrical data					
max. operation current [kA]	8.8	12	15	40	44
crit. current [kA]	(4.2K)		26(2.75T)	60(6T)	60(3,5T)
number of turns	60-120	96	56	100-450	93
number of panc.		12	8		
start up voltage [kV]	20	20	-	23	1.7
control voltage [kV]	3	·3	-	?	-
discharge cleaning [kV]	23	23	23·	?	?
discharge voltage [kV]	-	3	23	?	?
magnetic data					
inductance (air) [H]*		0.16	0.018	0.18-1.	0.034
stored energy of the single coil (air) [MJ]	*	11.5	2	6700(all coils)	32.9
induction at superconductor [T]		1.75	1.6	5-6	3.5
Ḃ [T/s]					
- start up		1.75	-	3 (max)	≅ 3
- discharge		-	150	-	
- disruption		80	-	(10?)	12
- disruption simulation	-	-	80	-	-
Position control during flat top					
- B_m = 2·ΔB [T]	0.048	0.048	0.08 (one double panc.)	(-1%·B_{max})	< 1% B_{max}
- frequency [Hz]	10	10	10	(~1?)	20

* values depending on turn number and flux.

Table 9: Comparison of the model coil
        Parameter of Tore Supra, Model Coil, Asdex-Upgrade and NET

capability.

2. Design of the TORE SUPRA Coil "ES"

2.1 Components for Coil "ES"

The major components, which have to be developed and fabricated are:

- Coil winding and impregnation using an internally cooled superconducting cable. The cable is the same as developed now for the model coil in task M 4.
- Coil vacuum vessel and radiation shield (80 K) with low time constant against pulsed magnetic fields ($\tau \lesssim 5$ ms).
- Current leads for 12 kA, 23 kV using the experience of the developments done so far at KfK and CEA (KfK is aiming at a current lead development for 40 kA, 23 kV).
- Mechanical support structure to bear the forces acting on the coil under normal load and fault conditions.
- Cryogenic supply system (preferably to be fitted into the existing TORE SUPRA cryogenic system).
- Coil diagnostics and protection.

2.2 Predesign of the Coil

In the reporting period predesign of the winding and pancake connection area of coil "ES" was terminated. The design is based on the same principles as for the model coil (task M 4).

During a workshop in March 1986, a first design of the mechanical supports and the vacuum casing was discussed. The design was based on 12 equidistant supports between winding and coil case in order to lower the shear strength in the winding pack. The casing itself is connected to the six legs of the iron yoke. As a consequence, the vacuum casing had to carry part of the load and therefore was relatively strong. So it was difficult to find a solution for the electrical separation of the vessel sections in order to minimize the eddy currents. During the discussion it was agreed to try to have a design with only 6 supports between winding and iron yoke. The coil supports allow for a radical thermal shrinkage of 11 mm and take up any eccentric force. The axial force on a support amounts to 35 metric tons, both tension and compression. The vacuum casing thus can be much less stiff and can easier be separated into 6 insulated sectors with time constants ≤ 5 ms, as compared to the previous design.

From the available shear strength data of present coil impregnations for Tokamak applications it was concluded, that it should be possible to reach the necessary shear strength of 10 MPa in the glass fiber/Kapton/epoxy insulation of the winding pack.

The revised design was again discussed in a workshop in August and will now be investigated in more detail.

The calculations of the eddy currents in the vacuum vessel and the associated forces during plasma disruption and burn control have been started in cooperation with the University of Graz.

3. Current Leads

3.1 Design for the Model Coil

For the test of the model coil a design was started for a 24 kA lead which should be used to test the model coil. The idea is to have a modular design which later could be upgraded to higher currents of 40-50 kA.

We tried to use parts which can be easily manufactured in our workshop therefore avoiding the need for special equipment. A first module which should be capable of 4 kA is now in progress. This module will be tested in one of our existing bath cryostats.

3.2 Design for the ES-Coil

For the ES-coil a special upgraded design of the TORE-SUPRA leads is made by CEA/France. This design will also be tested at KfK. Because of the special tooling needed for the fabrication any further upgrading to currents higher than 12 kA seems to be more difficult and to be to expensive, too.

Staff:
F. Beckenbach
S. Förster
G. Friesinger
U. Jeske
H. Katheder
P. Komarek
A. Nyilas
L. Schappals
G. Schenk
C. Schmidt
H.J. Spiegel
A. Ulbricht

M 9   Structural Materials Fatigue Characterization
        at 4 K

Joining of Structural Materials

The coil supports of NET require deep welds of steel
casings. The task aims at obtaining information on the
fatigue behaviour of welded steel at low temperature
and on inspection procedures.

The required materials for the development of the weld
process were ordered after the reception of the
tender. Delivery of the materials is expected by mid
of October 86. The materials chosen are 1.4429
($\sim$ 316 LN), 1.4436 ($\sim$ 316 L) and 1.4306 ($\sim$ 304 L). The
ordered quantity for each material is 5000 mm x
1500 mmx 30 mm. Supply of low sulphur (< 0.003%), low
carbon (< 0.02%) and low phosphorus (< 0.04%) were
guaranteed by the steel plant for the material 1.4306.
For the other two materials (1.4429 and 1.435) the
delivery of standard composition was proposed because
of metallurgical difficulties in case of carbon and
sulphur refinement due to the alloyed molybdenum. A
decrease of the sulphur and carbon in the alloy is
possible only for a heat in a large crucible, which
means the delivery of a quantity above 30 tons.

Filler material for the welds were determined. The
Material 1.4455 alloyed with nitrogen and manganese
will be used for all three types of stainless steels.
A call for tender for a supply of wire materials has
been recently done by the institution "Schweißtechni-
sche Lehr- und Versuchsanstalt, Duisburg" (SLV). The
same wire will be ordered from four different manu-
facturers to receive results considering the optimum
combination of plate material with wire.

The design of the flow cryostat which will be used as
mechanical test chamber was completed. Delivery from
the manufacturer is scheduled for February 87. The
design of the neccessary load frame and the machine
adaptation works are also completed, so that
immediately after receiving the cryostat preliminary
tests can be started.

Staff:
G. Hohnburger
H.P. Raber
S. Fischer
A. Nyilas

M 12   Low Electrical Conductivity Structures
Development

Low electrical conductivity is of importance for a number of NET coils being exposed to low temperature and variable magnetic fields. Within task M 12, compatibility of high strength electrical insulator materials and construction elements with the above requirements shall be examined.

Joining of Fibre Reinforced Plate Materials

Experiments have been carried out with glass fibre reinforced plastic (GFRP) to test the behaviour of joints between parts of plate material. Measurements of loss of the torque moment for a joint (metallic bolt/GFRP-plate) during cool down from ambient temperature to 77 K showed tightening of the joint. At ambient temperature the necessary load to open the bolt was found to be 80% of the initial tightening load. At 77 K the load to open was measured to be nearly equal to the value of the former thightening load at ambient temperature. This can be explained by different thermal expansion of the two materials stainless steel and GFRP.

Fig. 30: Loss of stiffness test of a glass fibre reinforced plastic section at ambient temperature

Loss of stiffness tests have been carried out with a U-type GFRP section, which simulates a corner section of a magnet casing. Section dimensions in mm were 183 x 380 x 183 at a length of 110 mm. No significant loss of section stiffness during cool down was obtained when the section had been assembled with 40 mm thick GFRP materials and stainless steel bolts. Fig. 30 shows the assembled section under test at ambient temperature. The load-displacement (at loading line) record could be obtained with specially built and calibrated clip gauges. The test at 77 K showed a similar loading behaviour as compared to the experiment at ambient temperature.

High Performance Fibre Materials

No European manufacturer could be found to produce GFRP-plates with R-glass fabrics. Different types of hybrid plate materials were ordered. The combination of materials includes glass, carbon and aramid fibres. The plates are 4 mm thick and suitable for strength, flexural and shear testing.

Staff:
G. Hohnburger
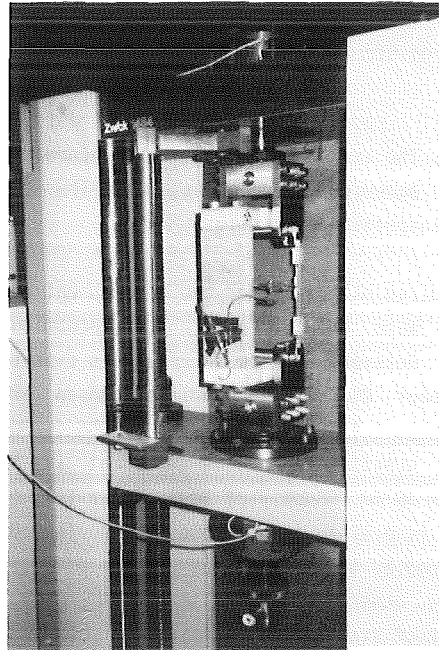J.P. Raber
S. Fischer
A. Nyilas

MAT 1.6   Development and Qualification of Type 1.4914
           Base Metal Properties

A fully martensitic steel (German denomination 1.4914) has been selected as a possible first wall and structural material for the Next European Torus.

After the procurement of the NET-heat (Nr. 53645) of reference material, the composition of which is given in Tab. 10, semifinished rods and plates with dimensions requested by the different EC laboratories have been manufactured. Most of the EC labs and industrial partners associated with the research programme on Type 1.4914 material have in the meantime been supplied with material.

1.4914 (Heat 53645)	
C	0.13
Cr	10.6
Ni	0.87
Mo	0.77
V	0.22
Nb	0.16
Si	0.37
Mn	0.82
S	0.004
P	0.005
B	0.0085
N	0.020
Other Components	Al 0.054
	Co 0.01
	Cu 0.015
	Zr 0.053

Table 10: Chemical composition of the NET-heat
          Type 1.4914 (wt.%)

In order to recommend a final heat treatment for this fully martensitic steel, investigations have been started in which the influence of austenitizing temperature (varied between 1050 and 1175°C) and the follow-on tempering treatment (680-780°C) on micro-structure and toughness are studied. Especially δ-ferrite formation, prior austenite grain size and structural homogeneity are investigated. The first preliminary results indicate that, in addition to the above parameters, also the fabrication steps for the production of plates with variable thickness between 1

and 20 mm, influence the microstructure and δ-ferrite formation.

For the material in all dimensions the following heat-treatment 950-980°C/2h + 1075°C/30min + 750°C/2h produces a homogenized, fully martensitic and δ-ferrite free structure (Fig. 31). Therefore this heat

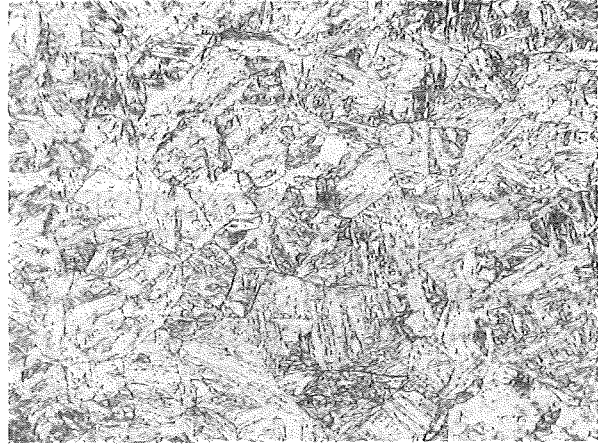

Fig. 31: The structure of 1.4914 steel after the
         preliminary reference heat-treatment

treatment should be used in further experimental in-vestigations as a preliminary reference heat-treat-ment.

Staff:
B. Dafferner
C. Wassilew

MAT 1.9   Pre- and Post-Irradiation Properties of
          1.4914 Martensitic Steel

It is the main objective of the present task to
investigate the influence of thermal cycling upon the
lifetime of first wall materials. As described in the
previous report a typical thermal loading procedure is
suggested and its influence upon lifetime is
investigated by means of two methods.

1. Mechanical Loading Equivalent

Assuming a homogeneous temperature distribution, a
mechanical loading cycle (i.e. stress/strain cycle)
equivalent to the suggested thermal loading cycle is
calculated. The latter is applied to solid (SGRIM) and
to hollow cylindrical test specimens (HGRIM), at
different constant temperatures, respectively (HGRIM
specimens are used for in beam investigations). These
tests reveal whether the mean strain (i.e. tensile,
compressive or zero) influences the number of cycles
to failure. Because the first specimen of the
martensitic steel 1.4914 was not available until
September 86, preliminary tests were conducted on SGRM
specimens from stainless steel type AISI 316 L (Ispra-
heat). In accordance with previous results obtained on
SS AISI 304 no influence was observed of the mean
strain upon lifetime at the test temperature of 650°C.
Results on AISI 304 have shown that this independency
is assured also for lower test temperatures.

There is a considerable delay in the preparation of
the SGRIM specimens from 1.4914. The only specimen
available at present was used to check whether HGRIM
specimens can be prepared by the same technique as
developed for AISI 316 L. Obviously, the prerequisite
heat treatment during manufacturing affects the
dimensional stability of the martensitic HGRIM
specimens. Preliminary tests conducted with the
specimen mentioned above indicate that under
comparable conditions the cyclic deformation behaviour
of the materials examined is different. Especially the
number of cycles to failure for 1.4914 is
substantially less than for AISI 316 L. Within
approximately 8 weeks martensitic test specimens SGRIM
will be available to start with systematic
examinations.

2. Thermal Loading (Thermal Fatigue)

In reality the temperature distribution in the first
wall will be non-homogeneous. Accordingly, stress
gradients will be generated which may lead to crack
formation and/or lead to growth of existing cracks. In
order to study the influence of temperature gradients
upon lifetime, as already reported, a method was
developed by means of which the HGRIM specimens are
heated ohmically so that within certain limits the
radial temperature gradient as well as the heating-
and cooling rate resp. can be controlled by an axial
gas flow. First experiments conducted on AISI 316 L
"free-ends specimens", in which the temperature in the
narrowest cross section was cycled between 550°C and
250°C, did not reveal any crack formation after 20000
cycles (this corresponds to several weeks of test
time). Calculations show that the stresses generated
in the "free-ends specimens" are too low to yield
fatigue damage. Therefore experiments are on the way
in which the same thermal loading is applied to
"fixed-ends specimens". Due to the expected very long
test times it is necessary to develop automatic test
rigs in order to increase the efficiency. Tests on
1.4914 will start as soon as specimens will be
available. Several methods for crack detection were
considered. Because in the above epxeriments the
fatigue damage was too weak to be revealed by current
metallography, the inspection of the specimens surface
was done by scanning electron microscopy (SEM). For
damage scales of interest, i.e. crack length of the
order of 0.1 mm, a mechanical device, in the past
successfully applied in quality control of cladding
tubes, seems appropriate for the present need.

Staff:
N. Baumgärtner
M. Bocek
C. Petersen
D. Rodrian
W. Scheibe
R. Schmitt
H. Schneider
W. Schweiger

MAT 1.11 Post Irradiation Fracture Toughness of Type
            1.4914 Martensitic Steel

It is foreseen to study the influence of fission
neutron irradiations on the impact properties of
1.4914 material. Emphasis is given to the problem of
DBT-temperature shift and to an eventual change of
impact energy as a function of irradiation temperature
and neutron fluence. In addition radiation hardening
and post-irradiation annealing behaviour will be
studied by tensile and hardness tests.

During the time period given above around 90
miniaturized Charpy-V-samples have been prepared for
the common JRC-ECN-KfK irradiation SIENA-E 198-14, in
which the temperature is varied between 250 and 475°C
and a fluence level between 3 and 32 dpa will be
covered. Samples with the preliminary reference heat
treatment (950-980°C/2h + 1075°C/30min + 750°C/2h) and
other heat treatments, in which the tempering
temperature has been varied between 600 and 750°C,
will be put in this experiment together with samples
taken in different orientations (LT, TL) to the
rolling direction of the ingot material. In addition,
tensile samples in the reference conditions have been
manufactured and will also be loaded into the
irradiation rig. The irradiation will start by the end
of 1986 in HFR.

Staff:
B. Dafferner
K. Ehrlich
C. Wassilew

MAT 2.2   In-Pile Creep-Fatigue Testing of Type 316
          and 1.4914 Steels

It is intended to study the in-reactor deformation and
the fracture behaviour of the two candidate structural
materials for NET with load cycling under tension.
The irradiation will take place in the central
position of the KNK II-reactor. Each irradiation rig
will consist of eight pressurized tube samples which
can individually be loaded by an internal gas
pressure. The rigs will be temperature controlled.

The external parameters for these tests have been
specified. Sample temperatures will be constant
between 400 and 550°C, dependent on the reactor
position. The inner pressure is variable between 100
and 450 bar, which corresponds for the given geometry
of tubes to a maximum tangential stress of 400 MPa.

The preparation work for this epxeriment has been
continued. The beginning of the irradiation is
scheduled for 1987.

Staff:
K. Ehrlich
L. Schmidt

MAT 6/MAT 13 Ceramics for First Wall Protection
and for rf Windows

SiC qualities of industrial manufacturers are to be tested concerning the durability of tiles to protect the first wall against plasma instabilities and disruptions. Insulator materials (like Al_2O_3, $MgAl_2O_4$, AlN) are to be selected with regard to their resistance to thermal crack formation by dielectric loss in rf-windows. These windows shall be applied to separate wave guides for ECR heating from the plasma vacuum.

Common KfK-CEA irradiation experiments with test specimens of the above-mentioned materials were started in OSIRIS-Saclay (April 1986, only insulator materials) and HFR-Petten (July 1986). The specimen temperatures are about 550°C in OSIRIS, 400°C and 1200°C in HFR. The fast neutron fluences will amount to about 1×10^{22} n/cm^2. An additional common HFR experiment with SiC and graphite specimens (the latter from CEA and KFA) will be prepared, which is to run at higher temperatures (800 - 900°C and 1500°C), but to a lower neutron fluence of about 3×10^{21} n/cm^2.

Measurements of material properties were continued in order to characterize the sample materials and to prepare for the evaluation of irradiation experiments. In addition to previous measurements, the thermal diffusivity of CVD-SiC was determined. The results together with the data on HIP-SiC are presented in Fig. 32. The thermal diffusivity of single crystal α-Al_2O_3 ($\perp$ to c-axis) has been measured and is shown in Fig. 33.

Fig. 33: Thermal diffusivity of α-Al_2O_3-single crystal ($\perp$ to c-axis)

Special effort was devoted to examining the thermal shock resistance of the materials investigated. The difference of critical temperature for thermal crack formation was measured by dipping cylindrical pellets of 13 mm diameter into molten metal of variable temperature. Fig. 34 shows the results. SiC, AlN, and

Fig. 32: Thermal diffusivity of HIP-SiC (above, up to 1450°C) and CVD-SiC (below)

Fig. 34: Thermal shock resistance of the ceramic materials investigated
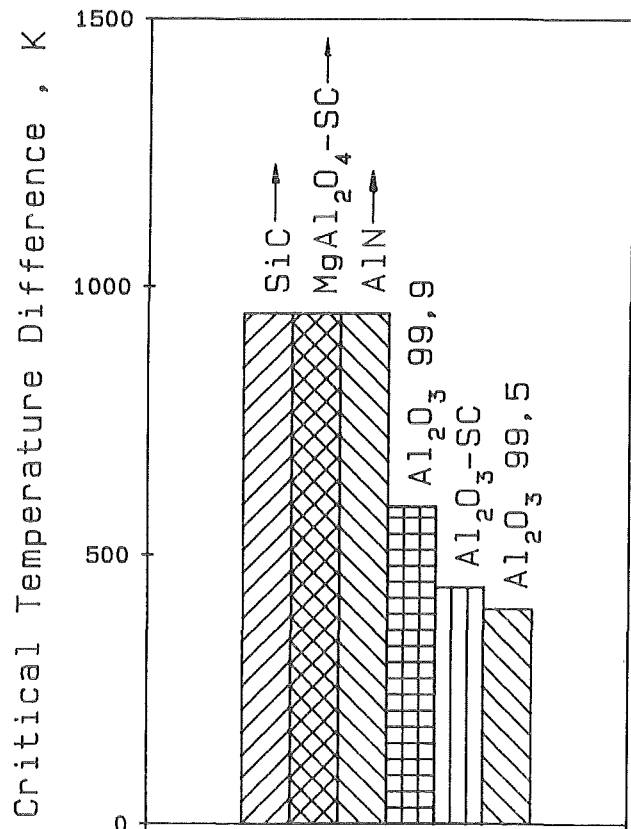
$MgAl_2O_4$-single crystal did not fail even at the maximum temperature difference of 950 K, which appears rather surprising for the Mg-Al spinel and has still to be analyzed in this respect. Some relevant material properties taken from the literature or resulting from KfK measurements are given in Table 11.

Material	α 20-1000°C 10^{-6}/K	k R.T. W/mK	E GPa	$\sigma_{f,b}$ MPa
Al_2O_3 S.C.	$\sim$P.C.	$\sim$40	350-470	450-690
dto KfK			330-420	355
97-99.5	7.7-8.6	22-32	330-380	280-400
KfK 99.5		32	370	205
KfK 99.9		30	380	300
$MgAl_2O_4$	7.6	25	180	130-280
AlN	5.4	100-140	300	250-450
dto KfK		77	310	270

Table 11: Properties of ceramic insulator materials, relevant to thermal crack formation

Concerning the measurement of dielectric loss at very high frequencies, an open microwave resonator (Fabry-Perot) has been used at 35 GHz to make a rough classification of the insulator materials investigated: Al_2O_3 single crystal showed the lowest level of loss tangent, comparable to $MgAl_2O_4$ single crystal, while the other polycristalline materials tended to higher values in the sequence of Al_2O_3 99.5, Al_2O_3 99.9, AlN-HIP. The dielectric loss of the isostatically hot-pressed AlN turned out to be too high to use the potential advantage of its good thermal conductivity, probably because of the considerable impurity of this material. But in the meantime a purer, sintered AlN quality appeared more able to compete.

Up to now, the _absolute_ accuracy of these 35 GHz measurements is questionable. Therefore measurements at lower frequencies have also to be considered. Results obtained from Q-meter measurements at 30 MHz are given in Table 12. Concerning the loss tangent of the oxide materials investigated, the same sequence resulted as mentioned for the 35 GHz measurements. The surprising performance of Al_2O_3 99.5 and Al_2O_3 99.9 may be due to an effect of the different grain size (10 µm/1 µm).

Materials	ϵ'	tan δ 10^{-4}
$MgAl_2O_4$ SC		<0.1
Al_2O_3 SC	9.8	<0.1
Al_2O_3 99.9	10.0	2.6
Al_2O_3 99.5	10.1	0.3

Table 12: Dielectric properties from Q-meter measurements at 30 MHz

Recent measurement at 10 GHz resulted in tan δ values $< 10^{-4}$ for Al_2O_3 single crystal and Al_2O_3 99.5. Tan δ is even likely to be considerably lower for the first material.

At present a new Fabry-Perot resonator system is being tested at 140 GHz, the frequency of choice for ECRH heating of large Tokamaks.

Staff:
M. Blumhofer
W. Dienst
G. Gausmann
H. Haase
R. Heidinger
B. Schulz
H. Zimmermann

MAT 9.2 Investigation of Fatigue under Dual Beam Irradiation

The Dual Beam Technique allows the production both of damage and of helium in thick specimens by simultaneous irradiation with high energy protons ($\leq$ 40 MeV) and alpha particles ($\leq$ 104 MeV) produced by two KfK cyclotrons.

1. Development of the Irradiation Facility

During the reporting period special effort was made to increase the beam current of the alpha particles from about 5 µ A to 10 µ A which necessitated to optimize the beam diagnostic modules. The helium loop for the cooling of irradiated samples which had been installed recently, was tested very successfully. This loop works with a helium pressure between 1 and 3 bar and with near-sound gas velocity.

The path of the proton beam is also completed and measurements of the beam quality indicated, that up to 10 µA the beam current and the beam homogeneity show a good time stability.

Meanwhile several proton and alpha particle irradiations have activated parts of the equipment. In order to avoid future handling problems, in particular after high current proton irradiations, measurements of the activated nuclei were done for a number of materials. Such activation data can be conveniently used not only to make a selection with regard to low activation elements and alloys, but also be taken as an alternative method to determine the irradiation dose of the specimens (dosimetry). However, additional systematic investigations have to be done in order to get reliable data for longterm activation under high energy proton and alpha irradiations.

2. Specimen Investigations

A set of sheet specimens made of AISI 316 L steel was homogeneously implanted with alpha particles at 600°C. Their tensile and creep properties are being tested together with sheet specimens made of 1.4914 martensitic steel irradiated in the last reporting period. Therefore a testing machine with a vacuum oven was built and is now in operation. Moreover, the complex heating system developed for future in-beam fatigue experiments was completed and tested.

Staff:

G. Bürkle   D. Preininger

A. Möslang   G. Przykutta

MAT 18   Development of Low Activation Ferritic-
         Martensitic Steels

First wall and blanket structures of fusion machines
will get activated during operation by the high
neutron fluxes, giving rise to problems in
reprocessing or waste disposal. To overcome these
problems, it is necessary to avoid the presence of
certain alloying elements (or some isotopes therefrom)
and to minimize impurity elements exhibiting
unfavourable activation properties.

A literature survey has shown that in recent years 9-
12% ferritic/martensitic steels have been devised in
which mainly Mo and Nb have been replaced by additions
of W or enhanced levels of V or Mn. The results
obtained show that for the modified materials the
standard of commercial alloys, like 1.4914, FV 448 or
HT9, has not been reached, especially with regard of
an adequate balance of tensile and impact properties.
However, improvements appear possible, by varying the
interstitial content and by a sophisticated
combination of other alloy constituents.

This aim will be pursued in cooperation with JEN-
Madrid.

Following the discussions at the MAT 18-Task Group-
Meeting of 30 October 1985 at Brussels and especially
considering the work done by UKAEA Culham + British
Steel Corp., the KfK task was revised in April 1986.
In coordination with the UK program, KfK/JEN will
proceed mainly along two lines:

a) investigation of the effect of Ce, Ta and Hf
   additions on the creep and impact properties of
   1.4914

b) investigation of the effect of a systematic
   variation of the δ-ferrite content on the
   mechanical properties of the 1.4914-type alloy.

At first an estimation of the "ferritizing power" of
Ta and Hf has been made based on the dependence of the
Cr-equivalent factor on the maximum extent of the γ-
phase in the relevant binary phase diagrams with Fe.
According to Fig. 35 the factor for both Ta and Hf
will be within the range 1.0 to 1.2. This knowledge is
of relevance in applying the Schaeffler diagram in
order to control δ-ferrite formation in the micro-
structure.
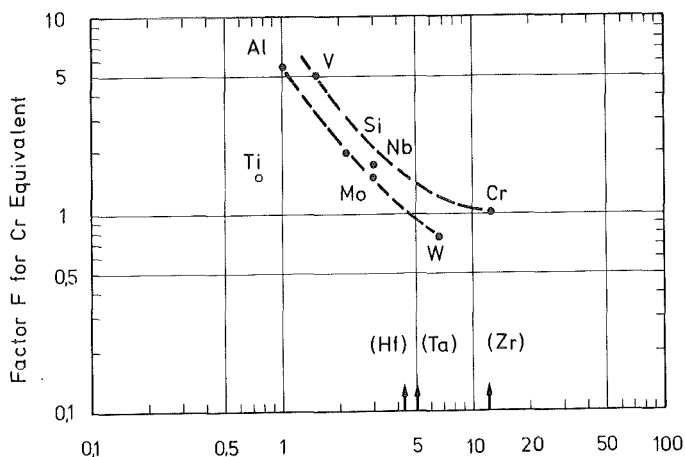
Fig. 35: Estimation of the Cr-equivalent factor F
         (Schaeffler diagram) for the elements Hf,
         Ta, Zr

The test materials (9 alloys covering point a) and b)
have been ordered at Saarstahl, Völklingen, and will
be delivered in October 1986. Heat treatments as well
as creep and instrumented impact testing will then be
carried out at KfK-IMF. The installation of the
testing devices will be finished in September 1986.

Staff:
K. Anderko
L. Schäfer
M. Schirra

N 1   Design Study of Plasma Facing Components

This task comprises design studies concerning first wall and first wall protection, and the investigation of divertor concepts for NET. The first wall concept reported here is based on a helium cooled steel structure protected by radiatively cooled small tiles. Two cooling concepts for the divertor are being investigated: Helium cooling and water cooling. This report deals with a helium cooled divertor. Investigations concerning a water cooled divertor design will be reported in the next semi-annual report.

a) First Wall with Radiatively Cooled Protection Tiles
First wall protection against impact of particles in operation and against plasma disruptions is considered necessary for NET. Graphite or ceramics are candidate protection materials. Since direct coatings can probably not be made thick enough to reach a sufficient life time, protection tiles and attachment methods are being developed. Conduction cooling of the tiles by a metallic bonding to the first wall structure causes detrimental stresses due to suppressed thermal expansion. Mixed conduction and radiation cooling of tiles that are mechanically pressed to the structure seems unpredictable since the contact pressure will be reduced by thermal and radiation induced creep.

Therefore, cooling by radiation alone is probably the most reliable heat transfer mechanism but it leads also to the highest tiles temperatures.

There are a number of concepts using radiation cooling. They are characterized by relatively large tile dimensions and use attachment methods like dove tails, support rails or bolts.

A new attachment method shown in Fig. 36 meets the following requirements:
- large ratio of radiating surface to plasma facing surface to lower the temperature
- small tiles and unrestricted thermal expansion to minimize the stresses
- short heat flow paths to the heat sink to minimize the temperature
- possibility of easy, remotely operated tile replacement

This concept is based on the use of small tiles which are fitted loosely between cooling tubes or channels.
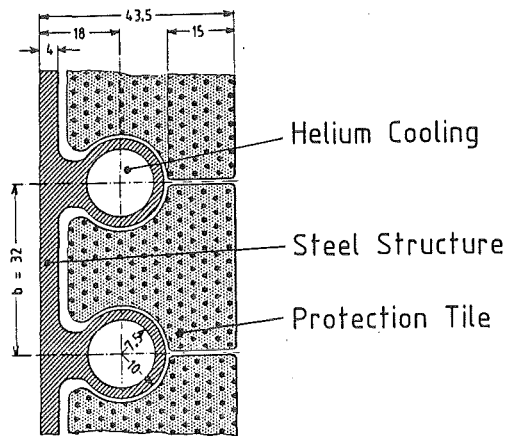

Fig. 36: First wall design with radiatively cooled protection tiles (reference case dimensions)

The gaps can be made large enough to allow free thermal expansion or radiation induced swelling. This minimizes thermal stresses such that it may allow the use of massive SiC rather than graphite tiles. The radiating surface is roughly twice as large as the plasma facing surface. Temperature distributions for graphite tiles and temperature and stress distributions for the underlaying first wall structure were calculated with a finite element computer code for steady and transient conditions. Heat loads typical for NET, emissivities $\varepsilon = 0.9$ on both sides of the gap between the tile and the cooling tube, and cooling with helium at 6 MPa and 300°C were assumed for the reference case. Table 13 shows the main results for this reference case. The maximum graphite temperature at the plasma-facing surface is close to 1400°C and the maximum temperature of the first wall steel structure mid-way between the cooling tubes is close to 520°C. Stresses in the steel structure are dominated by thermal stresses as a result of non-linear temperature distributions and suppressed bending of the structure along the tube axis. These stresses are secondary stresses; they arise when the system is heated to operating temperature and experience a cyclic change during each burn cycle.

In order to quantify the sensitivity with which temperatures and stresses respond to changes to the more important parameters, some parameters were modified in reasonable steps, but only one at a time relative to the reference case. The resulting maximum temperatures, stresses and time-dependent stress changes are also compared in Table 13.

Modified Parameter	Maximum Temperatures		Steel Maximum Thermal Stresses (von Mises)			
	Graphite	Steel	Bending of Tube Axis Suppressed		Free Bending	
			σ_{max}	$\Delta\sigma_{max}$ for 48 s Dwell	σ_{max}	$\Delta\sigma_{max}$ for 48 s Dwell
	°C	°C	MPa	MPa	MPa	MPa
Reference Case	1420	523	270	81	221	80
Reduced Emisivities of Graphite and Steel $\varepsilon_G = \varepsilon_{S1} = 0.8$	1488	535	295	80	228	79
Reduced Emisivitiy of Steel Wall (Flat Portion) $\varepsilon_{S2} = 0.15$	1428	498	219	79	200	79
Reduced Surface Heat Flux $q'' = 10$ W/cm²	1215	496	254	79	177	64
Increased Heat Conductivity of Unirradiated Graphite $\lambda_G = 50$ W/mK	1291	540	301	77	207	70
Reduced Distance b = 28 mm Between Cooling Tube Center Lines	1386	474	197	77	186	77

Table 13: Results for modifications of the reference
case parameters

Table 13 indicates that:
- More conservative emissivities of $\varepsilon_G = \varepsilon_{S1} = 0.8$ result in only slightly increased temperatures and stresses.
- A reduced emissivity (polishing) of the FW flat portion ($\varepsilon_{S2} = 0.15$) reduces the maximum steel temperature and stresses considerably.
- A reduced surface heat flux of $q'' = 10$ W/cm² results in much lower temperatures but stresses are reduced only slightly at suppressed bending.
- Increased heat conductivity of graphite (un- irradiated state) of $\lambda = 50$ W/(mK) results in lower maximum tile temperatures but in higher maximum steel temperatures and, correspondingly, in in- creased stresses at suppressed bending.
- Reduced distance between cooling tubes centerlines (small tiles) is the most effective tool to considerably decrease temperatures and stresses.

Parameter influences on stresses are less pronounced in the case of free first wall bending but time- dependent stress changes are nearly the same for both cases.

The FW concept presented includes radiatively cooled protection tiles that are sturdy and can freely expand thermally; the attachment method allows easy replacement by remote handling. A reasonable combination of the free design parameters allows to achieve maximum graphite tile temperatures below 1400°C, maximum FW temperatrures below 500°C, maximum von Mises stresses below 230 MPa and cyclic stress changes below 80 MPa during the burn cycle transient. Due to the FW design the maximum tile temperature is approximately 300 K lower than for an equivalent 25 mm thick flat tile. A first comparison of these values with allowable limits is encouraging.

As remaining open questions the thermal, mechanical, and chemical behavior at the contact points between tiles and FW structures need to be investigated and the utilization of SiC or SiC-coated graphite as tile materials should be examined.

Staff:
E. Diegele
G. Hofmann
S. Malang
K. Rust

b) Feasibility of a Helium Cooled Divertor
To avoid the detrimental consequences of a water leak into the plasma chamber the feasibility of a helium cooled divertor for NET was checked. Basis was the double null design in which the divertor plates are integrated into the inboard blanket segment. As a design principle the proposition of F. Moons was

selected in which poloidally running coolant tubes are drilled into a molybdenum block. However, for stress reduction the block was subdivided into 22 separate stripes with one coolant channel each. Fig. 37 shows a
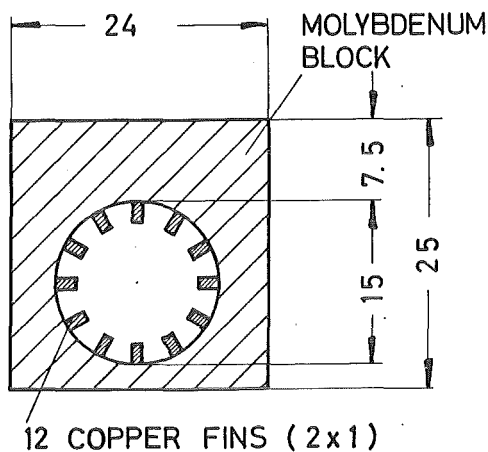
Fig. 37: Cross section of helium cooled divertor element

cross section through such an element. The copper coolant fins could be fabricated by pouring molten copper inside the molybdenum channel and subsequent machining. This design avoids the problem of repeated plastic deformations of the copper in presence of temperature cycles. The fins are interrupted in the axial direction as well. Table 14 shows the main results of the divertor thermohydraulic calculations.

Peak power density	5.1 MW/m^2
Divertor plate power	0.83 MW
He temp. inlet/outlet	100°C/140°C
He coolant pressure	8 MPa
He pressure drop	0.34 MPa
Molydenum max. temp.	730°C
Max. temp. gradient through plate thickness	600°C
Max. fin copper temp.	400°C

Table 14: Thermohydraulic data for helium cooled divertor plates

N 2   Shield Design Studies

Under this task the "in vessel shield blanket" will be treated. It is to replace the breeder blankets, at least for the first periods of NET operation. Therefore, one has to find a simple, safe, robust and low cost design with a sufficient shielding effect. Two versions are envisaged: a low temperature water cooled and a helium cooled concept.

A first study is related to the water cooled concept. Fig. 38 shows the cross section of a shielding blanket segment behind a first wall which, by lateral connection with the rear support structure, makes up a second containment.
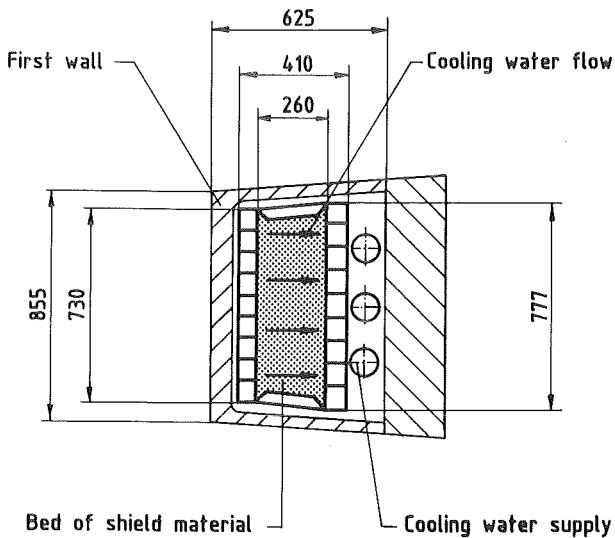
Fig. 38: Water cooled shield blanket

The blanket segment has been designed as one construction element of about 6 m height. It is composed of two rigid frames consisting of welded sheet metal plates which, together with the lateral walls, form a box-shaped cross section. The space between the front and rear walls has been compartmentalized by radially arranged sheet metal plates and filled with shielding material in the form of steel or lead balls of about 10 mm diameter. The cooling water enters from bottom into the cooling channels of the wall facing the plasma; it passes in radial direction through the bed of shield material and is collected at the top end of the rear cooling channels to be carried to the outside. The water volume in the cooling channels facing the plasma causes the neutron energy to be heavily reduced immediately behind the first wall. In order to obtain

a uniform flow of water through the shield material adapted to the heat generated, appropriately dimensioned nozzles will be provided in the front wall. The cooling water is heated from about 40°C to 70°C on the average. The proposed mean cooling pressure in the blanket will be 3 to 4 bar.

It has been shown in a first computation that the required neutron shielding effect is realized without problems by the blanket concept presented.

Staff:
E. Bojarsky
U. Fischer
H. Reiser

N 5   <u>Development of Theory and Tools for Evaluation</u>
           <u>of Magnetic Fields Effects on Liquid Breeder</u>
           <u>Blankets</u>

In a blanket of a fusion reactor the heat deposition
is concentrated near the first wall. This is shown as
an example in Fig. 39 for the self-cooled liquid metal
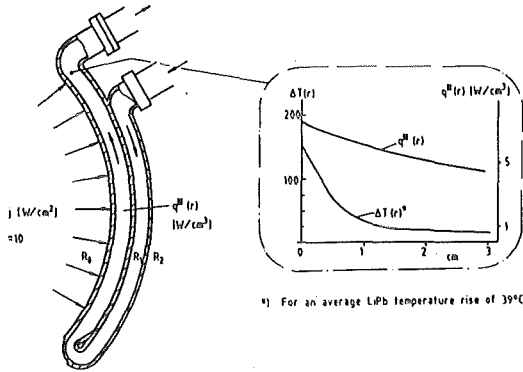

Fig. 39: Heat, velocity and temperature distribution
         in the LiPb flow channel of the NET outboard
         blanket

blanket as proposed by Malang /1/. If laminar slug
flow is assumed prevailing in the high magnetic field
of NET, this kind of heat deposition distribution
gives rise to a steep temperature gradient in the flow
duct. This results in high temperatures of the liquid
metal near the first wall so that the mean temperature
rise has to be kept low to avoid increased corrosion
attack. To decrease the mean temperature rise one has
to increase the flow of liquid metal resulting in an
increased pressure drop.

Increasing the velocity near the first wall equalized
by a decreased velocity at the second wall reduces the
first wall peak temperature remarkably as shown in
Fig. 40. In this figure the velocity and temperature
distribution of liquid Sodium-Potassium in an MHD flow
duct with a rectangular cross section, heated on one
side with a homogeneous heat flux j_o = 10 W/cm^2 are
shown for the case of a flat velocity profile across
the duct (without) and for the case of shifting the
flow through to the heated wall (with flow tailoring).

Walker and Picologlu /2, 3/ have shown how flow
distribution in a MHD duct flow can be directly
controlled by MHD and have proposed different types of
so called "MHD flow tailoring". In the frame of a
cooperation between Argonne National Laboratory (ANL)
and the Kernforschungszentrum Karlsruhe (KfK) a joint
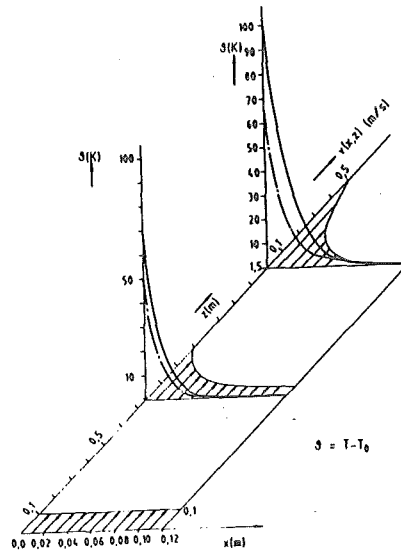
Fig. 40: Velocity and temperature distribution in a
         MHD flow duct with a rectangular cross
         section, heated on one side with a constant
         heat flux j_o = 10 W/cm^2, without and with
         flow tailoring

proof of principle experiment is undertaken to show
the viability of flow tailoring for further
improvements of the design of a selfcooled liquid
metal blanket for NET.

The test section will be designed and built by KfK.
The experiment will be conducted in the ALEX facility
at ANL, where also the analytical basis is worked out.
For the design the type of flow control with the
lowest additional MHD pressure drop was chosen.
Fig. 41 shows schematically how a blanket module based
on this type of flow control would look like. The
space between thin walled top and bottom sides is
modulated with respect to the magnetic field direction
while the distance between the sides parallel to the
magnetic field B (first and second wall) is kept
constant.

In Fig. 42 a draft of the flow tailoring test section
is shown. In order to demonstrate the intended effect
extensive instrumentation is foreseen: Pressure taps
transducers, a traversing mechanism and electrodes on
the duct wall surfaces to measure the pressure drop,
local velocities with different instruments and the
voltage distribution respectively.
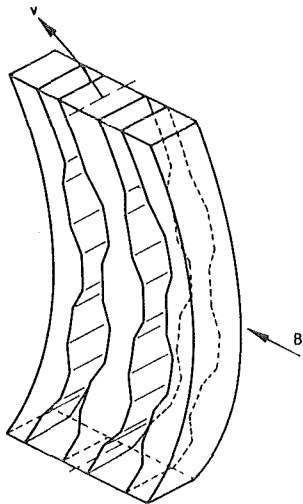
Fig. 41: Schematic view of a selfcooled liquid metal blanket module with flow tailoring by modulated separation walls

References:

/1/ S. Malang et al.: Liquid Metal Cooled Blanket Concept for NET, Proc. 14 Symposium on Fusion Techn., Avignon, Sept. 15-19, 1986

/2/ J.S. Walker and B.F. Picologlu: MHD Flow control as a Design Approach for Self-Cooled Liquid Metal Blanket of Magnetic Confinement Reactors, Proc. 6th Topical Meeting on the Technology of Fusion Energy, San Francisco, March 1985

/3/ J.S. Walker and B.F. Picologlu: Comparison of Three MHD Flow Control Methods for Self-Cooled Liquid Metal Blnakets, Proc. 7th Top. Meeting on the Techn. of Fusion Energy, Reno, Nevada, June 15-19, 1986

Staff:

G. Arnold   H. Kußmaul
L. Barleon   K.-J. Mack
V. Casal   A. Sterl
H. Kreuzinger   K. Thomauske
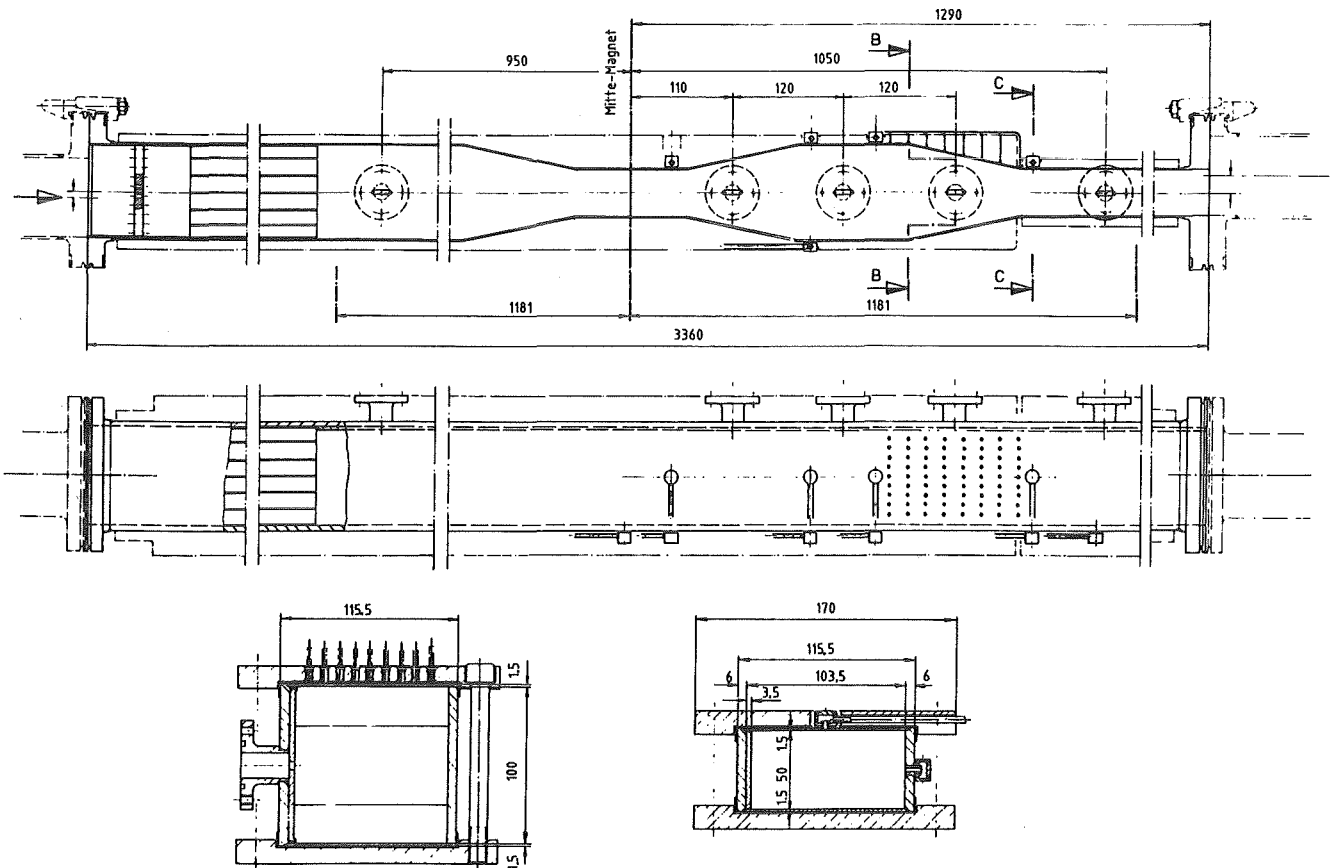
Fig. 42: Joint ANL-KfK flow tailoring test section FT 3, Version 1

RM 1   Background Studies on Remote Maintenance

Based on the results of the NET-studies "Pipe and
Vacuum Duct Connections" and "Vacuum Tight Connections
and Closures, Lip Welding and Cutting" the
development of components, such as pipe and electrical
connections, mechanical flange connections, cutting
and welding devices for pipes and flanges (the latter
connected by means of lip welding) has been started.

The task includes in particular the development of
pipe connections for
- water cooling systems
- breeder fuelling systems for breeding blankets with
  liquid metal (LiPb) as breeding material
- gas cooling systems
- purging systems with Helium as purge gas.

Based on the identification of the state of the art
presented in the reports of the NET Study Contracts
pipe connections were selected for modification and
further development. Fig. 43 shows as an example the
KfK-clamping ring connector. The design for the pre-
tests of pipe connectors up to 200 mm dia. has been
finished. The recommendation of a pre-testing program-
me is under preparation.

In parallel to the work on design, modification and
preparation of the first prototypes of pipe connectors
a universal lip-welding and -cutting system has been
designed. This system is able to weld the different
geometric configurations of openings and lip forms. In
addition the existing remotely operated KfK pipe-
welding system will be modified with respect to the
NET requirements (high pressure, elevated temperature
and low leak rate).

A test facility for integrated tests of all the
systems mentioned above is under design. To reduce
operation time it is foreseen to control the different
working stations with a computer control system.

Staff:
L. Gumb
B. Haferkamp
A. Schäf
M. Selig
M. Trettin
R. Ullrich
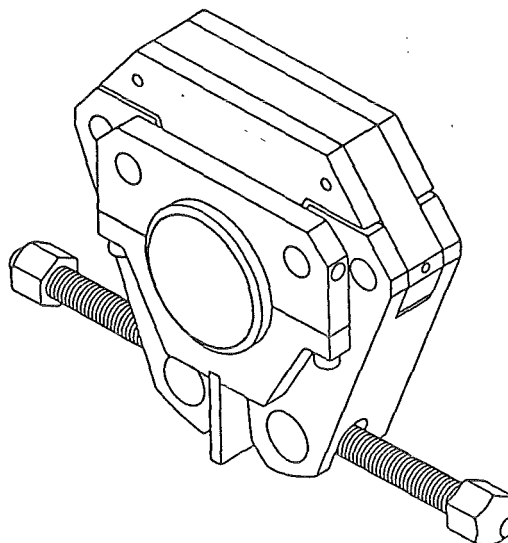
Fig. 43: KfK-Clamping ring connector

RM 2   Mechanical Components Assembly

The arrangement of blanket and divertor segments was investigated in order to prepare the concept for handling and positioning of in-vessel components. Two or three in-board segments per torus sector with and without integrated divertor plate were taken into account. The necessary steps for separate exchange of highly loaded components, such as divertor plates and first wall parts, are influencing the design of the handling tools. The position of the supply lines within the segments was analyzed for various blanket concepts.

After these investigations a common geometry of the components of a torus sector seems possible for the three NET blanket concepts (water cooled liquid breeder blanket, helium cooled solid breeder blanket and self cooled liquid breeder blanket).

Staff:
G. Böhme
B. Haferkamp
W. Link
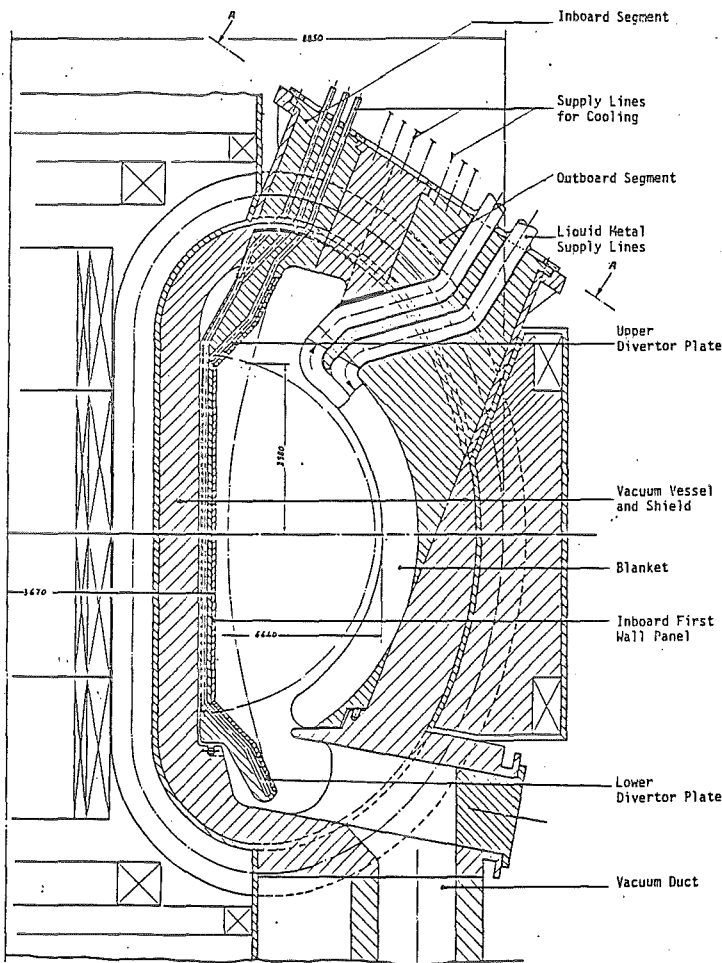
Fig. 44: KfK proposal of a liquid metal cooled
         blanket for NET

RM 3   Handling Equipment for In-vessel Components

Inspection, repair, and replacement of NET in-vessel components require special remote handling equipment. The organizations CEA, CEN/SCK, ENEA, JET, and KfK cooperate in the development of such equipment. The development is oriented towards handling of the following components which are considered as representative for all others: protection tiles for the first wall, divertor plates, active coils, and radiofrequency antennae. The principal equipment for the task is called "In-Vessel Handling Unit" (IVHU). It consists of

- a contained transfer unit (CTU)
- a transporter (an articulated boom or a vehicle represent the reference options selected as a result of the work performed during this report period)
- front-end effectors attached to the transporter for performing the proper task.

Out of the 9 sub-tasks of the RM3 work programme the following main activities are to be reported.

Sub-Task 1: Development of Concepts

The investigation of the 5 options for handling tool insertion into the vessel resulted in 5 different carrier or transporter concepts. In a first trade-off check list the most important details of the concept were composed. The main results are:

1. Insertion through an equatorial opening: 1/3 to 1/2 of the torus can be reached by a tool inserted through only one opening; this option seems to be very favourable.

2. Insertion through a divertor opening: the free space between divertor and torus is too small; more detailed investigation seems not to be justified.

3. Insertion through the opening of a blanket module by means of the CTU: 1/3 to 1/2 of the torus can be reached, however, much more time seems to be necessary, the control would be very complicated; no more work seems to be justified at present.

4. Insertion through an opening in the blanket plug: in addition to the disadvantages of option 3, this version suffers under narrow space and short reach of the tool and will not be taken into account

further on.

5. In-torus vehicle: this equipment can be inserted through a blanket opening and can approach all parts inside the vessel, the technical concept will be closer investigated and could be an alternative to option 1.

In addition to the above analysis a schematic concept for the kinematic system of transporter, TV-boom and various manipulator equipment was elaborated and proposals for the control modes were made.

Sub-Task 2: Overall Geometry Measurement

The technique for highly accurate remote geometry measurement has to be developed in order to allow in-situ measurement of components during shut-down periods. Such measurements will be necessary as changes of the geometrical dimensions of the components have to be anticipated. Thermal and stress cycling but also neutron induced swelling contribute to geometry changes over the lifetime of the components.

The approach to this sub-task at present emphasizes the measurement system architecture for both in-vessel and out-of-vessel application. The sensor to be used in the prototype implementation will be a high resolution laser theodolite (manufactured by Wild). The theodolite is equipped with computer controllable drives and digital readout. The overall system will consist of

- one theodolite mounted on an optical bench which permits two viewing positions to be used as a basis for triangulation (instead of using two theodolites in parallel)

- a micro-processor for control of the theodolite, for data analysis and as an interface to a CAD system

- a closed circuit TV camera which is used to position the laser dot on the component precisely

- a display monitor for displaying the camera picture with capability of overlaying a perspective view of a wireframe CAD model of the component

- software for controlling the system and for interfacing with a CAD system.

The IGES standard format for CAD data will be used for interfacing with CAD. Thus the measuring system will be independent from a particular CAD system and can be operated in connection with any CAD system that supports three-dimensional wireframe models (and the IGES standard).

For application of the system to in-vessel measurement the sensor will have to be replaced by equipment that is radiation hardened. Most likely a laser beam directed into the vessel through periscopes (which are to be used for various in-vessel inspection purposes) will have to be used.

The equipment for the system has been installed. Initial tests to control the theodolite from the micro-processor were successful.

Sub-Task 6: Boom Position Monitoring

This sub-task concentrates on two issues:

1. the development of a computer based remote control system that integrates manual and automated control capabilities for boom positioning,

2. the development or improvement of special sensors to be used in conjunction with this system.

A more global survey of sensors suitable for boom position monitoring application is being carried out under sub-tasks 8 and 9 (see below).

Based on the experience with the control system of the articulated boom the architecture of an overall control system for the NET in-vessel handling unit is presently being designed. The system has three levels of control:

1. the drive control system with feedback from sensors related to individual degrees of freedom,

2. the position and autonomous sub-task control system (including collision avoidance) with multiple sensor feedback,

3. the task control system which includes the human operator in the feedback loop through an appropriate man-machine interface.

The computer graphics supported man-machine interface for boom position monitoring is persued in parallel for JET and NET. The system architecture and the hardware are the same in both cases so that JET will constitute a test-bed for the NET oriented system. The software, however, will be different as the development for NET will have to allow for more flexibility while the JET components geometry is totally definded. A high-performance computer graphics workstation (the IRIS 3020 from Silicon Graphics) has been delivered to JET. A KfK delegate to JET has started to develop the JET oriented software. KfK has decided to order the same hardware. Software development has started on other computer equipment (Intel computers with Tektronix display) and will be implemented to the IRIS workstation as soon as it becomes available. For transferring geometrical data of the handling unit and its operating environment from a CAD system to the control system data base a data format in accordance with the CAD*I proposal was defined and implemented.

A very robust proximity sensor has been developed (see Fig 45). The sensor will be practically insensitve to the radiation and temperature conditions of the environment. A test program for investigation of the performance characteristics of this sensor has been established.
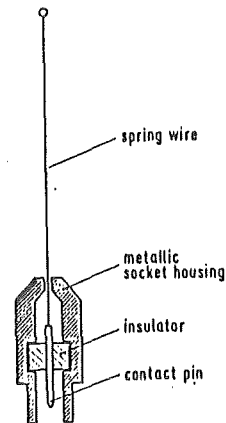
Fig. 45: The KfK whisker type proximity sensor: The sensor is basically a stainless steel wire that will produce an electrical signal when it short-circuits with its support upon deformation due to contact with an obstacle.

Sub-Task 8 and 9: Environmental Conditions
                   (Radiation, Temperature)

A market survey on sensors for boom position
monitoring has been performed. The survey was directed
towards sensors that are capable of or might have the
potential for being improved to operate at the
radiation levels and temperature conditions prevailing
inside the vacuum vessel. This activity is performed
in close cooperation with CEN/SCK.

Staff:
G. Böhme
J. Hübener
H. Knüppel
W. Köhler
I. Kornelson
U. Kühnapfel
K. Leinemann
H.A. Rohrbacher
E.G. Schlechtendahl
J. Schröder
P. Schultheiß

S+E 1 Radioactive Effluents

Releases of high amounts of molecular tritium (HT) cause a contamination of soil and plants by formation of tritium water (HTO) and organically bound tritium (OBT).

To quantify the conversion rate of HT in soil and plants under realistic conditions, KfK is participating in the French Tritium Release Experiment during September/October 1986. Representative plants and soil cores from Germany will be exposed to the plume at 800 m distance downwind and analyzed later in laboratory for HTO and OBT. At the same location the tritium concentration of the air will be measured by a tritium monitor and by an HT/HTO-sampling system.

In April 1986 a background measuring programme was performed on the planned site for the release experiment. Plant and soil samples were taken away at 600 m distance downwind from the stack and analyzed for HTO and OBT. Because of the varying tritium background on the site it was decided to make background measurements just before the release, to get correct reference values.

In the preparation time for this experiment experience was gained for the later tasks:

- Test of several methods for taking away undisturbed soil cores, which can also be used for planned laboratory measurements.

- Preparation of plants, which will be exposed to a tritium atmosphere.

- Development of an HT/HTO-sampling method.

There are still technical problems with the climatic chamber, which is foreseen for the exposure of plants with HT under controlled conditions. Therefore the first tests with H_2 and HT have been delayed.

An automatic oxidizer for combustion of dried plants and soil has been delivered. Calibrations were made for the determination of OBT.

The separation method for organic plant material has been improved and tested with contaminated plants. Wheat seedlings (300 g fresh weight after exposure) have been labelled with 4.5×10^6 Bq HTO by watering in a climatic chamber. Work has been started to separate the organic substances.

Future Activities:

- Analyzation and interpretation of plant, soil and air samples which will be received from the tritium release experiment.

- First tests in the climatic chamber with H_2 and HT.

- Further improvement of the separation method for organic plant material.

Staff:
S. Diabaté
D. Honig
L. König

S+E 4.1.2 Safety Aspects of the Cryosystems

In order to investigate the buckling behaviour of the cryostat of NET a simplified strategy for the analysis of the elastic stability is under development.

Originally the proposed method (now called the first order approximation) was intended to give a simplified procedure to solve the classical linearized buckling behaviour. The theoretical assessment of Malmberg /1/, dealt with this first order approximation approach. The conclusion was that additional sample problems should be studied. Therefore calculations for plates and shells have in the mean time been repeated under different boundary conditions. The results underline, that a reasonable assumption of the buckling shape plays an important role in the accuracy of the calculated buckling loads.

Although the first order approximation method considers the imperfect geometry, the strong nonlinear influence of these defects cannot be taken into account sufficiently. As reported in /2/ the proposed method has been generalized by higher order approximations. Further development is under way.

For a first crucial test axially compressed circular cylinders have been chosen where accurate test results for nearly perfect and well defined imperfect samples are available /3/. The second order approximation proved to be able to predict the strong reduction of the buckling load (knockdown factor > 0.3) with an accuracy of ca. 25 % which is a fairly good result compared to more elaborate methods.

As to the computing effort comparisons have been performed with the FEM-code ABAQUS /4/ where the buckling option was used. A first result is, that the new method can reduce the computing time approximately by the factor of 2 in the case of a perfect cylinder. This comparison will have to be completed for imperfect cylinders, where nonlinear ABAQUS-calculations will have to be performed.

References:

/1/ T. Malmberg "Theoretical Assessment of a Proposal for the Simplified Determination of Critical Loads of Elastic Shells", KfK 4113 (1986)

/2/ Semi-annual Report April - September 1985 KfK 3979 (October 1985), EUR 9611e

/3/ N. Waeckel, J.F. Jullian "Experimental Studies on the Instability of Cylindrical Shells with Initial Geometric Imperfections in Recent Advances in Nuclear Component Testing and Theoretical Studies on Buckling" PVP-Vol. 89 (1984)

/4/ ABAQUS, update 4.4 Hibbit, Karlsson and Soransen Inc.

Staff:
B. Dolensky
R. Krieg
T. Malmberg
S. Raff

S+E 4.1.3 Safety Aspects of Superconducting Magnets

In the first step the TESPE-S magnet safety programme mainly consists of the investigation of different fault operations with each fault being studied separately. This procedure has to precede later destructive experiments in order to accomodate them safely and to interpret their results.

A second 5-coil experiment was performed. (TESPE-S contains an arrangement of six coils). Azimuthal magnetic forces between two magnets next to the missing coil were measured by piezoelectric force transducers mounted on the outer support ring. At currents of about 1 kA the coils moved closing the small inter-coil gaps so that a first force signal could be recorded. Up to 2.4 kA the expected quadratic current dependence was observed (Fig. 46), while
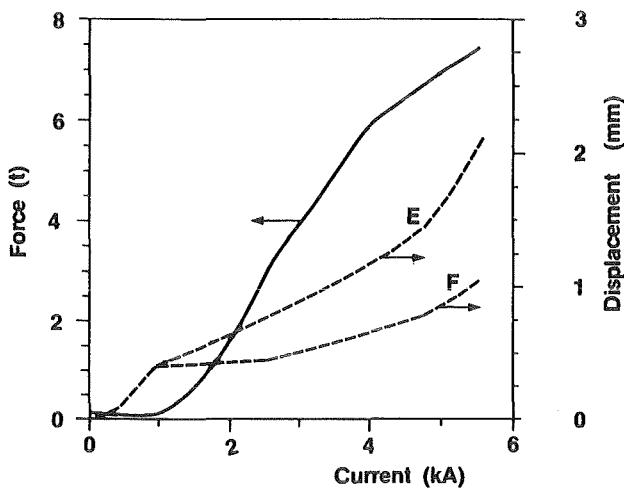

Fig. 46: Reactive forces and azimuthal displacements as functions of system current

beyond this current value and even more above 4 kA the increase of force was significantly slower. Obviously a growing part of the azimuthal forces was taken by the central support. The explanation for this behaviour is found when the action of the centering magnetic forces is taken into account which compress the central support structure and coil fixture thereby enhancing the torsional stiffness of the arrangement. This finding is in agreement with the results of the buckling measurements reported earlier.

First loss-of-cooling experiments were performed. One of the coil-cooling loops was equipped with a heat exchanger in order to warm up the selected coil to 5-

10 K. With gas cooling at a temperature of 5.8 K the coil current was run up to 3 kA, i.e. 43 % of the operating current at 4.3 K, without indications of instabilities. A series of such experiments will follow in the next period. - In a second set-up, cooling of a shorted coil with a circulating current of 2500 A was turned off and heated gas took the coil up to quench. Using a simple two-region model, quench analysis showed that the quench spreads very rapidly, allowing the energy to be distributed over a large fraction of the coil. As the windings were transparent to helium, the gas flow determined the thermal transport.

Reconstruction of the helium venting line required for further loss-of-vacuum experiments has been completed. The experimental set-up for flooding the insulation vacuum with helium gas and for measuring evaporation rate, pressure and temperature increase inside the magnets and liquid helium tanks was installed.

Within the theoretical study on safety of magnet system components, analysis of the TESPE-S energy dump system was finished. Its unavailability in case of a required dump is calculated to be 1.1×10^{-2} per demand in the 90% confidence limits of 4.6×10^{-4} and 4.8×10^{-2}. Main contribution to unavailability arises from the control unit, which however can be improved so that its contribution is reduced to the same order of magnitude as for the other subsystems.

Staff:
P. Duelli
W. Geiger
A. Grünhagen
L. Hütten
K.P. Jüngst
H. Kiesel
G.W. Leppelmeier
G. Obermaier
H. Schnauder
F. Spath
E. Süss
A. Wickenhäuser

S+E 5.4   Overall Plant Accident Scenarios for NET

Besides the component related safety studies performed
under the topics S+E 2 and S+E 4.1 this work
concentrates on the interactions of the different
components and systems and the integral behavior of
the whole plant.

The main objectives are

- to identify and to investigate significant accident
  sequences where the plant as a whole or a major part
  of its components are involved with regard to the
  consequences for personnel, public and the plant
  itself, and

- to identify critical components from both plant
  damage and safety points of view in order to orient
  R+D and to give guidance to the choice between
  different design options (see also S+E 5.5).

To initiate this work at a stage where essential
parameters of the plant are not yet fixed, safety
considerations of important components of NET (e.g.
blanket and magnetic coils) will be performed in a
first phase.

The first component considered is the blanket. So for
some of the blanket-designs proposed for NET different
accident scenarios and their consequences are being
investigated. As a starting point the events discussed
in the American Blanket Comparison and Selection Study
are taken. If possible and meaningful, experience from
fission reactors is introduced.

Typical initial events considered for a blanket are:

- loss of coolant
- local or global coolant-flow reductions
- external forces
- induced forces
- consequences of failures identified.

The main idea of the work is to identify weaknesses in
the designs with respect to safety and to provide the
designers with this information.

Staff:
R. Meyder

S+E 5.5   Development of Safety Guidelines for the
           Design of NET

The establishment of safety related guidelines for the
design of NET shall support the general approach to
safety in design, and thus, shall help the designers
to   integrate   in an   iterative   process   safety
considerations into the design at an early stage of
the design procedure.

In the framework of a special working group, the NET
Design Safety Guidelines Working Group (DSGWG), it is
intended to elaborate a document in two parts: (1.)
general safety guidelines and (2.) design specific
safety guidelines for NET. The safety guidelines will
provide targets for the design of NET, particularly
radiation exposure targets.

Different contributions to a first draft version of
the General Safety Guidelines for the Design of NET
were made. On behalf of the DSGWG the first version of
the general guidelines was compiled on the basis of a
previous paper. In the next future,   further
discussions are intended within the DSGWG, especially
concerning the structure of the document,   the
contents, and the degree of detailed description. The
first part of the document is scheduled to   be
available by end of 1986.

Staff:
W. Kramer

T 6   Industrial Development of Large Components for
       Plasma Exhaust Pumping

On behalf of the Commission of the European
Communities (CEC) a working group of CEA and KfK
elaborates the specifications and conducts the
development of large vacuum components for NET. Two
alternative solutions for plasma exhaust gas pumping
are pursued in parallel: mechanical pumps and cryo-
pumps. The large components required (high vacuum
pumps, roughing pumps, and valves) are not
commercially available at present. It is planned to
develop them within T6.

Technical specifications have been prepared for
turbomolecular pumps, roughing pumps and valves. A
feasibility study for turbomolecular pumps is carried
out by industry. The contract for another study
concerning valves will be placed in the near future.
The invitation to bid for roughing pumps is being
prepared.

In the industrial feasibility study for turbomolecular
pumps of 50 000 l/s pumping speed (helium reference)
the following preliminary results have been obtained
by the Pfeiffer company.

Using the aluminum alloy Al Zn Mg Cu 1,5 yields a
maximum circumferential speed for the rotor of
470 m/s. With a disk diameter of 1500 mm, a rotational
frequency of 100 Hz and with a blade length of 300 mm
for the input disk, the required volume flow rate of
50 000 l/s can be realized.

Transmission probabilities of gas molecules through
the channels between the blades of a turbopump in and
against the pumping direction depend on the blade
angle, on the overlapping of the blades and the ratio
v/u of the blade speed over the mean thermal velocity
of the molecules. These probabilities were calculated
by Kruger, Shapiro and Maulbetsch dependent on the
above given parameters.

With the aid of these data disks with different blade
lengths and blade angles were designed and volume flow
rate and compression ratio of each disk were
calculated.

Based on the specified volume flow rate data of the
roughing pump the number of different rotor disks were
optimized to attain the required vacuum data with a
minimum length of the rotor. 17 disks are needed in 4

different disk forms.

The required throughput of 165 mbar l/s (He reference)
can only be attained in the non molecular flow range
at decreasing values of pumping speed and compression
ratio. Calculations of the gas throughput were done by
means of an extrapolation of the cut-off pressure in
the compression ratio curves of turbopumps with
different sizes.

Result: A throughput in the range of 115 - 180 mbar
l/s dependent on the deviations of the extrapolated
test data is feasible. The calculation was checked by
the experiment with a pump TPH 5000 and different
roughing pumps.

With the given gas desorption rates from the plasma
chamber the torus pressure curve during dwell time was
calculated for 115 and 180 mbar l/s maximum gas
throughput for 12 and 16 pumps on the torus. With 16
pumps the minimum pressure will be attained after 9
seconds and with 12 pumps after 13 seconds.

The ultimate pressure depends on the compression ratio
of the turbopumps and the ultimate pressure of the
roughing pump on the one hand and on the desorption
rate and the pumping speed of the pumps on the other
hand. To get maximum pumping speed for the turbopump
at 10^{-10} mbar the forepump needs a minimum pumping
speed of 1 - 0.1 l/s in the lower 10^{-4} pressure range.

Two drafts have been made of a rotor design. The first
one with a shaft penetrating all disks and a second
one with disks without central holes fastened together
with axial bolts.

Two shaft ends are fastened on the input and output
sides of the rotor to support the bearings and the
motor. The first solution proved inadequate because of
too high mechanical strain in the disks. For the
second draft the strain was calculated in the roots of
the blades and in the disks. With an exponential
sectional profile the radial and tangential strains
are equal and constant over the whole disk radius:
max. 180 N/mm in the disks, max. 150 N/mm in the
blades.

In transversal magnetic fields, eddy currents are
induced in the disks and in the shaft of the rotor.
These currents heat up the rotor. The rotor
temperature depends on heat generation and heat losses
by radiation between rotor and stator of the pump.

When using the aluminum alloy Al Zn Mg Cu 1.5 the rotor temperature must not exceed 120°C. The possible heat flow at this temperature will be generated by the motor, the magnetic bearings and the above mentioned eddy currents. The maximum eddy current heat power can be calculated if the losses of the magnetic bearings and the motor are known.

Preliminary data of the pump are:

Vacuum data
Volume flow rate He:	57 000 l/s
Volume flow rate H_2:	56 000 l/s
Compression ratio H_2:	$1,1 \times 10^7$
Compression ratio N_2:	$> 10^9$
Compression ratio He:	10^9
Throughput He:	115 - 180 mbar l/s

Rotor data
Diameter:	1500 mm
Rotational frequency:	100 Hz (6000 rpm)
Circumferential speed:	471 m/s
Number of disks:	17
Length of disk range:	1650 mm
Length of rotor:	2870 mm
Mass of rotor:	2130 kg
Momentum of inertia:	254 kg m^2
Energy:	5×10^7 Ws
Temperature raise at baking without energy removal:	15 °C
Material of disks:	Aluminium alloy

Staff:
U. Kirchhof
H. Lukitsch
A. Mack
D. Perinić

T 10 A <u>Plasma Exhaust Purification by Means of Cryosorption on Molecular Sieves or Alternative Adsorbents</u>

The fuel cycle of a fusion reactor requires processes for the removal of impurities from several gaseous streams, such as the plasma exhaust gas, the solid blanket coolant, the blanket sparge gas, etc. Among the processes presently under discussion cryosorption may be cited. However, for an evaluation of the suitability of this alternative a number of experimental data are still missing. To fill this gap, a laboratory loop, designed to investigate the adsorption on type A zeolite of certain relevant impurities (CO, CO_2, CH_4, NH_3, H_2O etc.) from a He or H_2 carrier gas is now under construction. First experiments will concentrate on the measurement of adsorption isotherms of the pure species as well as of gaseous mixtures at temperatures above 80°K. Particular attention will be directed towards the co-adsorption of hydrogen. For this purpose tritiated protium will be employed ($\geq$ 100 m Ci/l). Gaseous tritium will be determined with a small ionization chamber of own construction (detection limit < 1 m Ci/l). Exchange reactions will be followed by liquid scintillation counting. Permanent trapping of tritium in the zeolite, which has been found to occur at about 250°C, i.e. during regeneration, and which appears to be due to a phase transformation of the zeolite, will be investigated by techniques developed in our laboratories. The loop will have a volume of 1 liter, cooling will be carried out with a two stage cryogenerator. For gas analysis a gas chromatograph, a mass spectrometer and several other specific detector methods, such as UV derivative spectroscopy, capacity detection, etc. will be used.

<u>Staff:</u>
R.-D. Penzhorn

T 10 C/   Plasma Exhaust Gas Purification by Use of
10 E   Hot Metal Getters

Purification of the plasma exhaust gas can be achieved by various technical processes. Besides the method of diffusion through a palladium/silver membrane and cryogenic methods, also hot metal getters are known to have the capabilities of either retaining gaseous impurities from helium/hydrogen gas mixtures or of separating hydrogen isotopes from the other gas constituents by hydride formation, depending on temperature. In order to investigate the feasibility of such getters for NET, an experimental program has been started looking into both applications:

a) Absorption of low Z impurities on hot metal beds (T-10 C)
b) Absorption of (D, T) on heated metal beds (T-10 E)

The main objectives are:

- to study the absorption and desorption behavior of hydrogen as well as the irreversible uptake of gaseous impurities like O_2, N_2, CO, CO_2, or CH_4;

- to demonstrate the purification efficiency and capacity of various getter materials for realistic operational conditions, i.e. with tritium gas at pressures as close as possible to 1 bar.

The program will be carried out in three steps:

1. Design and construction of a laboratory scale tritium-compatible facility;

2. Inactive tests with H_2 and He plus different combinations of impurity gases for basic investigations of non-uranium getter materials such as Zr/Al, Zr/V/Fe alloys; characterization of the most relevant parameters; examination of the gettering properties of additional elements like, Cr, Mn, Ni, Ti, Sn, Mo, La, Y.

3. Validation of the main results with tritium; investigation of isotopic and ageing effects.

The concept of the facility which is currently under construction includes the following main components:

Test gas supply: Pressure gas bottles containing H_2, He, and the impurity gases can be connected with either a 10 l or a 100 l recipient for preparation of the test gas mixture. Tritium will be supplied from a uranium storage vessel. The recipients will be evacuated and baked at 300°C before being filled with the test gases.

Vacuum system: In order to avoid ingression of ambient gases and to allow for tritium operation the whole loop was designed according to the rules of UHV (ultra high vacuum) technology.

Getter beds: Up to 4 getter beds are installed which can be exposed either separately or in series. At the beginning, the properties of SAES getters ST-101, ST-198, and ST-707 will be investigated in the temperature range 200 - 800°C.

Gas analysis: The concentration of the impurities before purification will be in the order of 1% relative to hydrogen and should reach of 10^{-4} to 10^{-6} after purification. As analytical tools, a mass spectrometer and a gas chromatograph with He ionization detector will be used. The latter can also be applied to detect the different hydrogen isotopes with sufficient sensitivity. In addition, FT-IR spectrometry is being prepared as a method for the analysis of compounds containing hydrogen isotopes.

Glove box: The whole loop including all pumps and analytical instruments will be enclosed in a large glove box which will be operated with an inert atmosphere of nitrogen during the tritium test series.

Staff:
H. Albrecht
T. Kastner
E. Willin

T 10 H Plasma Exhaust Purification Applying Catalysts

Current concepts under consideration for the removal of impurities from the plasma exhaust of a fusion machine forsee the employment of a palladium silver alloy diffuser cascade for the separation of the process gas into a pure heavy hydrogen fraction fed into the isotope separation system and a noble gas stream containing up to 16 mol % of tritiated (Q_2O, CQ_4, NQ_3, Q_2 with Q = D,T) and non-tritiated (He, Ar, O_2, CO, CO_2, etc.) impurities. D,T present in the impurities of the noble gas stream and also existing as residual molecular hydrogen must be recycled. In addition the noble gas stream needs to be decontaminated to a high degree prior to its discharge into the atmosphere.

At KfK a process for the recovery of D,T from the noble gas stream, involving a CO oxidation step, an O getter bed, a diffuser membrane for hydrogen permeation and a cracking catalyst for CH_4 and NH_3 is presently under development. In this report attention is focused on the oxidation of CO over hopcalite and on the synthesis, self-radiolysis and catalytic cracking of tritiated ammonia and methane.

Experiments on the selective oxidation of CO were carried out in a laboratory loop having a total volume of 25 l. All gases subject to investigation were diluted with He and circulated over hopcalite with a flow rate of 4.5 - 5.7 l/min. Hopcalite was found to be a rather porous material with a specific surface area of 233 m^2/g. At low temperatures it tends to adsorb gases reversibly without however losing much of its catalytic activity; at temperatures about 220°C it decomposes yielding O_2.

When a mixture of 19.3 mol % NH_3 was passed over 10 g of hopcalite at 200°C for a period of 2 h, no measurable reaction took place. Also methane was not significantly oxidized at these temperature. Carbon monoxide instead was rapidly and completely oxidized to carbon dioxide even at a temperature of 25°C (Fig. 47a). A material balance ($[CO_2]_t/[CO]_0 \ll 1$) indicates that a large fraction of the produced CO_2 remains adsorbed on the hopcalite. Heating the hopcalite up to 200°C after completion of the reaction caused the release of the adsorbed CO_2, i.e. $[CO_2]_t/[CO]_0 \sim 1$. If the reaction was carried out at 200°C the oxidation was completed in less time and almost no adsorption of CO_2 occured (Fig. 47b). As apparent from the data in Fig. 47a oxidation of CO is characterized by a very
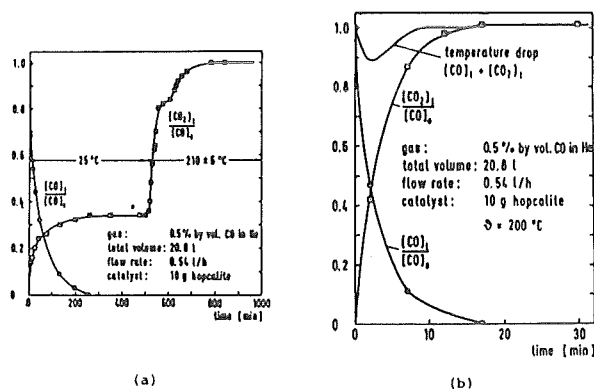

(a)   (b)

Fig. 47: Oxidation of CO over hopcalite (a) at 25°C followed by heating up to 210°C and (b) at 200°C

rapid initial reaction. The importance of this initial reaction is demonstrated by the results presented in Fig. 48. It is seen that even at - 17°C practically
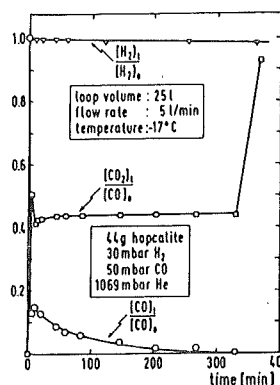
Fig. 48: Oxidation of CO in the presence of H_2 and He over hopcalite at -17°C. After completion of the reaction (330 min) the catalyst was heated up to 200°C, which caused liberation of the adsorbed gas.

all CO is oxidized to CO_2 within a few minutes when the amount of hopcalite is quadrupled.

Considerable effort has been invested into the study of the catalytic cracking reaction of NH_3 and CH_4 on various catalysts. From screening experiments with Fe, CO, Pd, Ru and Ni catalysts it was concluded that the fastest kinetics at the lowest temperature can be achieved with a Ni catalyst supported on Al_2O_3. On this catalyst CH_4 is cracked reversibly. Up to 80% of the C deposited on the catalyst by the cracking reaction can be converted back into CH_4 via reaction with H_2 at 570°C.

During the course of a collaborative effort with TSTA, Los Alamos, first experience on the handling and on the properties of highly radioactive NH_3 and CH_4 were gained. Starting from an equimolar mixture of H_2 and T_2, CH_2T_2 and $NT_{1,5}H_{1,5}$ were synthesized from Al_4C_3 and Mg_3N_2, following techniques developed under cold conditions in KfK. The self-radiolysis of CH_2T_2 and $NH_{1,5}T_{1,5}$ as well as the effect of NH_3 on the self-radiolysis of CH_2T_2 were determined. The catalytic decomposition of $NH_{1,5}T_{1,5}$ and CH_2T_2 on a Ni catalyst was demonstrated on a Ni catalyst employing a test loop built at KfK and shipped to TSTA. Presently these data are being evaluated.

Staff:
M. Glugla
K. Günther
K. Nolte
R.-D. Penzhorn
K.-H. Simon

Studies for NET/INTOR

Design of TF Coils for NET

The NET TF Coil Design Study continued with the aim of identifying critical paths and components for design and construction of the toroidal field coils and by preparing solutions for the identified problems. In the period under review finite element stress calculations on TF coils, superconductor and central vault of the torus were completed, the basis for ac-loss calculations was settled, and the technical specification of the superconductor was elaborated for industrial feasibility studies.

The cross section of the 16 kA-superconductor is shown in Fig. 49. The Roebel-process will be applied for
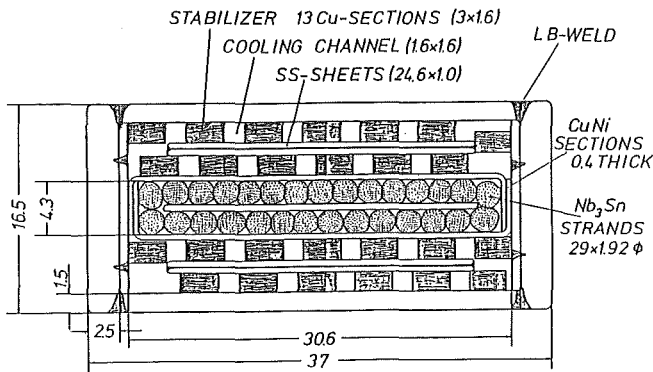

Fig. 49: Cross section of 16 kA superconductor for NET-TF coils (KfK design)

pre-fabrication of the stabilizer whose geometry was chosen to ensure high electrical stability, low ac-losses, acceptable helium pressure drop and ease of manufacture. Verification of this concept will be obtained from manufacture and test of the subsize conductor ordered from industry (see M 3).

Methods and formulae required for calculation of various ac-loss components in the TF superconductor were elaborated. Clearly, the losses are dominated by the coupling currents induced between strands of the superconducting core. The parameter "effective transverse resistivity cannot be calculated with the required accuracy and has therefore to be measured for each actual conductor to get reliable numbers for the losses.

The finite-element stress analysis of the

superconductor and the coil in the central vault led to design figures for coil casing, superconductor and winding pack. For given dimensions of the cross section in the central vault, optimization for low stresses requires minimum thickness of the winding pack in radial direction, i.e. maximum radial thickness of the coil case (Fig. 50). Two critical regions were identified. First, the local maximum shear stress within the windings reaches just the tolerable limit of 30 MPa. Second, slip between winding pack and coil casing can only be avoided at the side walls but not at the toroidal wall which
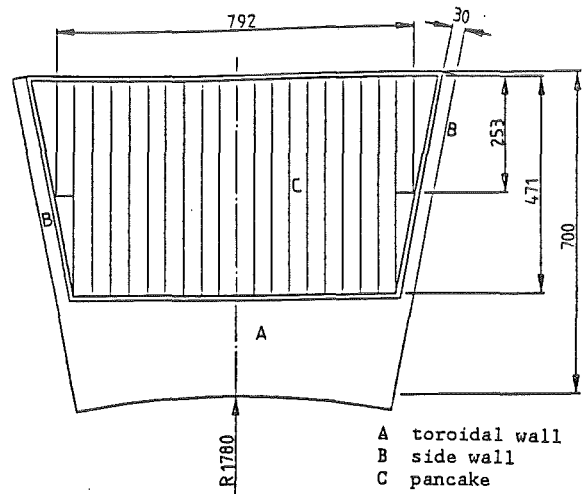
Fig. 50: Cross section of one TF coil in the central vault

leads to an enhancement of maximum toroidal stress in the windings by 14%. Within the conductor significant stresses occur in the corners of the steel jacket caused by small radii, but they can be kept at tolerable levels. With these results the stress-analysis part of the TF coil study was completed and a global analysis of the torus will be new be performed by NET.

Stress and Lifetime Calculations for First Wall and Blanket Structural Components in NET

The study "Stress and Lifetime Calculations" was terminated. In this investigation a lifetime prediction for the first wall of NET was outlined considering failure due to fatigue crack growth. The aim was to show the general procedure of lifetime calculations, to demonstrate the principal behaviour of plasma facing structures, to explain the radiation effects

and to give a first idea of the expected lifetime from a view point of fatigue.

The analysis includes five steps:

(1) Transient temperature distributions during a load cycle are calculated using the finite element method (FEM).

(2) Related elastic thermal stresses during a load cycle are determined using FEM also. These stresses represent the cyclic load causing fatigue crack growth. The important influence of the mean stress is taken into account by the

(3) Calculation of changing stress caused by irradiation creep and swelling on the basis of a semi-analytical model. In Fig. 51 the time dependent stresses are shown for two locations in the wall.
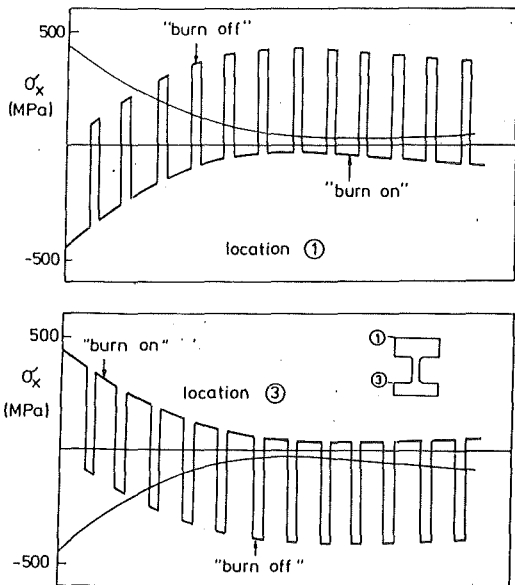

Fig. 51: Cyclic stresses in the wall (SS316CW) due to cyclic reactor operation

(4) Stress intensity factors are calculated assuming cracks in various positions in the first wall structure. Real pre-existing surface cracks are described by semi-elliptic cracks as shown in Fig. 52. Starting with the initial geometric data (a_i, c_i) the <u>average stress intensity factors</u> were calculated for the points A and B using the weight function method. If ∂S_A and ∂S_B denote virtual extensions of the crack area S in the depth or in

the width, the averaged K-values are given by

$$\overline{K_A} = \frac{H}{\overline{K_{rA}}} \int \sigma(x,y) \frac{\partial u}{\partial S_A} r \, dS$$

$$\overline{K_B} = \frac{H}{\overline{K_{rB}}} \int \sigma(x,y) \frac{\partial u}{\partial S_B} r \, dS$$

where u_r is the crack opening displacement field for a reference load case and $\overline{K_{rA}}$, $\overline{K_{rB}}$ are the accompanying stress intensity factors.
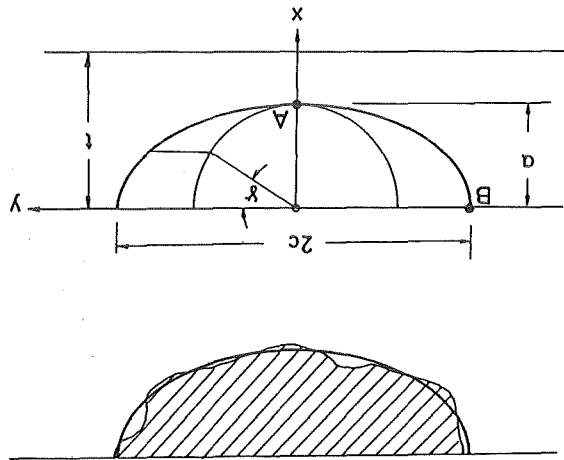
Fig. 52: Model of a real surface crack by a semi-elliptic crack

(5) Crack extension computations are performed by means of a modified Forman equation allowing to predict the time to failure.

$$\frac{da}{dN} = \frac{C_1 \lambda^m [f\Delta K - \Delta K_0]^n}{K_{Ic} - \lambda f \Delta K}$$

A threshold ΔK_0, below which no crack growth occurs, and an acceleration of crack growth rate near the critical stress intensity factor K_{Ic} are taken into account.
In this equation

$$\lambda = \frac{1}{1-R} \qquad \text{with } R = K_{min}/K_{max}$$

The quantity ΔK, responsible for the crack extension, is given by the difference between the maximum (K_{max}), and minimum value (K_{min}) during each cycle

$$K = K_{max} - K_{min}$$

The crack increments for each cycle were added to the previous values:

a → a+ Δa

c → c+ Δc

and the shape of the crack was assumed to remain semi-elliptical.

For the following cycles the whole procedure had to be repeated as long as the maximum averaged K-factor reached the dose dependent fracture toughness K_{Ic} or the crack tip at point A penetrated the structure. In this cycle failure of the wall was stated.

In a parametric study the geometric shape of the cracks was altered.

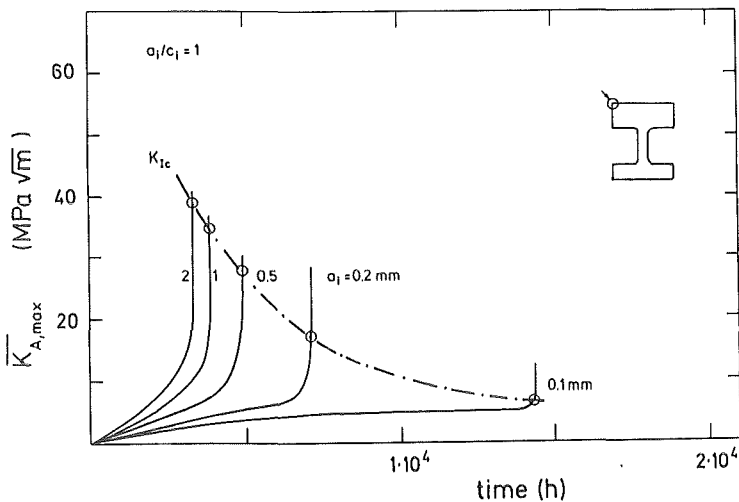In Fig. 53 the influence of the intitial crack depth

Fig. 53: Influence of the crack depth on lifetime for SS316CW

is represented for semicircular cracks situated at the plasma faced surface. Failure of the wall can be stated to occur at the intersections with the K_{Ic}-curve; they are marked by small circles where the maximum K-value reaches the fracture toughness. It is evident that the lifetime resulting from this conditions increases with decreasing crack size.

The effect of the aspect ratio a/c can be seen from Fig. 54. Maximum lifetimes are found for semi-circular cracks.
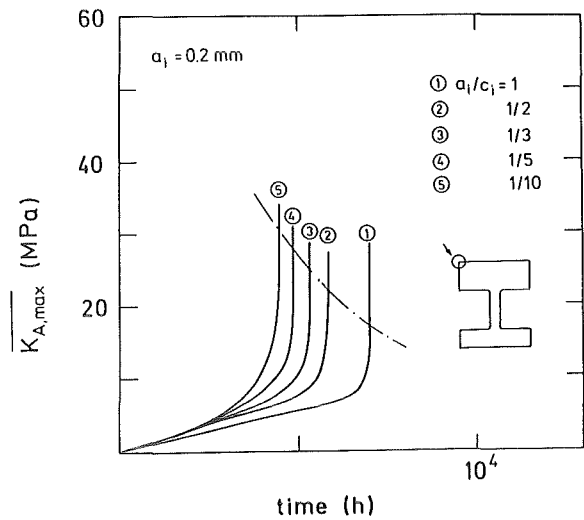
Fig. 54: Influence of the initial aspect ratio a_i/c_i on life time for SS316CW

A comparison between lifetimes calculated for austenitic steel SS316CW and martensitic steel 1.4914 is shown in Fig. 55. Because of the influence of the significantly lower thermal stresses due to the lower coefficient of thermal expansion and the higher thermal conductivity it was expected that martensitic steel should be superior to austenitic steel.

At least for front wall cracks this superiority can be seen in Fig. 55 where the lifetime data of martensitic steel are compared with the results obtained for austenitic steel.

All fracture mechanical failure calculations are strongly influenced by the irradiation embrittlement of the structural material. Whilst fracture toughness data are available for unirradiated and for thermally aged materials, data of irradiated materials are deduced indirectly from tensile test results. These sources of error will remain as long as reliable K_{Ic}-measurements on irradiated material are not available. Therefore the lifetimes calculated in this report should be considered as rather indicative. Nevertheless, the importance of influencing factors can be demonstrated by the parametric studies given here.

Fig. 55: a) Lifetime diagram for 1.4914
        b) Comparison of lifetime data SS316DW/1.4914

Formulation of Initial Design Equation for Type 1.4914
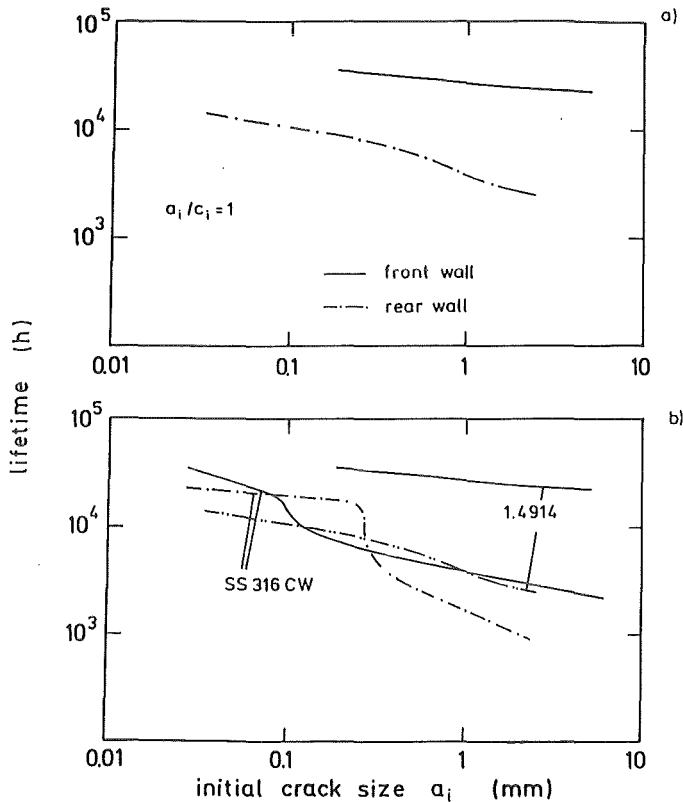Martensitic Steel (Summary of the Study Report)
Part A: Properties of Unirradiated Material

A fully martensitic steel (German denomination 1.4914)
was selected as a possible first wall and structural
material for NET. The existing experimental data of
this steel and of the comparable group of 9-12% Cr
ferritic-martensitic steels have been compiled.
Initial property equations have been formulated, where
possible. These equations should, however, be used as
a basis for exploratory studies only rather than for
engineering design.

In Chapter 1 a survey is given on the constitution,
the hardenability and the γ-α-transformation behaviour
of Type 1.4914 steel in comparison to other 9-12% Cr
bearing ferritic-martensitic alloys. A preliminary
recommendation for the optimum thermomechanical
pretreatment of this material is given.
Chapter 2 deals with the physical properties of this
material. Equations for thermal expansion, density,

thermal conductivity, specific heat and electrical
resistivity have been formulated. The data on
magnetization, permeability and coercive force and
their dependence on material composition and
pretreatment give only a general tendency for the 12%
Cr ferritic-martensitic steels. Further investigations
on this topic are necessary.

The mechanical properties are summarized in Chapter 3.
The elastic data are resonably well known and
correspondingly, "design equations" have been
formulated. Tensile-, creep- and creep-rupture data
have been generated for Type 1.4914 alloy so that
property equations dependent on composition and
pretreatment can be given.

Fatigue and fatigue-creep data are very scarce for the
class of 9-12% Cr steels. The ones available allow
however the conclusion that for small strain
amplitudes very similar results can be expected. A
quantitative formulation of the fatigue crack growth
over a broad temperature range is available for the
alloys HT9 and 9Cr-1Mo mod.. The data of 1.4922, the
unstabilized version of 1.4914 fit well into this data
set. Finally an initial property equation for the
impact energy of 1.4914 in Charpy-V tests has been set
up.

In Chapter 4 the corrosion behaviour of 9-12% Cr
steels in liquid lithium and lithium-lead is reviewed.
The data indicate a better compatibility of these
steels when compared with the austenitic reference
materials, but the limits in the upper operational
temperature are severe, namely $\sim$ 500°C in Li-Pb
eutectic and $\sim$ 550°C in liquid lithium. Data on liquid
metal embrittlement of Type 1.4914 material are
scarce. The general corrosion resistance in pure water
and in steam atmospheres is very good for 9-12% Cr
steels. This good corrosion resistance might be
reduced if the water chemistry is changed and heat
flux loadings are expected. Sensitivity to stress
corrosion phenomena is low if tempered materials are
used. Exposure of 9-12% Cr steels to helium does not
seem to pose any longterm problems with respect to
oxidation or decarbonization up to 600°C.

There exists a broad technical experience of welding
for the unstabilized version of Type 1.4914, as
reviewed in Chapter 5. The routine procedure is TIG-
welding and a well investigated heat-treatment during
and after the welding procedure has to be applied.
Property degradations due to welding can be general be

avoided by this procedure.

In Chapters 6 and 7 the hydrogen solubility, diffusivity and permeability data in 9-12% Cr steels are described and formulated in equations. Also the influence of hydrogen on the low temperature embrittlement is discussed. The results are of a very qualitative nature since synergistic effects stemming from a parallel irradiation or stress corrosion cracking are not taken into account.

Evacuation Behaviour of NET-Design Alternatives

On request of the NET-team supplementary parametric calculations about the NET evacuation behaviour were carried out. The results confirm that with the specified vacuum pumping capacity the required start vacuum conditions can be realized in all areas of the vacuum chamber within a reasonable time. The two blanket concepts do not differ remarkably in their evacuation behaviour. However, it should be mentioned that the data base of outgassing rates applicable to large vacuum installations like NET is by far not adequate at present. This work should therefore be considered as a first best estimate analysis made in this complex field. Because of the small gap widths in the vacuum chamber, pressure differences of up to two orders of magnitude prevail even after four days of evacuation. The conductivity of the divertor channel has a dominating impact on the effective pumping speed and in this way on the vacuum conditions reached.

An updated version of the final report concerning the NET study contract "Evacuation Behavior of NET-Design Altervnatives" was prepared. The results were published also in a paper presented at the 14th Symposium on Fusion Technology, Avignon, Sept. 1986. The computer code VAKMAP, developed under the study contract was streamlined and documented.

With a view to the proposed NET follow-up study contract about the "Simulation of the Vacuum Performance of NET-DN" the conductivity value of a more compact divertor channel and vacuum duct arrangement was determined using Monte Carlo techniques. The new study contract will be focussed on the vacuum behaviour during dwell time. In the development of the code VAKMAP this application was already taken into account.

Development of Helium Cryopumping Materials and Preliminary Design Concept of Cryocompound Pumps for NET

Experimental investigations are under way at KfK with the aim to develop and optimize porous active cryosorption surfaces for helium pumping from the plasma exhaust gas. In these investigations a multitude of combinations of materials for the sorbent, bond, and the cold wall are tested and the bonding techniques are investigated to select the best suited candidates. A test matrix was worked out.

In a first test series sorbent materials, which had been fixed to the 500 mm diameter carrier plates using various bonding techniques, will be examined for their resistance to temperature cycling. The temperature cycling experiment has been designed for simultaneous, automated testing of up to ten specimens. The specimens are moved alternately into an LN bath (~78 K) and an electric tubular furnace (300°C) through pneumatic drive. It is intended to subject each specimen to up to 100 cycles. The components of the test device have been built, assembly is under way.

Fig. 56: Activated carbon test specimen brazed onto a copper plate

The specimens which will survive cyclic loading without damage, will be examined for their capacity of helium cryosorption in a second test setup. After degassing at 300°C, the specimens will be exposed to helium gas. The increase of gas pressure at equilibrium above the specimen after heating is taken

as a measure of the sorption capacity of the specimen. With this testing facility the adsorption isotherms can be recorded for individual specimens. Construction of the test arrangement is under preparation.

As a final step, after the sorbent/bonding agent/wall combinations have been preselected, vacuum pump tests will be performed on a technical scale. This implies specimens of 400 mm diameter tested under conditions as expected for a NET cryopump (temperature, gas load, gas composition). The experiments include endurance test of selected samples. The whole arrangement was designed and industry was invited to bid for the cryogenic system. The experimental part of the study will carried out under a fusion technology research contract.

Staff:
G. Böhme
H.U. Borgstedt
E. Diegele
K. Ehrlich
T. Fett
R. Flükiger
B. Haferkamp
J. Hanauer
G. Hartwig
W. Höhn
K.P. Jüngst
B. Kammerer
U. Kirchhof
P. Komarek
M. Kuntze
K. Leinemann
S. Leistikow
A. Ludwig
J. Lühning
H. Lukitsch
A. Mack
R.A. Müller
D. Munz
A. Nyilas
D. Perinic
C. Petersen
D. Preininger
G. Schanz
M. Schirra
R. Schmitt
M. Selig
F. Spath   E. Ternig
K. Stamm   A. Ulbricht
E. Süss   D. Zimmerlin

Development of ECRH Power Sources at 150 GHz

The initial experiments have been started after delivery of the magnet system as the last required component. A series of tests to prepare the microwave operation of the gyrotron is under way. Presently, processing of the gun is in progress.

1. Magnet

The superconducting magnet system manufactured by industry has been accepted for preliminary operation. It was found that this magnet quenched, when the backing coil was activated. Nevertheless the required beam could be achieved with an increased velocity spread by elongating the gun intersection.

In the first experiment, the magnet has been successfully qualified for this modified operation. Axial and azimuthal field profiles were verified together with the magnet alignment.

For the second experiment, forming of particular field profiles was facilitated by computer control of the individual magnet currents. Quench protection by the computer is being developed in addition.

In both experiments, the cryogenic and the helium reprocessing systems have been operated reliably over extended periods.

A completely redesigned magnet system, which incorporates modified conductors, structural reinforcements and additional steering coils is under construction.

2. Gyrotron

The prefabricated gyrotron modules have been assembled and outbaked before insertion into the magnet. After full assembly of the gyrotron and the auxiliary systems, high voltage durability of the related components has been verified with and without magnetic field.

At present, the electron gun is being processed to form an adequate beam.

3. Diagnostics

In addition to the measurement of all essential operating parameters, special instrumentation for beam and microwave diagnostics during the initial experiments has been installed.

Beam diagnostics consist of

- thermo-sensors distributed over the thin-walled stainless steel collector
- infrared imaging of the collector temperature distribution
- X-rays observed along the collector

Microwave diagnostics include

- power measurement by a volume absorbing liquid calorimeter
- fast frequency measurement by a simple channelized receiver with a harmonic superhet front end

To measure the beam properties at the location of the microwave cavits, a destructive beam analyzer to replace the resonator inside the magnet borehole was constructed.

4. Theory

A self consistent code to describe the beam-field interaction in the gyrotron resonator has been developed. The wave equation for the radiofrequency field profile includes a source term and is solved simultaneously with the equation of electron motion. Some of the programs in the package have been vectorized. The code has been applied to the TE_{03}-mode gyrotron under study and is being used in design studies for high order modes.

Staff:

W. Baumgärtner	B. Jödicke
E. Borie	M. Kuntze
H. Budig	R. Lehm
G. Dammertz	A. Möbius
F. Graf	N. Münch
P. Grundel	H. Oppermann
G. Haubrich	B. Piosczyk
R. Hietschold	G. Redemann
G. Hochschild	H. Stickel
A. Hornung	R. Vincon
K. Jentzsch	H. Wenzelburger

External Contributors:

K. Behm and team	(Valvo, Hamburg)
E. Jensen et al.	(TU, Hamburg-Harburg)
M. Kitlinski et al.	(IHE, Univ. Karlsruhe)
M. Thumm et al.	(IPF, Univ. Stuttgart)
O. Dumbrajs	(Abas, Leopoldshafen)
E. Edgecombe	(Univ. Cambridge, UK)

Publications:

E. Borie, O. Dumbrajs: Calculation of Eigenmodes of Tapered Gyrotron Resonators, International Journal of Electronics, Vol. 60, No. 2, p. 143, February 1986

M. Kitlinski, W. Wiesbeck, G. Hochschild: Four-Antenna Mapping System for Identification of Modes in High-Power Gyrotron. MIOP '86 - Mikrowellentechnik und Optoelektronik, 10.-12. Juni 86, Wiesbaden, Vol. 3

M. Kitlinski, G. Hochschild, W. Wiesbeck: Reflection Monitor for an Oversized Circular Waveguide. 16th European Microwave Conference 86, Dublin, Ireland, September 8-12, 1986

Appendix I: Table of Fusion Technology Contracts

Task Code No.	Title	KfK Departments
B 1	Blanket Design Studies	IMF III, INR, IRB, IT
B 2	Development of Computational Tools for Neutronics	INR
B 6	Corrosion of Structural Materials in Flowing Pb-17Li	IMF I, IMF II
B 6.3	Fatigue of Structural Steel under Liquid Eutectic Environment	IMF I, IMF II
B 9	Tritium Extraction based on the Use of Solid Getters	IT
B 11-16	Development of Ceramic Breeder Materials	IMF I, IMF III, INR, IRCH
B 15.3	End of Life of Solid Breeding Materials in Fast Neutron Flux	IMF I, IMF III, INR
M 1	The Large Coil Task (LCT)	ITP
M 3	Development of Composite High Field Superconductors	ITP
M 4	Superconducting Poloidal Field Coil Development	ITP
M 8	Design and Construction of a Poloidal Field Coil for TORE SUPRA as NET-Prototype Coil	ITP
M 9	Structural Materials Fatigue Characterization at 4 K	ITP
M 12	Low Electrical Conductivity Structures Development	IMF IV, ITP
MAT 1.6	Development and Qualification of Type 1.4914 Base Metal Properties	IMF II
MAT 1.9	Pre- and Post-Irradiation Properties of 1.4914 Martensitic Steel	IMF II
MAT 1.11	Post Irradiation Fracture Toughness of Type 1.4914 Martensitic Steel	IMF II
MAT 2.2	In-Pile Creep-Fatigue Testing of Type 316 and 1.4914 Steel	IMF II, IMF III
MAT 6/ MAT 13	Ceramics for First Wall Protection and for rf Windows	IMF I
MAT 9.2	Investigation of Fatigue under Dual Beam Irradiation	IMF II
MAT 18	Development of Low Activation Ferritic-Martensitic Steels	IMF II

N 1	Design Study of Plasma Facing Components	INR, IRB, IRE
N 2	Shield Design Studies	IMF III
N 3	Development of Procedures and Tools for Structural Design Evaluation	IMF IV
N 5	Development of Theory and Tools for Evaluation of Magnetic Fields Effects on Liquid Breeder Blankets	IRB
N 6	Studies of Pepple Beds of Ceramics Compounds	INR
RM 1	Background Studies on Remote Maintenance	IT
RM 2	Mechanical Components Assembly	IT
RM 3	Handling Equipment for In-vessel Components	IDT, IRE, IT
S+E 1	Radioactive Effluents	HS
S+E 4.1.2	Safety Aspects of the Cryosystems	IRE
S+E 4.1.3	Safety Aspects of Superconducting Magnets	IDT, IRE, ITP
S+E 5.4	Overall Plant Accident Scenarios for NET	IRE
S+E 5.5	Development of Safety Guidelines for the Design of NET	IRE
S+E 6	Licensing Activities	PKF-PL
S+E 7	Accident Consequence Assessment for Fusion Reactor	AFAS, INR
T 6	Industrial Development of Large Components for Plasma Exhaust Pumping	IT
T 10 A	Plasma Exhaust Purification by Means of Cryosorption on Molecular Sieves or Alternative Adsorbents	IRCH
T 10 C/ 10 E	Plasma Exhaust Gas Purification by Use of Hot Metal Getters	IRCH
T 10 H	Plasma Exhaust Purification Applying Catalysts	IRCH
	Development of ECRH Power Sources at 150 GHz (This task is part of the Fusion Physics Programme of the EC.)	IDT, IK

Appendix II: Table of NET Contracts

Theme	Contract No.	Working Period
Stress and Lifetime Calculations for First Wall and Blanket Structural Components in NET	155/84-5/FU-D/NET	6/84 - 5/86
TF-Coil Design	183/84-12/FU-D/NET	12/84 - 3/87
Availability of the LCT Plant	210/85-9/FU-D/NET	10/85 - 12/87
Availability of the TESPE Device	211/85-9/FU-D/NET	10/85 - 12/86
An Assessment on the Feasibility of the Permeation Methods for Tritium Extraction from $Li_{17}Pb_{83}$ Blankets	223/86-2/FU-D/NET	2/86 - 8/86
Development of Helium Cryopumping Materials and Preliminary Design Concept of Cryocompound Pumps for NET	224/86-4/FU-D/NET	6/86 - 12/86
Study on the NET TF Pancake Tests	240/86-6/FU-D/NET	5/86 - 4/87
Engineering Problems of NET Blanket Testing and Blanket Insertion Strategy	243/76-6/FU-D/NET	7/86 - 7/87

Appendix III: KfK Departments contributing to the Fusion Project

Kernforschungszentrum Karlsruhe GmbH   Telephone (07247) 82-1
Postfach 3640   Telex 7 826 484
D-7500 Karlsruhe 1   Telefax/Telecopies (0)07247/82 5070
Federal Republic of Germany

KfK Department	KfK Institut/Abteilung	Director	Ext.
Applied Systems Analyses Department	Abteilung für Angewandte Systemanalyse (AFAS)	Dr. H. Paschen	2500
Central Data Processing and Instrumentation Department	Hauptabteilung Datenverarbeitung und Instrumentierung (HDI)	DP. H. Stittgen	5600
Central Safety and Security Department	Hauptabteilung Sicherheit (HS)	Prof. Dr. H. Kiefer	2660
Institute for Data Processing in Technology	Institut für Datenverarbeitung in der Technik (IDT)	Prof. Dr. H. Trauboth	5700
Institute for Nuclear Physics	Institut für Kernphysik II (IK)	Prof. Dr. A. Citron	3502
Institute for Materials and Solid State Research	Institut für Material- und Festkörperforschung (IMF)	I. Prof. Dr. F. Thümmler II. Dr. K. Anderko III. Prof. Dr. K. Kummerer IV. Prof. Dr. D. Munz	2918 2902 2518 4815
Institute for Neutron Physics and Reactor Engineering	Institut für Neutronenphysik und Reaktortechnik (INR)	Prof. Dr. G. Keßler	2440
Institute for Reactor Components	Institut für Reaktorbau- elemente (IRB)	Prof. Dr. U. Müller	3450
Institute for Radiochemistry	Institut für Radiochemie (IRCH)	Prof. Dr. H.J. Ache	3200
Institute for Reactor Development	Institut für Reaktor- entwicklung (IRE)	Prof. Dr. D. Smidt	2550
Central Engineering Department	Hauptabteilung Ingenieur- technik (IT)	Dr. H. Rininsland	3001
Institute for Technical Physics	Institut für Technische Physik (ITP)	Prof. Dr. P. Komarek	3500

Appendix IV: Fusion Project Management Staff (PKF-PL)

Nuclear Fusion Project -	Project Manager	Dr. J.E. Vetter	5460
Project Management Group	Secretariate	I. Sickinger, I. Pleli	5461/5466
	Administrator	Dr. D. Finken	5462
Projekt Kernfusion -	Blanket, Test Facilities	DI. H. Sebening	5464
Projektleitung	Superconducting Magnets, ECR-Heating	Dr. J.E. Vetter	5460
	Tritium Technonolgy, Materials	Dr. H.D. Röhrig	5463
	Safety, Remote Handling	DI. A. Fiege	2668